POLITECNICO DI TORINO

Collegio di Ingegneria Chimica e dei Materiali

Corso di Laurea Magistrale
in Ingegneria Chimica e dei Processi Sostenibili

Tesi di Laurea Magistrale

Population Balance Modelling of bubble sizes in gas-liquid flows with complex physical properties

Application of the quadrature method of moments to stirred tanks and bubble columns

Relatore

prof. Daniele MARCHISIO

Candidato

Eleonora GILLI

Marzo 2020

Ai miei genitori.

Contents

0. Introduzione

La presente tesi di laurea qui presente riassume il lavoro svolto presso il centro ricerche francese Institut Français du Petrol-Energie Nouvelle (IFPEN) situato a Solaize, Lione (Francia), in particolare, presso il dipartimento di modellazione e sviluppo di processo (Luglio-Dicembre 2019).
Lo scopo di questo lavoro è l'utilizzo di un approccio modellistico zero-dimensionale per testare e validare diversi modelli di coalescenza e rottura in sistemi bifase quali colonne a bolle e reattori agitati, con una visione del loro uso in sistemi complessi di tipo biologico e organico, al fine di predirne la distribuzione della dimensione delle bolle.
Dunque, questo lavoro può essere contestualizzato nello sviluppo di modelli, usati come strumenti per la progettazione di reattori multifase, in quanto capaci di predirne l'idrodinamica. Tali modelli trovano una applicazione in diversi settori dell'ingegneria chimica, tra cui i più i più interessanti, sono il campo della produzione dei biocombustibili e quello della 'Green Chemistry' in generale.
Per la validazione dei modelli di coalescenza e rottura sono stati sfruttati gli studi sperimentali fatti da Gemello (2018) e Cappello (2019), rispettivamente per colonne a bolle e reattori agitati contententi aria-acqua e i risultati sperimentali di Chaumat et al. (2007) and IFP-NT Vonner Roesler (2018) per sistemi di liquidi organici.
Una volta convalidati, tali modelli sono stati poi implementati in simulazioni di fluidodinamica computazionale (CFD) tridimensionali tramite il software ANSYS Fluent.
Tramite questo studio è stato possibile individuare dei modelli per la coalescenza e rottura che forniscono un' accurata predizione della dimensione delle bolle in varie condizioni operative per i sistemi gas-liquido analizzati.
L'importanza di avere una buona previsione della dimensione delle bolle risiede nel fatto che l'idrodimamica dei sistemi multifase e le dinamiche di scambio interfase (di material e di energia) dipendano da questa variabile.
Il lavoro è strutturato nel modo seguente:
Il capitolo 0 è un sommario esteso, scritto in lingua italiana, che riassume ciò che è contenuto nei capitoli successivi della tesi di laurea.
Il capitolo 1 contiene un'introduzione generale che spiega lo scopo della tesi e dà una breve descrizione del lavoro svolto.
Il capitolo 2 riporta una breve revisione bibliografica che riassume ciò che fino ad ora è stato fatto in questo ambito e che è stato riportato in letteratura.
Il capitolo 3 descrive l'idrodinamica delle colonne a bolle e dei reattori agitati, in particolare descrivendo i regimi e le principali proprietà di questi sistemi.
Il capitolo 4 descrive le condizioni operative adottate da Gemello (2018), Cappello (2019) e dagli altri autori negli esperimenti i cui risultati sono stati usati per la validazione dei modelli.
La prima parte del capitolo 5 riporta i concetti di bilancio di popolazione e del metodo dei momenti al fine di introdurre gli strumenti usati per il lavoro svolto. Inoltre sono stati riportati l'approccio usato e i principali risultati ottenuti dalle simulazioni fatte con approccio 0D.
La seconda parte del capitolo descrive il setup adottato nelle simulazioni di fluidodinamica computazionale, l'implementazione del bilancio di popolazione e i risultati ottenuti.
Il capitolo 6 riassume le principali conclusioni, prospettive future e i limiti di questo lavoro.

0.1 Contesto

I modelli che descrivono i fenomeni di coalescenza e rottura delle bolle rappresentano degli utili strumenti per il design di reattori e bioreattori multifase in quanto sono capaci di predirne l'idrodinamica. Questi modelli sono in grado di predire la distribuzione della dimensione delle bolle in diversi tipi di flussi e trovano perciò un ampio range di applicazione: è possibile infatti applicarli nel campo dei biocombustibili e anche in quello della 'Green Chemistry'.
I biocombustibili sono considerati come una forma di energia rinnovabile e, perciò, ultimamente occupano molto spazio nell'ambito della ricerca in quanto tutto ciò che riguarda la sostenibilità ambientale sta ottenendo molta attenzione, sia per la salute dell'ecosistema e sia in concomitanza con la previsione di riduzione a livello mondiale di altre fonti di energia non rinnovabili.
In genere con questo termine ci si riferisce ai combustibili liquidi che vengono impiegati nell'ambito dei trasporti e che vengono prodotti a partire dalle biomasse (piante o rifiuti di origine biologica). Tra i biocombustibili più comuni troviamo il bioetanolo e il biodiesel.
Il vantaggio dell'utilizzo di questo tipo di prodotti consiste nel fatto che essi hanno un impatto ambientale più contenuto rispetto ai combustibili fossili.
Infatti le biomasse e i biocombustibili che derivano da esse, durante la combustione, emettono in atmosfera anidride carbonica in quantità pari a quella assorbita dagli organismi vegetali durante la loro crescita, evitando così di rilasciare nuova anidride carbonica in atmosfera.

Figura 1 ciclo dei biocombustibili

0.2 Idrodinamica dei sistemi gas-liquido

I reattori gas-liquido, come le colonne a bolle o i reattori agitati, sono ampiamente usati in diversi processi di tipo chimico e biochimico per le loro eccellenti caratteristiche di trasferimento di massa e calore e per la semplicità di costruzione. Tuttavia, il comportamento idrodinamico, essenziale per la progettazione e lo scale-up del reattore, presenta una certa complessità.
L'idrodinamica di questi sistemi dipende dalle condizioni operative e dalla loro geometria sia a livello globale che locale.

La frazione volumica totale di gas, nota anche in inglese come "global gas hold-up" è un'importante proprietà per lo studio di questi sistemi in quanto influenza il trasferimento di massa all'interno dell'apparecchiatura. Può essere calcolato come il rapporto tra il volume di gas e il volume totale e dipende dalla velocità superficiale del gas Vsg.

$$\alpha_g = \frac{V_g}{V_g + V_l}$$

In letteratura è possibile trovare diverse correlazioni per la valutazione di questo parametro che sono valide a diverse condizioni operative.

La Potenza P rappresenta un'altra importate proprietà per il design dei reattori agitati. Questo parametro dipende dal diametro D e dalla velocità N dell'agitatore, la densità della fase liquida ρ_l e il numero di Potenza N_p.

$$P = \rho_l N^3 D^5 N_p$$

Il numero di Potenza è stato calcolato tramite la correlazione di Bujalski et al. (1987) che presenta la seguente forma:

$$N_p = 2.5 \left(\frac{x}{D}\right)^{-0.2} \left(\frac{T}{T_0}\right)^{0.065}$$

Dove x rappresenta lo spessore dell'agitatore, T è il diametro dell'apparecchiatura, mentre T_0 è un diametro di riferimento pari a 1 m. In questo lavoro N_p è pari a 4.66.

Nel caso di reattori agitati in cui è presente una fase gassosa, la Potenza P_g è diminuita rispetto al caso di assenza di fase gassosa e tale riduzione può esssere misurata tramite la relative power demand (RPD). Diverse correlazioni sono state proposte per il calcolo di tale grandezza e in questo lavoro è stata sfruttata quella fornita da Gabelle et al. (2011) in quanto essa è stata validata per un ampio intervallo di condizioni operative.

$$P_g = P \ \max\left[\left(\frac{P_g}{P}\right)_{lim}; exp\left(-15.36 {N_P}^{0.16} {Q_G}^{0.62} T^{-1.7} \left(\frac{D}{T}\right)^{0.51}\right)\right]$$

0.2.1 Regimi di flusso

Colonne a bolle

Diversi regimi sono individuabili all'interno di queste apparecchiature al variare della velocità superficiale del gas e del diametro della colonna. I principali regimi sono (Fig.2):

- Omogeneo;
- Di transizione;
- Eterogeneo;
- Slug flow.

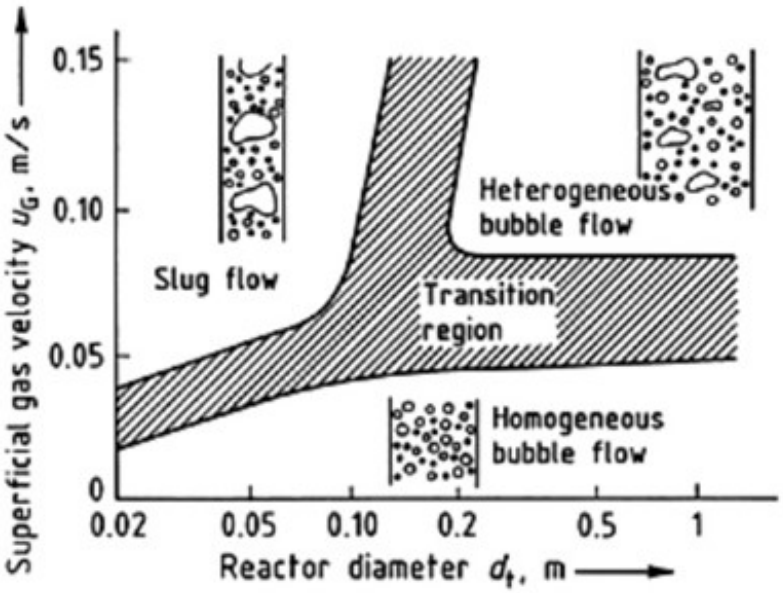

Figura 2 Regimi di flusso in una colonna a bolle

Il regime omogeneo (o fluidizzazione omogenea) avviene a bassi valori della velocità superficiale ed è caratterizzato da bolle di piccola dimensione e velocità pressochè uniformi. La distribuzione delle bolle è uniforme e i fenomeni di rottura e coalescenza sono praticamente assenti, dal momento che le interazioni tra le bolle sono deboli. Inoltre, il gas hold-up cresce linearmente all'aumentare della velocità superficiale del gas stesso.
Il regime eterogeneo invece si osserva ad alti valori di velocità superficiale e in colonne ad impiego industriale (cioè di diametro grande). Caratteristiche di questo regime sono le larghe bolle con breve tempo di residenza. L'incremento del gas hold-up all'aumentare della velocità superficiale del gas è più graduale, i fenomeni di rottura e coalescenza delle bolle diventano più rilevanti portando a una distribuzione della dimensione delle bolle più ampia.
Infine a valori di velocità ancora più alti, in colonne con diametro piccolo è possibile osservare un regime definito fluidizzazione a bolle in cui è possibile osservare grosse bolle che causano grandi differenze di pressione e fluttuazioni della portata liquida.

Reattori agitati

Sulla base della velocità dell'agitatore e delle diverse traiettorie delle bolle all'interno di un reattore con turbina di tipo Rushton, è possibile individuare diversi regimi quali: flooding, loading e completa ricircolazione. Questi regimi sono descritti da due numeri adimensionati (Lee and Dudukovic, 2014): il numero di flusso (Fl) e il numero di Froude (Fr) che, rispettivamente, rappresentano il rapporto tra le portate di gas e quella spinta dall'agitatore, e il rapporto tra l'accelerazione dovuta all'agitatore e la gravità.
Il regime di Flooding si verifica quando la dispersione della fase gassosa è assente o quasi, dal momento che l'energia prodotta dall'agitatore non è sufficiente a rompere le bolle. Perciò le bolle risalgono lungo l'albero rotante senza finire nella zona al di sotto dell'agitatore. La presenza di questa zona inutilizzata comporta una perdita in termini di Potenza, un basso gas hold-up e una bassa miscelazione, riassumibili in una ridotta performance del reattore.
Aumentando Fr o diminuendo Fl, cioè aumentando la velocità di rotazione dell'agitatore, la dispersione aumenta e il gas circola ovunque andando anche nelle regioni inferiori (Fig.3).
Al fine di avere una buona miscelazione e favorire il trasferimento di materia è necessario che all'interno dell'apparecchiatura ci sia una completa dispersione della fase gassosa; ciò è verificato

quando la velocità minima dell'agitatore è pari a N_{cd} (Yawalkar et al., 2001), cioè la minima velocità di agitazione al di sotto della quale si ha un'incompleta dispersione del gas all'interno dell'apparecchiatura.

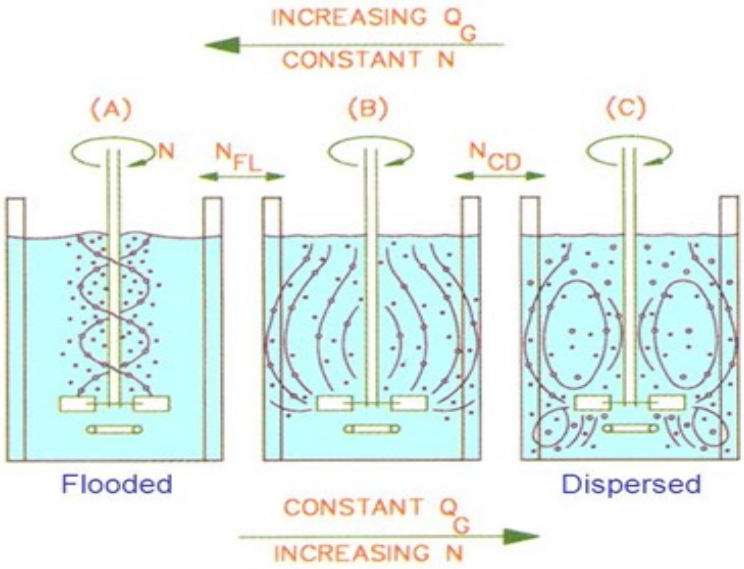

Figura 3 Regimi di flusso di un reattore agitato

0.3 Metodologia

Questa tesi si basa sullo studio di modelli di rottura e coalescenza capaci di predire la dimensione delle bolle in varie condizioni operative, in sistemi gas-liquido quali colonne a bolle e reattori agitati. In particolare, un approccio 0D è stato utilizzato per testare e validare i diversi modelli e, una volta validati, i modelli sono stati implementati in simulazioni 3D di fluidodinamica computazionale per uno studio sull'idrodinamica.

L'approccio 0D assume che entrambe le fasi siano perfettamente miscelate e che ci sia omogeneità spaziale, comportando costi computazionali veramente bassi (Buffo et al., 2016). Il vantaggio di questo approccio consiste nel poter testare molti modelli in breve tempo, superando l'ostacolo legato all'uso di normali simulazioni transitorie in 3D di fluidodinamica computazionale che richiedono un tempo estremamente elevato per fornire i risultati a diverse condizioni operative.

Il linguaggio di programmazione VBA, in Excel, è stato utilizzato per scrivere un codice contenente il modello 0D. Il codice si basa su un metodo iterativo dove il valore del diametro medio di Sauter, calcolato con l'iterata precedente, viene utilizzato per calcolare i termini di coalescenza e rottura che permettono di calcolare il momento di secondo ordine e che, a sua volta, è usato per calcolare il nuovo valore del diametro delle bolle fino ad otterene il valore allo stazionario.

Tra le varie correlazioni presenti in letteratura, è stata fatta una selezione e le principali sono state testate.

In uno studio precedente, Gemello (2018) aveva proposto un set di kernels capace di prevedere la dimensione delle bolle in una colonna a bolle contenente aria-acqua. Lo scopo di questo lavoro è stato quindi quello di usare l'approccio 0D sul sistema in questione al fine di testare diversi modelli e verificare che i risultati ottenuti da Gemello (2018) siano ancora verificati o che, al più, si trovi un set di kernels alternativo, in grado di fornire risultati in accordo con i dati sperimentali.

L'approccio 0D è stato applicato anche al caso di un reattore agitato contenente anch'esso aria-acqua su cui, in precedenza, Cappello (2019) aveva già fatto degli studi. In questo caso, i diversi kernels di

coalescenza e rottura sono stati testati al fine di trovare quelli in grado di riprodurre i dati sperimentali ottenuti da Cappello (2019), dal momento che gli studi fatti fino ad ora su questi sistemi sono ancora poco validati o necessitano di essere migliorati.
Si è cercato inoltre di sfruttare tale metodo per riuscire a trovare un set di kernels comune in grado di descrivere in modo soddisfacente la distribuzione della dimensione delle bolle in entrambi i sistemi.
Infine, è stato dato uno sguardo all'uso di questi modelli in sistemi più complessi, di tipo organico: gli esperimenti fatti da Chaumat et al. (2007) su una colonna a bolle contenente cicloesano e quelli fatti da IFP-NT Vonner Roesler (2018) con esano sono stati usati per la validazione dei modelli testati con l'approccio 0D.
In seguito, una volta validati, i modelli testati nel caso del reattore agitato sono stati implementati in alcune simulazioni di fluidodinamica computazionale per permettere di ottenere delle previsioni più accurate sull'idrodinamica del sistema.
Per aiutare a raggiungere la convergenza, inizialmente le simulazioni sono state lanciate disaccoppiando il bilancio di popolazione dal calcolo dell'idrodinamica (one-way coupling), e, solo successivamente, calcolarli di nuovo in contemporanea (two-way coupling).
Quindi partendo da simulazioni completamente sviluppate, in cui si è assunta dimensione constante delle bolle e mandate a convergenza, è stato poi implementato il bilancio di popolazione tramite la funzione UDF (User-Defined Function). È stato inoltre introdotto uno scalare UDS (User-Defined Scalar) che rappresenta il momento di secondo ordine normalizzato rispetto alla frazione volumica delle fase gassosa:

$$\mu_2 = \frac{m_2}{\alpha_g}$$

Lo scalare è stato inizializzato all'ingresso basandosi su una distribuzione log-normale centrata nel valore medio del diametro delle bolle ed è stato inoltre inizializzato su tutto il volume attraverso inizializzazione patch.
Infine, per poter controllare i diversi parametri e i rispettivi valori sono state poi aggiunge 8 UDM (User-Defined Memories).
L'andamento della fase discreta è stato quindi predetto considerando l'influenza della fase continua sulla fase discrete stessa ed è stato calcolato il diametro di Sauter a diverse condizioni operative e poi confrontato con i risultati ottenuti dall'approccio 0D.

0.4 Modellizzazione: strumenti usati

0.4.1 Bilancio di Popolazione

Nei sistemi gas-liquido di tipo disperso, la distribuzione della dimensione delle bolle (BSD) gioca un importante ruolo nel determinare il comportamento idrodinamico, la miscelazione e il trasferimento di materia. A tal proposito è necessario considerare questa relazione al fine di ottenere dei risultati accurati. Il bilancio di popolazione (o population balance model, PBM) è un modello in grado di simulare tale distribuzione della dimensione delle bolle dal momento che tiene in considerazione i fenomeni di coalescenza e rottura.
Il PBM è un promettente strumento sia in ambito accademico che industriale ed è stato per la prima volta formulato da Hulburt and Katz (1964) per scopi di ingegneria chimica.
Prima di approfondire tale concetto, è necessario chiarire altri aspetti relativi al bilancio di popolazione, quale ad esempio la funzione di densità numerica (NDF).
Quando si utilizza un approccio Euleriano, la fase dispersa è generalmente descritta da una NDF. Questa funzione $n_\xi(t, x, \xi)$ identifica l'intera popolazione della fase dispersa e descrive come tale

popolazione sia distribuita rispetto alle proprietà d'interesse (ad esempio, il vettore della coordinata interna $\xi=(\xi_1, \xi_2, \ldots, \xi_M)$ all'interno del dominio computazionale, ad ogni istante.
Integrando la NDF rispetto a tutti i possibili valori, si ottiene la concentrazione numerica totale *N(t,x)*:

$$\mathrm{N} = \mathrm{m}_{\xi,0} = \int_{\Omega\xi} \mathrm{n}_\xi(\xi)\mathrm{d}\xi$$

N(t,x) è il numero totale di entità per unità di volume situate al tempo t in un punto x e corrisponde al momento di ordine zero della funzione di densità. In generale, il momento k-esimo della NDF può essere definito come:

$$\mathrm{m}_{\xi,\mathrm{k}} = \int_{\Omega\xi} \xi_1^{\mathrm{k1}} \ldots \xi_{\mathrm{M}}^{\mathrm{kM}} \mathrm{n}_\xi(\xi)\mathrm{d}\xi$$

L'equazione del bilancio di popolazione è scritta in termini della NDF e può essere derivata come un bilancio delle bolle in una regione fissata del dominio computazionale (Ramkrishna, 2000).
Il numero di elementi all'interno del volume considerato cambia risultando nella seguente equazione (Marchisio and Fox, 2013):

$$\frac{\partial}{\partial t}\left(\int_{\Omega x} dx \int_{\Omega\xi} d\xi\, n_\xi\right) + \int_{\Omega\xi} d\xi \int_{\partial\Omega x} (n_\xi \boldsymbol{u}) \cdot dA_x + \int_{\Omega x} dx \int_{\partial\Omega\xi} \left(n_\xi \dot{\xi}'\right) \cdot dA_\xi = \int_{\Omega x} dx \int_{\Omega\xi} d\xi\, S_\xi$$

Dove **u** è il vettore velocità delle bolle, ξ' indica la variazione della generica coordinate interna, Ω_x è il volume di controllo nello spazio fisico, mentre Ω_ξ quello nello spazio delle fasi e S_ξ tiene in considerazione alcuni fenomeni riguardanti la fase discreta, tra cui la collisione tra bolle.
Applicando alla precedente equazione il teorema di Reynolds-Gauss e imponendo le condizioni iniziali relative alla variabile tempo e le condizioni al contorno per lo spazio fisico e quello delle fasi, tale equazione può essere risolta analiticamente o con metodi numerici.
Inoltre, quando la popolazione della fase discreta è descritta da un'unica coordinata interna (ad esempio la dimensione delle bolle L) e le bolle sono caratterizzate dalla loro distribuzione di velocità, l'equazione del bilancio di popolazione prende il nome di equazione generalizzata (GPBE), includendo la velocità delle bolle come una variabile interna.

$$\frac{\partial n_L}{\partial t} + \frac{\partial}{\partial x} \cdot (\boldsymbol{u} n_L) + \frac{\partial}{\partial L} \cdot (G_L n_L) = S(L)$$

Dove G_L rappresenta l'entità di variazione della lunghezza della particella, mentre *S(L)* tiene conto dei fenomeni tra cui coalescenza e rottura.
Nel caso quindi di una popolazione descritta usando solo la dimensione delle bolle come coordinata interna, il *k-esimo* momento della NDF può essere definito come segue:

$$m_{L,k} = \int_0^\infty n_L(L) L^k dL$$

Applicando questo momento all'equazione precedente:

$$\frac{\partial m_{L,k}}{\partial t} + \frac{\partial}{\partial x} \cdot \left(\boldsymbol{u}_{L,k} m_{L,k}\right) = k G_{L,k-1} m_{L,k-1} + S_{mk}$$

Dove l'entità media della variazione del *k-esimo* momento e il termine sorgente sono rispettivamente:

$$G_{L,k} = \frac{\int_0^\infty G_L n_L(L) L^k dL}{\int_0^\infty n_L(L) L^k dL}$$

$$S_{mk} = \int_0^\infty S_L L^k dL$$

Il termine sorgente tiene conto solo dei fenomeni di coalescenza e rottura dal momento che il trasferimento di materia è trascurato in questo lavoro. Perciò questo termine può essere scritto come la somma dei termini relativi al fenomeno della coalescenza e quello della rottura e, in particolare, entrambi I fenomeni contribuiscono con due termini: nascita e morte.

I termini che appaiono nel termine sorgente sono i seguenti:

- La nascita di nuove bolle dovute alla rottura della bolla madre B^B;
- La nascita di una nuova bolla dovuta alla coalescenza di due bolle più piccole B^C;
- La morte della bolla madre in seguito alla sua rottura D^B;
- La morte delle due bolle che per coalescenza ne formano una nuova D^C.

Sommando i termini di nascita e sottraendo quelli di morte, la forma esplicita del termine sorgente risulta in:

$$S(L) = \frac{L^2}{2}\int_0^L \frac{h\left((L^3+\lambda^3)^{\frac{1}{3}},\lambda\right)}{(L^3-\lambda^3)^{\frac{2}{3}}} n_L\left((L^3+\lambda^3)^{\frac{1}{3}}\right) n_L(\lambda)d\lambda - \int_0^\infty h(L,\lambda)n_L(L)n_L(L)d\lambda + \int_L^\infty \beta(L,L')g(L')n_L(L')dL' - g(L)n_L(L)$$

Dove *g(L)* rappresenta il kernel di rottura, *β(L,L')* è la funzione di distribuzione delle bolle figlie, mentre *h(L,L')* è il kernel della coalescenza.
Diversi modelli di coalescenza e rottura sono disponibili in letteratura e sono stati usati in questo lavoro al fine di individuare quelli capaci di fornire una corretta previsione della dimensione delle bolle.

0.4.2 Metodi per risolvere il PBM: Metodo di quadratura dei momenti (QMOM)

Molti metodi sono stati proposti e sviluppati per risolvere il bilancio di popolazione e possono essere classificati approssimativamente in tre categorie:

1. Metodi delle classi (CM);
2. Metodi Monte Carlo (MCM);
3. Metodo dei momenti (MOM);

A differenza dei metodi delle classi e Monte Carlo che richedono un alto costo computazionale per raggiungere un livello di accuratezza accettabile, il metodo dei momenti fornisce una buona accuratezza con una bassa spesa computazionale.
Con l'utilizzo di questo metodo nasce però un problema noto come 'problema della chiusura' dal momento che, come evidenziato da Buffo et al. (2012), non è sempre possibile scrivere le equazioni principali in termini dei momenti. Per superare tale ostacolo sono stati proposti diversi metodi numerici di chiusura, tra cui il metodo proposto da McGraw (1997) basato su una formula di quadratura (QMOM).
La nuova classe di metodi consiste nella ricostruzione della NDF come la somma di funzioni di base (ad esempio Delta di Dirac) e le equazioni dei momenti sono risolte calcolando il termine sorgente attraverso una quadratura gaussiana.
Il vantaggio legato al metodo QMOM risiede nel fatto che esso è molto adatto ad essere accoppiato con solvers di fluidodinamica computazionale e risulta estremamente accurato anche con un basso numero di nodi come dimostrato negli studi di Marchisio et al. (2003) e Marchisio e Fox (2005). Per queste ragioni tale metodo è stato adottato per la risoluzione del bilancio di popolazione.
Il problema della chiusura (ridotto al seguente integrale) viene risolto con il QMOM con una formula d'interpolazione:

$$I = \int n(\xi)f(\xi)d\xi \approx \sum_{i=1}^{N} f(\xi_i)\, w_i$$

Dove w_i rappresenta i pesi, ξ_i rappresenta i nodi della formula d'interpolazione, N è il numero di nodi, mentre dall'altra parte, $n(\xi)$ è la NDF non nota, ξ è la generica coordinata interna (come la dimensione delle bolle) e $d\xi$ è l'intervallo d'integrazione.
Questo schema numerico, che permette di risolvere l'integrale, è costruito partendo dai momenti trasportati della NDF, dal momento che i suoi momenti sono i soli ad essere noti e la quadratura gaussiana rappresenta questo tipo di schema (Marchisio and Fox, 2013).
È noto che una formula di quadratura di ordine N possa essere calcolata dai suoi primi $2N$ momenti ed è noto anche il fatto che il QMOM è estremamente accurato anche con un numero di nodi molto basso; perciò vari studi hanno adottato N=3, tracciando i primi sei momenti della distribuzione della dimensione delle bolle. Dunque in questi casi è necessario risolvere sei equazioni addizionali dei momenti per la fase gas:

$$\frac{\partial}{\partial t}(\rho_g m_k) + \nabla \cdot (\rho_g m_k \boldsymbol{u}_g) = \rho_g S_{mk}$$

Dove ρ_g è la densità della fase gas, u_g è la velocità media della fase gas, è m_k il momento di ordine k della BSD e rappresenta il termine sorgente normalizzato per il k-esimo momento legato ai fenomeni di rottura e coalescenza.
Il generico momento di ordine k della BSD è definito come:

$$m_k = \int_0^{\infty} n(L) L^k \, dL \approx \sum_{i=1}^{N=3} w_i L_i^k$$

In particolare, i momenti di basso ordine della distribuzione della dimensione delle bolle corrispondono a specifiche proprietà della distribuzione, come riassunto nella seguente tabella:

Momento di ordine k-esimo	Proprietà fisica della distribuzione
Momento di ordine zero	Numero totale di bolle per unità di volume
Momento di prim'ordine	Lunghezza totale
Momento di second'ordine	Legato all'area superficiale
Momento di terz'ordine	Legato al livello di gas

Tabella 1 significato dei momenti di basso ordine della distribuzione della dimensione delle bolle

Il momento può essere ulteriormente normalizzato rispetto alla frazione volumica locale della fase gas:

$$m_k = \mu_k \alpha_g$$

Perciò l'equazione di trasporto dei momenti diventa:

$$\frac{\partial}{\partial t}(\rho_g \alpha_g \mu_k) + \nabla \cdot (\rho_g \alpha_g \mu_k \boldsymbol{u}_g) = \rho_g S_{mk}$$

Il termine sorgente che appare nell'equazione di trasporto mostrata qui sopra può essere calcolato usando una formula di quadratura, rendendo perciò necessario l'utilizzo del noto algoritmo di inversione per determinare gli N nodi e pesi dai 2N momenti della BSD (Gemello, 2018).
Ulteriori dettagli teorici riguardanti il metodo adottato sono forniti nei capitoli successivi o nel libro scritto da Marchisio and Fox (2013).
Come detto precedentemente, il QMOM con numero di nodi pari a N può essere calcolato tracciando i primi 2N momenti della BSD; contrariamente a ciò, questo lavoro si basa sull'idea che sia sufficiente un solo diametro medio delle bolle per descrivere l'effetto della rottura e della coalescenza. Infatti, l'ipotesi è quella di risolvere solo l'equazione di trasporto del momento di second' ordine per calcolare il diametro medio di Sauter ($d_{32} = m_3/m_2$) dal momento che m_3 è legato al gas holdup che è noto.
In questo caso per il calcolo si considera un unico diametro L (i=j=1) e il termine sorgente presenta la seguente forma:

$$S_{m2} = \frac{6\alpha}{\pi L}\left[\frac{3\alpha}{\pi L^3} h(L,L)\left(2^{\frac{2}{3}} - 2\right) + g(L)\left(\frac{b^2}{L^2} - 1\right)\right]$$

Quest' ipotesi semplificativa è accettabile dal momento che la differenza di predizione del diametro di Sauter con il metodo QMOM e con l'approccio semplificato è minore del 2.5%. Inoltre, il vantaggio di questo approccio risiede nella velocità e semplicità con cui è possibile calcolare il diametro di Sauter: è necessario risolvere una sola equazione invece che cinque come richiesto con il metodo QMOM (nel caso più comune in cui si adotta un numero di nodi pari a tre).

0.5 Simulazioni CFD: Set-up

Dopo la validazione dei modelli di coalescenza e rottura, il bilancio di popolazione è stato implementato in simulazioni di fluidodinamica computazionale. L'inserimento del bilancio di popolazione in simulazioni di fluidodinamica computazionale ha lo scopo di rendere le previsioni dell'idrodinamica più precise.
In questo lavoro è stato simulato un reattore agitato in 3D tramite ANSYS Fluent 2019 R2, in transitorio e a diverse condizioni operative: la velocità di agitazione è stata variata tra 600 e 997 rpm, mentre la velocità superficiale del gas tra 0.00415 m/s e 0.0415 m/s.
Le principali caratteristiche relative alla geometria e mesh adottate sono riportate nella seguente tabella:

Tipo turbina	Rushton a sei pale
Diametro apparecchiatura (T) [m]	0.1
Diametro turbina (D) [m]	T/3
Locazione della turbina dal fondo (h_D) [m]	T/3
Diametro sparger [m]	0.06
Sezione simulata	1/6 dell'intera apparecchiatura
Periodicità	Lungo la direzione azimutale
Griglia [num. di celle]	621200
Condizione in uscita	Degassing
Metodi di discretizzazione spaziale	
Gradiente	Least squares cell based
Pressione	PRESTO!
Scalare, quantità di moto, energia cinetica turbolenta, dissipation rate turbolenta	Second order upwind
Frazione volumica	First order upwind
Residui	1e-9 per lo scalare 1e-6 per tutte le altre quantità
Fattori di sotto-rilassamento	
Densità, forze e viscosità turbolenta	1
Frazione volumica	0.5
Energia cinetica turbolenta, dissipation rate turbolenta	0.8
Scalare	0.1
Dimensione del passo temporale	0.001 (considerando il numero di CFL)

Tabella 2 principali caratteristiche relative alla geometria e mesh usate nelle simulazioni di CFD

Per quanto riguarda invece i modelli usati, per descrivere la fluidodinamica è stato adottato l'approccio Eulero-Eulero la cui teoria si basa sull'idea che entrambe le fasi continua e dispersa sono considerate come compenetranti e continue, introducendo così il concetto di frazione volumica di ogni fase poichè il volume occupato da una fase non può essere occupato dall'altra. Per ogni fase vengono risolte le

equazioni di conservazione: l'equazione di continuità e quella di Navier-stokes dove assumiamo che il trasferimento di massa tra le fasi sia assente.
L'approccio Eulero-Eulero include tre diversi modelli multifase; tra questi è stato adottato il modello Euleriano il quale risolve un set di N equazioni di conservazione per ogni fase, mentre la pressione è condivisa. Il vantaggio di questo modello consiste nel fatto che il numero di fasi secondarie è limitato solamente dalla capacità della memoria o da problemi di convergenza.
Essendo il sistema considerato gas-liquido con la fase gassosa dispersa in quella liquida, esistono delle forze interfacciali tra le due fasi, tra cui quella controllante in questo tipo di sistemi è la forza di drag. Generalmente, le altre forze vengono trascurate.
Per semplificare il codice di CFD, in questo lavoro sono state considerate la forza di drag, la forza di massa virtuale con un coefficiente costante e la forza di dispersione turbolenta, mentre le restanti forze sono state trascurate.
La forza di drag rappresenta la resistenza causata dalla risalita delle bolle lungo il reattore attraverso il liquido e influenza sia la velocità relativa delle bolle che la frazione volumica della fase gassosa.
Diverse leggi che descrivono la forza di drag sono state proposte e ANSYS Fluent ne mette a disposizione alcune. In questo lavoro è stata adottata la correlazione proposta da Grace et al. (1978) che generalmente viene usata per flussi bifase di tipo gas-liquido.
Dal momento che le simulazioni sono state condotte in regime turbolento, è stato adottato il metodo RANS (Reynolds-averaged Navier-Stokes equations) e, in particolare, per adattare i modelli di turbolenza a due-equazioni a sistemi multifase, è stato utilizzato il modello di turbolenza dispersa. Quest'ultimo modello calcola l'equazione della turbolenza solo per la fase continua e considera il fenomeno della turbolenza come indotto dalla fase dispersa. Inoltre, tra i modelli di turbolenza disponibili, è stato adottato il realizable k-ε che ha mostrato stabilità e costi computazionali accettabili per il sistema in questione.
Infine, per tenere in considerazione le parti rotanti (agitatore e pale) del reattore, si è adottato il sistema di riferimento noto come moving reference frame (MRF). L'apparecchiatura è stata perciò divisa in due zone: la zona in movimento, comprendente anche parte del fluido che circonda l'elemento che ruota, e nota come rotore e quella statica nota come statore.

0.6 Risultati principali

Come detto precedentemente, diversi kernels di rottura e coalescenza sono stati testati con l'approccio modellistico zero-dimensionale.
I test condotti sui due sistemi hanno mostrato come alcuni modelli fossero completamente incapaci di riprodurre i dati sperimentali: infatti prevedendo un effetto errato della velocità superficiale del gas o dell'energia di dissipazione, si ottengono bolle di dimensione troppo grande o troppo piccola.
In altri casi i modelli hanno dimostrato di avere il giusto andamento della curva che rappresenta il diametro di Sauter al variare della velocità superficiale, ma di essere nell'intervallo di magnitudine sbagliato. Perciò è stato quindi introdotto un fattore correttivo in grado di centrare i risultati rispetto al diametro medio sperimentale:

$$corr_{factor}^{n} = corr_{factor}^{n-1} * \frac{L_{exp}}{L_{0D}}$$

Esso rappresenta il prodotto tra il valore ottenuto con l'iterazione precedente e il rapporto tra il valore medio sperimentale e quello medio calcolato con l'approccio 0D. Tale costante moltiplicativa viene moltiplicata al kernel di coalescenza in quanto inizialmente si è pensato che il problema di una scorretta previsione dei risultati fosse legato ad una valutazione errata del fenomeno della coalescenza e che perciò andasse ponderato.

Dopo aver applicato il fattore correttivo, alcuni modelli hanno comunque mostrato disaccordo con i risultati sperimentali, mentre altri hanno fornito una previsione esatta della dimensione delle bolle, in accordo con l'andamento osservato sperimentalmente.
Per quanto riguarda il caso della colonna a bolle contenente aria-acqua, questo studio ha confermato che il set di kernels proposto da Gemello (2018) è in grado di riprodurre i risultati sperimentali con un errore di approssimazione del 5%. Lo studio ha anche evidenziato come un altro set (il modello di Laakkonen et al., 2006 per la rottura, quello di Prince e Blanch, 1990 per la frequenza di collisione e per l'efficienza di coalescenza il modello di Chesters, 1991) sia altrettanto capace di fornire una buona predizione con un errore del 7%. Il grafico seguente riporta i risultati citati (Fig.4):

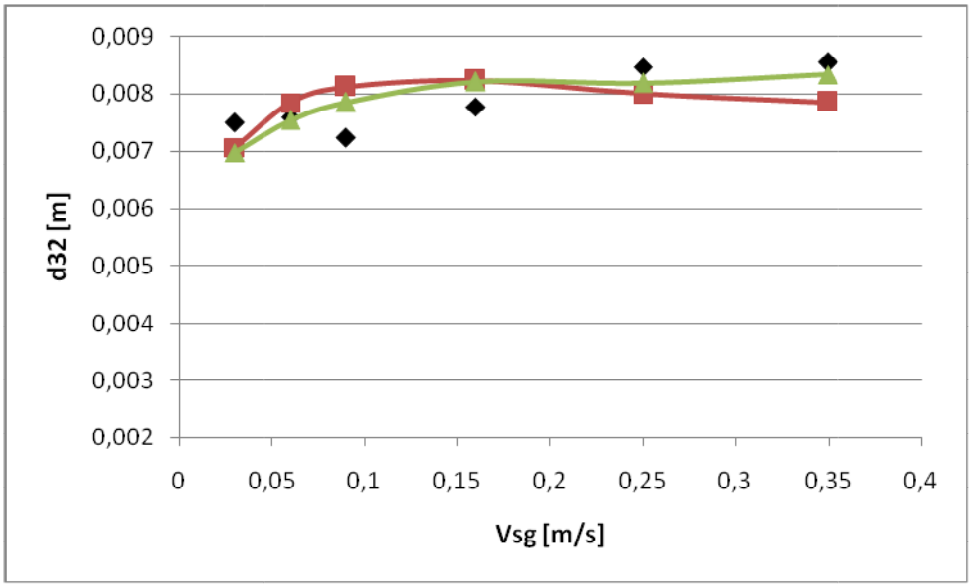

Figura 4 grafico riportante il diametro di Sauter al variare della velocità superficiale del gas misurato sperimentalmente (♦), fornito dal set di modelli proposto da Gemello (2018) (▲) e dal set di modelli costituito da il modello di Laakkonen et al. (2006) per la rottura, quello di Prince e Blanch (1990) per la frequenza di collisione e per l'efficienza di coalescenza il modello di Chesters (1991) (■)

Anche per il reattore agitato, è stato possibile trovare un set di modelli (il modello di Laakkonen et al., 2006 per la rottura, quello di Prince e Blanch, 1990 per la frequenza di collisione e per l'efficienza di coalescenza il modello di Coulaloglou e Tavlarides, 1977) in accordo con i dati sperimentali raccolti da Cappello (2019) (errore medio del 5%).
Per quanto riguarda invece lo studio di sistemi più complessi, di tipo organico, l'idea era di testare la capacità dei modelli trovati per il caso semplice di aria-acqua di predirre la dimensione delle bolle anche nel caso di sistemi caratterizzati da proprietà fisiche complesse. Purtroppo i modelli hanno fallito nella previsione, evidenziando la necessità di uno studio più approfondito, magari di tipo sperimentale in cui i fenomeni di coalescenza e di rottura vengono analizzati separatamente.
L'approccio 0D è stato inoltre adottatto per testare varie combinazioni di modelli e trovare quali fossero in grado di descrivere contemporaneamente entrambi i sistemi contenenti aria-acqua all'interno. Il set composto dal modello di Laakkonen et al. (2006) per la rottura, quello di Prince e Blanch (1990) per la frequenza di collisione e il modello di Chesters (1991) per l'efficienza di coalescenza, ha dimostato di descrivere in modo relativamente buono la dimensione delle bolle sia all'interno della colonna a bolle che del reattore agitato con un errore medio di approssimazione di circa 13%.
Nella tabella seguente vengono riassunti i set di kernels che sono stati validati per i diversi sistemi:

Sistema	Colonna a bolle	Reattore agitato	Entrambi i sistemi

Modello di rottura	Laakkonen et al. (2006)	Laakkonen et al. (2006)	Laakkonen et al. (2006)
Frequenza di collisione	Prince e Blanch (1990)	Prince e Blanch (1990)	Prince e Blanch (1990)
Efficienza di coalescenza	Lehr et al. (2002)	Coulaloglou e Tavlarides (1977)	Chesters (1991)

Tabella 3 Riepilogo dei modelli capaci di riprodurre la dimensione delle bolle nei diversi sistemi

Lo studio del reattore agitato è poi proseguito implementando il set di kernels validato in precedenza in simulazioni di fluidodinamica computazionale. Il bilancio di popolazione è stato infatti introdotto attraverso una UDF e sono state lanciate varie simulazioni a diverse condizioni operative. Questo lavoro preliminare (One-way coupling) ha consentito di verificare che il diametro medio di Sauter previsto con l'approccio 0D fosse in accordo con quello previsto attraverso queste simulazioni di fluidodinamica computazionale e, di conseguenza, in accordo con i dati sperimentali. I risultati ottenuti con i due diversi approcci si discostano al massimo del 15% confermando che l'approccio 0D è un ottimo metodo per testare velocemente diversi modelli. Di seguito sono riportati e messi a confronto, sulla sinistra, una rappresentazione schematica del reattore agitato simulato sperimentalmente da Cappello (2019) con i valori locali del diametro di Sauter in diverse zone dell'apparecchiatura e, sulla destra, il corrispondente contour plot del reattore simulato tramite ANSYS FLUENT alle stesse condizioni operative (Fig.5). Tale confronto evidenza quindi ciò che è stato precedentemente detto: i risultati sono in accordo tra loro, discostando al massimo del 15%.

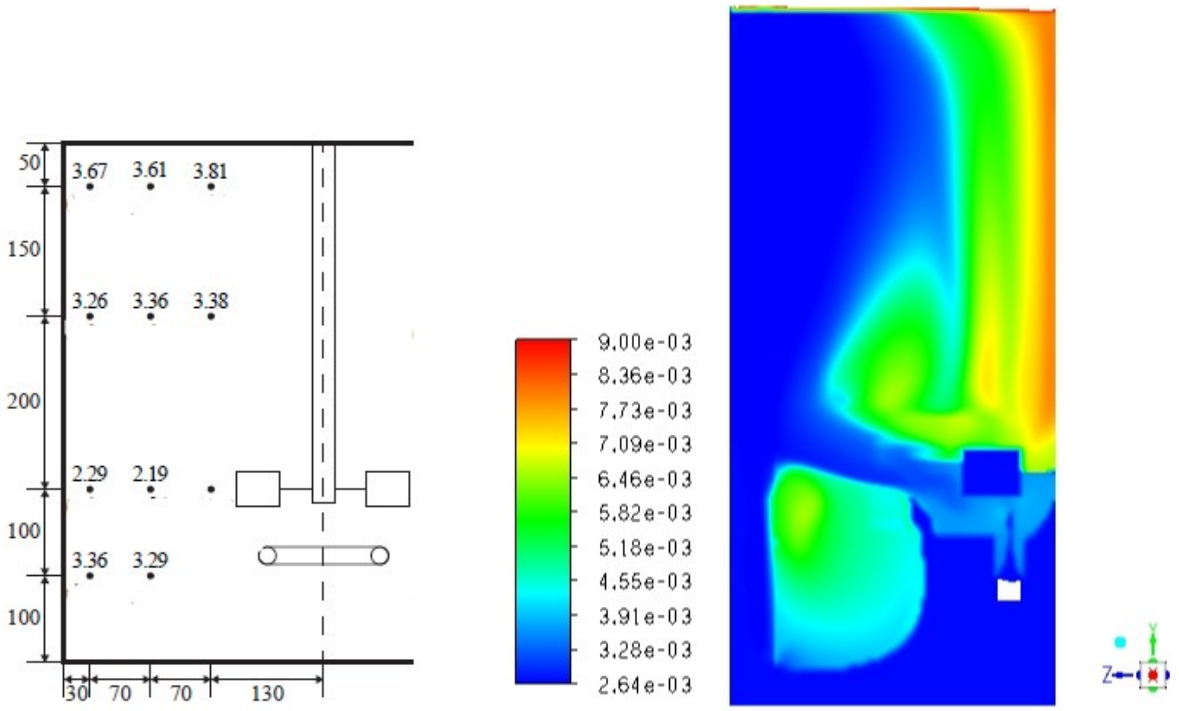

Figura 5 confronto del valore locale del diametro di Sauter misurato sperimentalmente da Cappello (2019) (da cui è stata presa l'immagine sulla sinistra) e il contour plot di tale grandezza simulata tramite ANSYS Fluent alle stesse condizioni operative

Infine è stata testata l'influenza del valore di inizializzazione del diametro delle bolle sul risultato finale ed è stato osservato come questo parametro abbia solo un debole effetto. Perciò per le simulazioni si è deciso di adottare come diametro iniziale il valore medio sperimentale.

0.7 Conclusioni e prospettive future

Lo scopo di questa tesi consisteva nello studio di modelli di rottura e coalescenza capaci di prevedere la dimensione delle bolle in varie condizioni operative, in sistemi gas-liquido quali colonne a bolle e reattori agitati.
Grazie all'utilizzo di un approccio 0D è stato possibile testare i diversi modelli e individuare quelli in grado di riprodurre i risultati ottenuti sperimentalmente sia per il caso delle colonne a bolle che dei reattori agitati. Lo studio fatto per la colonna a bolle studiata già in precedenza da Gemello (2018) ha confermato la validità del modello proposto dall'autore e ha permesso di trovare un altro set di kernels come valida alternativa. È stato inoltre possibile individuare un set di modelli capace di descrivere il diamero medio di Sauter all'interno di un reattore agitato e, infine, è stato trovato un set che si trova in accordo con entrambi i dati sperimentali della colonna a bolle e del reattore agitato. La ricerca di un set di kernels capace di descrivere contemporaneamente i due sistemi si basa sull'idea di trovare delle correlazioni che abbiano ampia validità di applicazione in termini di condizioni operative, geometria e tipo di sistemi.
È stato inoltre possibile dimostrare come l'approccio 0D sia in grado di fornire una predizione della dimensione delle bolle che è in stretto accordo con i valori ottenuti dalle simulazioni One-way coupling di CFD. Questo risultato è importante in quanto conferma come tale approccio sia un utile strumento per il test e la validazione di modelli in breve tempo e con costi computazionali veramente bassi, superando l'ostacolo legato alle simulazioni di CFD che richiedono un tempo estremamente elevato per confrontare i vari modelli tra loro e fornire i risutati.
Purtoppo però lo studio fatto su sistemi con proprietà fisiche più complesse non ha fornito risultati soddisfacenti e ha sottolineato la necessità di uno studio più approfondito per riuscire a comprendere i risultati ottenuti, magari focalizzandosi sugli effetti della reologia per simulare più accuratamente i bioreattori.
Un'altra prospettiva futura in merito a questo lavoro consiste nel proseguire lo studio facendo delle simulazioni di CFD dove si tenga conto non solo dell'influenza della fase continua su quella dispersa, ma anche viceversa (Two-way coupling) in modo da avere una previsione più accurata delle proprietà idrodinamiche e poter valutare il trasferimento di massa all'interno del sistema.

1.Introduction

This thesis represents the work done during the internship carried out in Institut Français du Petrol-Energie Nouvelle (IFPEN) based in Solaize, Lyon (France), in the Department of Process conception and modeling (July-December 2019).

The main aim of this work is the use of a 0D approach for the study of models of coalescence and breakage in gas-liquid systems such as bubble columns and stirred tank reactors, under the heterogeneous flow regime, providing suitable models to predict correctly the bubble size for different operating conditions. Besides, the use of these kernels in more complex systems is investigated.

To reach this goal the experimental data carried out in air-water systems by Gemello (2018) for bubble columns and Cappello (2019) for stirred tank reactors have been used, since they allow the validation of bubble breakage and coalescence kernels. On the other side, the experiments carried out by Chaumat et al. (2007) and IFP-NT Vonner Roesler(2018) have been used for the investigation of these models in organic liquids.

In particular, this experimental database is useful to decouple breakage and coalescence phenomena.

Hence, to achieve the aim of the work, a preliminary work has been done by carrying out 0D simulations with VBA in order to test several models and then these models have been implemented in three-dimensional transient Eulerian-Eulerian CFD simulations with ANSYS Fluent.

Sets of kernels have been carried out which provides an accurate bubble size prediction in different operating conditions for stirred tank reactors and bubble columns.

The importance of finding models capable of carrying out good prediction of the bubble size is due to the fact that in dispersed gas-liquid systems, the bubble size distribution influences the phase structure and interphase force, which, in turn, determine the multiphase hydrodynamics such as spatial profiles of gas holdup, velocities of the phases and mixing and mass-transfer behaviors. In particular, the Population Balance Model is (PBM), which considers breakage and coalescence phenomena as source terms, is an effective method to simulate the bubble size distribution (BSD).

The structure of the work is presented below:

In chapter 1 a general introduction of the objective of the thesis and a brief description of the work done during the internship have been presented.

In chapter 2 a literature review has been presented that explains which is the work done previously by different authors and why it is important to consider the coupling of Population Balance model and CFD simulations to predicts bubble size properly.

In chapter 3 both the bubble columns and stirred tanks reactors hydrodynamics have been described in order to provide a general background that is necessary to understand the topic and the work done in this internship.

In chapter 4 it has been summarized the general setup and operating conditions adopted by Gemello (2018),Cappello (2019) and the other authors to obtain the experimental data that have been used in this thesis.

In the former part of chapter 5 the concepts of Population Balance Model (PBM) and Quadrature Method of Moments have been introduced in order to explain the theory which this work has been based on. Besides, the approach used and the results obtained from the 0D simulations have been showed and discussed.

In the latter part of chapter 5 the work done with CFD code has been presented and discussed, introducing the CFD-PBM coupling adopted in this part of the work. Besides a general description of the geometry, mesh and setup adopted for these simulations has been provided.

In chapter 6 the main conclusions and the limits of this work have been reported and some perspectives have been suggested for future works.

2.Literature review

Gas–liquid systems are encountered in many industrial processes. Stirred tanks, bubble columns, air loop reactors are very common gas–liquid contactors and they recover an important role in different chemical engineering fields. In particular, in these kind of systems many important chemical reactions are usually carried out (e.g., oxidations, hydrogenations, alkylation, hydroformylation, chlorination, Fischer-Tropsch synthesis, etc.)(Buffo et al., 2016).

However, their hydrodynamics are really complex, strongly dependent on geometry, the flow parameters of both phases (e.g. volumetric flow rate, flow regimes, etc.) and their fluid properties (e.g. gas holdup distribution, gas-liquid mass transfer coefficient, etc.). Furthermore, multiphase flows are characterized by the existence of interfaces between the phases and the discontinuity of associated properties (Liao et Lucas, 2010).

In particular, for stirred tanks, their hydrodynamics are very complicated because of the interactions between flow around the rotating impellers and stationary baffles as stated by (Sommerfeld et Decker, 2004).

These reactors generally work under turbulent conditions, in order to provide good gas dispersions and consequently enhance the mass and energy transfer rates, allowing for the reduction of the overall costs (Buffo et al., 2016).

Therefore, the simulation of gas-liquid systems under these turbulent conditions plays a key role and it gets necessary in order to have a better understanding of the complexity of the multi-phase flow of the stirred tanks and bubble columns, and then better controlling of corresponding processes.

Thanks to the increasing computational power, Computational Fluid Dynamics (CFD) is playing a more and more important role in their investigation, design, and scale-up, and it is going to replace traditional methods based on semi-empirical correlations.

These correlations are used to estimate the flow regime and corresponding flow characteristics. The problem linked to this kind of approach is the limited range of validity: only geometries and operating conditions similar to those experimentally observed make it possible to use these empirical correlations. However, measured experimental data are not completely abandoned because they are needed to validate the developed computational model (in fact, in literature it is widespread to combine experimental results with CFD modeling to validate the latter);moreover, CFD analysis is used in the chemical industry to direct and optimize the experimental campaign, rather than replace it (Petitti et al., 2010).

In the past, the study of stirred tanks by mean of CFD modeling was only focused on single-phase liquid flow; then works on multiphase systems started to appear in the literature and nowadays this field has been continuously expanding and the predictive capabilities of CFD modeling are getting better and better.

Several authors focused their works on CFD modeling of stirred tanks; however, among the early works about gas-liquid tanks, some of the proposed modelling methods are based on simplifying hypothesis which represent limitation on the predictive capability of the models themselves.

For example, in the work of Morud and Hjertager (1996), experimentally determined impeller boundary conditions have been used instead of simulating directly the impeller, thus limited predictive capability of the model is obtained.

Other studies done by Harvey and Greaves (1982) and Placek et al. (1986) performed steady state simulations in two-dimensional grids under the assumption of axial-symmetry and impeller and baffles were represented by source/sink of momentum; but in this way the inability to solve three-dimensional structures has been highlighted.

To overcome this issues, three-dimensional simulations were carried out by (Brucato et al., 1989, 1990; Gosman et al., 1992; Ranade et al., 1989, 1990), still modeling the stirrer as a momentum source or by means of boundary condition methods.
Then, Tabor et al. (1996) and other authors developed the Sliding-Mesh (SM) and the Multiple Reference Frame (MRF) approaches, showing that the MFR approach is less computationally intensive and gives a good accuracy.
To describe the multiphase systems various model are available: the main approaches are the Eulerian-Lagrangian and the Eulerian-Eulerian approach.
The Euler-Lagrange point-particle model calculates the continuous phase using the average Navier-Stokes equations and the motion of each bubbles is calculated separately. Due to the high numerical effort to calculate the motion of a large number of bubbles, this method is applied restrictively to low volume fractions of gas phase and low number densities of the bubbles (Lehr et al., 2002). Furthermore, this method has the difficulties of considering the forces on the deformable bubbles and breakup and coalescence of the bubbles, even if it has the advantage of a clear physical description (Wang et al., 2006).
On the other side, the Euler-Euler has a numerical cost comparatively small and, in this case, both the continuous and the dispersed phases are treated as interpenetrating continuous media described by conservation equations written in fixed coordinates.
These methods have been applied to gas-liquid reactors and gave good results, so they were proved to be promising (Gosman et al., 1992).
Another important issue, deeply investigated in the recent past and still subjected to some controversy, is the treatment of turbulence (Petitti et al., 2010). Turbulence is a key element in CFD simulations since it has a main role in coalescence and break-up of bubbles and it enhances heat and mass transfer rates.
Different accurate turbulence approaches can be used for gas-liquid flows such as direct numerical simulation (DNS), large-eddy simulation (LES) or Reynolds-Averaged Navier-Stokes approach (RANS).
Several studies showed that the Reynolds-Averaged Navier-Stokes approach provides acceptable predictions: Montante et al. (2007) modeled gas-liquid dispersion in a stirred vessel by RANS-based CFD simulations. However, other authors such as Sun et al. (2006) and Wang et al. (2006) employed a k-ε turbulence model in their work without acomplete success in predicting the two-phase flow. In accordance with these results, Lane et al. (2005) stated that the turbulent dissipation rate is not well predicted by the RANS k-ε turbulence model.
Although the accuracy of this model is not so high, the RANS approach represents the only feasible way for the use on industrial problems and real geometries, because the DNS and the LES approaches have quite high computational costs even if they result in a more accurate prediction.
Many authors took also into consideration different grid refinement methods. Scargiali et al. (2007) performed steady CFD simulations of gas-liquid stirred vessel and studied the influence of grid refinement and the role played by the turbulent dispersion force, the lift force and virtual mass force on the gas holdup. The obtained results were in reasonable agreement with experiments and so the authors concluded that the grid size may significantly affect the prediction, while the effect of the analyzed forces was negligible (they played a secondary role) in determining the distribution of gas holdup.
Furthermore, it has been proved by many works in the literature (one of those is the work of Gao et al., 2016) that the grid size may influence the predictions of turbulence quantities in systems such as stirred tanks, where it is possible to notice strongly localized velocity gradients. In fact, Gao et al. (2016) simulated multiphase stirred vessels by coupling CFD and PBM and showed that the power number calculated from the torque applied to the walls stabilizes after grid refinements.

Another important aspect considered in CFD simulations is the role of the interfacial forces, several studies were done in order to clarify the contribution to the final prediction of the model by each force, especially for global properties (e.g. global gas holdup). As known, the motion of the bubbles is determined by interactions between the two phases and among the bubbles themselves. Such interactions are usually described through different interfacial forces that appear in the momentum balance equation.

According to the analysis of Khopkar et al. (2005), Scargiali et al. (2007) and Montante et al. (2007) the effect of the drag and buoyancy forces largely predominates in gas-liquid stirred tanks. So, for this reason, many authors such as (Laakkonen et al., 2006; Pettiti et al., 2010; Gimbun et al., 2009; Buffo et al., 2016) decided to not include the effect of the virtual mass, lift and turbulent dispersion force in their works.

Since buoyancy does not depend on the relative motion of bubbles with respect to liquid, its formulation is easy and depends on the local volume fraction of the gaseous phase through the definition of a mixture density (Buffo et al., 2016). On the contrary, the drag force correlation was the subject of several investigation present in literature. The correct specification of the drag force is important: the bubble slip velocity is determined by a balance between drag and buoyancy forces and, in turn, the bubble slip velocity affects local BSD, gas holdup and hence the mass transfer area.

Different models have been proposed that consider the rise of a bubble in a stagnant, therefore laminar, liquid (among those there is for example the one proposed by Scargiali et al., 2007); however this could be incorrect since in turbulent flows a bubble is subjected to turbulent eddies that causes the bubble to accelerate and decelerate continuously and also the effect of bubble crowding must be included.

For this reason, the modification of drag coefficient by turbulence has been studied in the last years and various correlations for the previously mentioned drag coefficient were proposed. Brucato et al. (1998) made measurements of particle settling velocities in turbulent flow and found that these velocities were reduced to a percentage of the value in the stagnant case. They also proposed a correlation for the drag coefficient developed for solids but still suitable for bubbles which Khopkar et al. (2005) modified for the gas-liquid stirred vessel simulation.

Other studies related specifically to gas bubbles have mainly been based on a computational approach: Lane et al. (2005) proposed a new method of calculating drag coefficient which takes into account the effect of interaction between bubbles and turbulent eddies, showing good agreement with experimental data.

Many other authors proposed their correlations for the drag coefficient such as Schiller and Nauman (1933), Ishii and Zuber (1979), Tomiyama et al. (2002) and many others.

Ishii and Zuber, 1979 proposed a drag coefficient for fluid-fluid systems dependent on the swam effect, whereas the expression of Tomiyama et al. (2002) is suitable for isolated bubble and was obtained from experiments on contaminated air-water systems.

Since the drag coefficient under dilute conditions is different from the dispersion one, the effect of bubble crowding and micro-scale turbulence were included through a bubble swarm function. Some expressions for the swarm factor were formulated in the latest years by Simmonet et al. (2007, 2008) and by Roghair et al. (2011, 2013b) not considering the effect of breakage and coalescence on BSD. Buffo et al. (2016), accounting for local bubble polydispersity through the GPBE, proposed a power-low correction based on the works of both Wen and Yu (1966) and Ishii and Zuber (1979).

Anyway, to evaluate properly the drag force and its coefficient, it is necessary to evaluate correctly the local bubble size distribution.

Early works performed on the gas–liquid stirred tanks made use of a uniform, mono-dispersed bubble size throughout the tank(e.g.Wang et al., 2006; Deen et al., 2002; Scargiali et al., 2007).

Generally, the results obtained in these studies are in fair agreement with experimental data as this assumption often represents a significant limitation to a faithful description of gas-liquid reactors which show strong inhomogeneities in the Bubble Size Distribution (BSD).
For example, Deen et al. (2002) developed a gas-liquid flow CFD model considering only drag force between the two phases and fixing both the bubble diameter and the gas-liquid dispersion level. These assumptions lead to the overestimation of mean axial gas velocities, while liquid velocities and mean radial gas velocities agreed well with experimental data.
Unfortunately, the assumption of a fixed bubble diameter represents a significant limitation to an accurate description of gas-liquid reactors since many researches showed there is a wide distribution of the bubble size within the reactor under heterogeneous regime. This simplification limits such models to the homogeneous regime because the bubble size distribution in such a condition is narrow and the bubble interaction is relatively weak. Therefore, it is important to consider in detail the local bubble behavior: in fact the bubble behavior influences the flow regime transition because the occurrence of large bubbles is the major phenomenon that causes the transition from the homogeneous to the heterogeneous regime (Wang et al., 2006).
For these reasons, authors such as Bakker (1992, 1994) started adopting a population bubble density model (BDM) by adding an equation for bubble number density, considering physical transport, break up and coalescence in a one-way coupling approach. Both overall and local predictions of gas holdup and mass transfer coefficient gave good agreement with experimental data, but the analysis was limited to few operating conditions.
In recent years, many studies coupled CFD simulations with Population Balance Model (PBM) in order to evaluate the local bubble size (Lane et al., 2002, 2005; Moilanen et al., 2008; Gimbun et al., 2009; Venneker et al., 2002).
For example, Venneker et al. (2002), in their work, presented a model able to predict local gas fraction and bubble size distributions for stirred vessel under turbulent gas dispersion, based on Population Balance Model (PBM). As the authors stated, the model predictions are encouraging to conclude that the use of population balance equations is a promising technique to study dispersed flows. In fact, they highlighted that the main advantage of using PBM in CFD simulations is that bubble-bubble interactions are explicitly considered. Therefore, compared to models with mono-dispersed bubble size, studies on mass transfer in dispersed flows can be carried out more accurately.
The advantages of the CFD-PBM coupled model, as written in the article of Wang et al. (2006), are the following:

1. combines the ability of CFD to calculate the entire flow field and the ability of the PBM to calculate the local bubble size distribution;
2. implements the PBM into the CFD framework so that bubble breakup and coalescence can be taken into account, so the CFD-PBM coupled model can determine the bubble size evolution in different flow regimes;
3. takes into account the influence of the bubble size on the interphase interaction so that the CFD-PBM coupled model has the ability to predict the flow behavior in different flow regimes;
4. predicts the local bubble size distribution and gas holdup from which the local gas–liquid interfacial area can be determined.

In the majority of the cases, satisfactory results were obtained for the local bubble size, but an adjustment of some of the empirical constants of the models has been required.
In the formulation of the BDM proper bubble breakage and coalescence kernels were not included, whereas the equations for bubble size were lumped together and expressed in terms of critical Weber number and energy dissipation rate without modelling the frequency and efficiency of both bubbles and bubble-eddy collisions.

Since the bubble breakup and coalescence models are very important for proper prediction of bubble size distributions in different flow regimes, a full Population Balance model is thus much preferable.
Several methods had been developed to solve the Population Balance Equation and there are three main groups they belong to: classes methods (CM), Monte Carlo methods (MCM) and moment methods.
The group of Classes methods contains all the methods where the space of internal coordinates is discretized. The issue of this group of methods is that it is characterized by high computational costs to obtain an acceptable accuracy, especially when the inhomogeneities of the physical space are considered.
The other group named Monte Carlo Methods is based on the solution of stochastic differential equation capable of reproducing a wide number of artificial realizations of the analyzed system (Zhao et al., 2007). In order to achieve a solution very close to the reality, a very high number of artificial realizations are used and hence resulting in high computational costs. Therefore the Monte Carlo Methods were used only for simplified cases as validation.
A good compromise between computational expense and accuracy is achieved by the method of moments. Initially was formulated by Hulburt and Katz (1964) for particulate systems.
The idea behind this method (Standard Method of Moments, SMM) is the integration of the internal coordinate and the BSD is determined through its moments which represent the scalarsthat the CFD code solves the equations of transport for. One of the advantages of SMM is that a low number of moments (equal or less than 4) is required to obtain an acceptable accuracy ,but, as stated by Marchisio et al. (2002), this method has some limitations: only size-dependent growth rate, size-independent coalescence/aggregation and breakage kernels can be treated accurately, since, for realistic processes, it is not always possible to write the governing equations in terms of the moments themselves (Buffo et al., 2012), leading to the so called «closure problem».
Several closures have been proposed to overcome this issue and, in particular, the Quadrature Method of Moments (QMOM) can be used for this aim. The QMOM is a method based on the SMM where the number density function (NDF) representing the population is assumed to be the sum of Dirac delta functions and where, through a Gaussian quadrature, the transport equations of lower-order moments can be written in terms of the lower-order moments themselves (Petitti et al., 2010).
QMOM was firstly proposed by McGraw (1997) and then validated by Marchisio et al. (2003) for break up and coalescence problems.
The advantage related to this method is that QMOM is very suitable to be coupled with CFD solvers (Marchisio et al., 2003a; Petitti et al., 2010) and it results extremely accurate even with a very low number of nodes (Marchisio et al., 2003; Marchisio and Fox, 2005). For this reason, the QMOM was firstly adopted in this work to solve the Population Balance model.

3.Gas-liquid systems hydrodynamics

3.1 Gas Holdup

Gas holdup α_g is an important parameter in this type of systems since it affects gas-liquid mass transfer within the vessel. It can be calculated as the ratio between the volume of the gas and the total volume and can be related to superficial gas velocity Vsg.

$$\alpha_g = \frac{V_g}{V_g + V_l}$$

Different authors studied this parameter and their correlations are available in the Literature.

3.2 Flow regimes in Bubble Columns

Depending on superficial gas velocity and column diameter, different flow regimes can be identified inside the vessel, such as homogeneous, transition, heterogeneous and slug flow regimes (Fig.6).

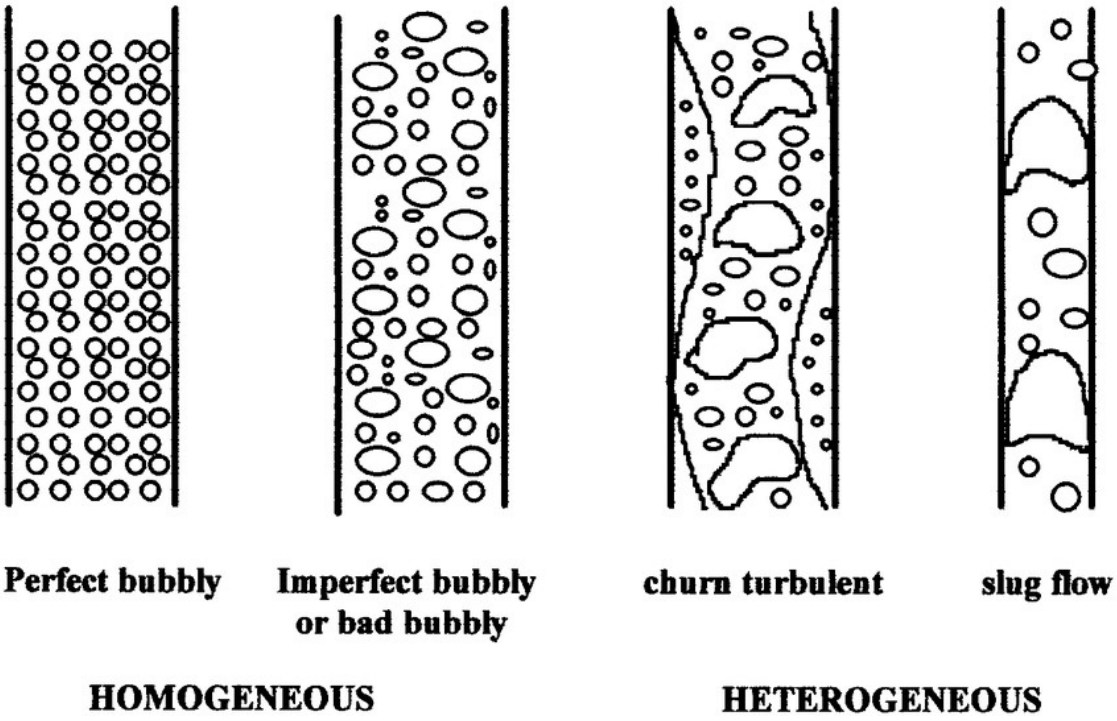

Figura 6 Different flow regimes in Bubble Columns

The homogeneous or bubbly regime occurs at low superficial gas velocities and it is characterized by bubbles of almost uniform small sizes and rise velocities. The bubble distribution is uniform and the breakage and coalescence phenomena are practically absent (weak bubble interactions). In particular, in the homogeneous regime the gas holdup increase linearly with increasing superficial gas velocity.
On the other side instead, the heterogeneous regime (or churn-turbulent regime) occurs at high superficial gas velocities. It is characterized by unsteady flow patterns and large bubbles with short residence times, leading to a slower increase in the gas holdup with the superficial gas velocity; the bubble breakage and coalescence become relevant and lead to a wide bubble size distribution. This flow regime is usually observed in large diameter columns (industrial-size).
At higher superficial gas velocity, especially with small diameter columns, it is possible to observe the slug flow regime which is characterized by huge gas bubbles that cause large pressure and liquid flow rate fluctuations.

3.3 Flow regimes in Stirred Tank Reactors

In a baffled aerated stirred tank equipped with a Rushton turbine it is possible to identify different flow patterns based on the trajectories of bubbles within the vessel. In particular the regimes are flooding, loading and fully recirculated and can be described using two dimensionless numbers (Lee and Dudukovic, 2014). These numbers are the Flow Number (Fl) and the Froude Number (Fr) and they represent respectively the ratio between the gas flow rate and the impeller driven flow rate, and the ratio between the impeller driven acceleration and gravity.

Flooding regime occurs when there is little or no gas dispersion because the energy provided by the impeller is not able to break up bubbles; thus they rise along the shaft, leading to less on no gas in the region below the impeller. Therefore the lower part of the vessel is wasted resulting in poor performance of the STR (namely loss in power consumption, low gas holdup and poor mixing within the tank).

By increasing the Fr number or decreasing the Fl number (both by increasing the impeller rotational rate), the flow regime reaches a more dispersed state and gas circulates not only in the upper part of the vessel, but also into the lower region(see Fig.7). The minimum impeller speed needed to have a complete dispersion of the gas in the liquid phase in STR is the so called N_{cd} (Yawalkar et al., 2001), below which it results in incomplete dispersion of the gas.

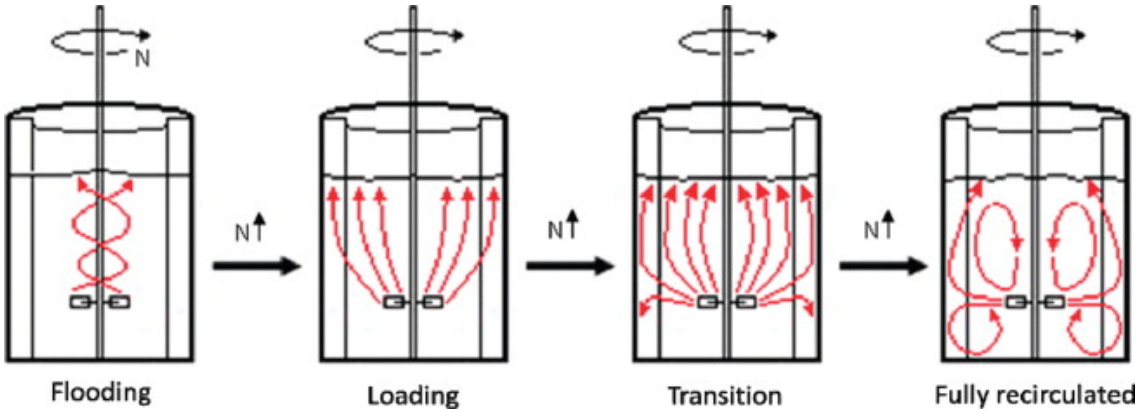

Figura 7 Different flow regimes in Stirred tanks (Mueller and Dudukovic, 2010)

3.4 Power Draw in Stirred Tank Reactors

Power input P is another import parameter for the process and mechanical design of agitated vessels. This parameter can be related to the diameter D and speed N of the impeller, the liquid phase density ρ_l and the power number Np.

$$P = \rho_l N^3 D^5 N_p$$

The power number has been calculated with the correlation of Bujalski et al. (1987) that can be expressed as following:

$$N_p = 2.5 \left(\frac{x}{D}\right)^{-0.2} \left(\frac{T}{T_0}\right)^{0.065}$$

Where x represents the thickness of the impeller, T the vessel diameter and T_0 is a reference tank diameter equal to 1 m. Hence a value of Np equal to 4.66 has been used in this work for the simulated tank.

The power draw in aerated stirred tanks ,P_g, is lowered than in ungassed system and the relative power demand (RPD) let estimate this reduction. In this work the RPD was calculated with the correlation proposed by Gabelle et al. (2011) since it is validated for a wide range of operating conditions and can be expressed as: $P_g = P \ \max\left[\left(\frac{P_g}{P}\right)_{lim}; exp\left(-15.36 {N_P}^{0.16} {Q_G}^{0.62} T^{-1.7} \left(\frac{D}{T}\right)^{0.51}\right)\right]$

4.Experimental Data

To validate bubble coalescence and breakage models it is necessary to carry out a set of data at different operating conditions. In this work, two different sets of experimental data have been used for bubble columns and stirred tank reactors, referred to air-water systems: the database obtained by Gemello (2018) have been used for the case of bubble columns, whereas the data of Cappello (2019) for stirred tank reactors.

Two different but similar objectives are linked to the use of air-water data collected for bubble columns and stirred tanks: the experimental observations in bubble columns have been used to verify the validity of the set of kernels proposed by Gemello (2018) orto find an alternative set of models able to reproduce the experimental data; whereas the data carried out by Cappello (2019) in stirred tanks have been used for the validation of one or more bubble coalescence and breakage models among the available ones in the literature, testing whether or not the 0D approach is also valid for STRs.

Besides, in this work, experimental data of more complex systems (organic) have been collected in order to investigate the ability of these models to predict the bubble size in case of complex physical properties. In particular, we used the experiments done with cyclohexane by Chaumat et al. (2007) and the ones done with hexane at different pressures by IFP-NT VonnerRoesler (2018).

A brief overview of their work will be shown in the following paragraphs.

4.1 Experimental setup of air-water bubble columns

Gemello (2018) made the experiments with air and water in a 0.4 m diameter cylindrical bubble column at atmospheric pressure, for values of superficial gas velocity that vary in the range of 0.03 m/s to 0.35 m/s. The initial liquid height (without gas) is equal to 4 diameters (H/D=4), while the total column height is about 8 diameters. The author used two different spargers in order to analyze the effect of the sparger itself on hydrodynamics and bubble dimensions, but the data used in this work are all referred to the sparger with 92 holes of 2 mm diameter.

Regarding the way to obtain the experimental data, different techniques have been used as follows:

- the difference of liquid height before and after gas injection have been used to measure the global gas volume fraction:

$$\alpha_g = 1 - \frac{H_0}{H_f}$$

- the local gas volume fraction measured by using a 1C conical mono-fiber optical probe;
- the liquid velocity by using a Pavlov tube (Forret, 2003) measuring the differential pressure between two opposite holes, with a sampling frequency of 400 Hz;
- the Sauter mean diameter by using the cross-correlation (CC) technique firstly presented by Raimundo (2015). This technique quantifies the similarity of two signals of two optical probes, analyzing them simultaneously. The time-averaged horizontal diameter of the bubbles is obtained by using the CC signal. The cross-correlation function can be calculated as follows:

$$CC = \frac{\int_0^{t_{exp}} signal_A(t) signal_B(t) dt}{t_{exp}}$$

For a more detailed explanation of these techniques, refer both to Gemello (2018) and Raimundo (2015, 2016).

4.2 Stirred tanks experimental setup

As previously mentioned, the experimental data of air-water carried out byCappello (2019) have been used in this work to validate bubble kernels in stirred tanks. Experiments were carried out in a

cylindrical glass tank with flat bottom and a diameter T=0.3 m. The height of the liquid is equal to the diameter of the vessel, corresponding to a volume V of 0.021 m^3. A single six-blade Rushton turbine with a diameter D=T/3 was placed at a distance h_D=T/3 from the bottom of the vessel and provided the agitation inside the vessel. Moreover, four equispaced rectangular baffles were located inside the tank together with a 0.06 m diameter ring sparger (located in between the impeller and the bottom) (h_s=T/5). The tank was also equipped with a sparger composed by 21 holes of 1 mm of diameter. The superficial gas velocity (Vsg) have been varied in the range of 4-40 mm/s, while the impeller speed (N) ranged between 600 and 997 rpm. The correlation proposed by Gabelle et al.(2011) was used to calculate the relative power draw (RPD):

$$\frac{P_G}{P_0} = \max\left[\left(\frac{P_G}{P_0}\right)_{lim} ;\ exp\left(-15.36\, N_P^{0.16} Q_G^{0.62} T^{-1.7} \left(\frac{D}{T}\right)^{0.51}\right)\right]$$

Where Q_G is the gas flow rate in m^3/s, $(P_G/P_0)_{lim}$ is the constant value of RPD at high gas flow rate that depends on the geometry of the impeller: a value equal to 0.33 was measured by Gabelle (2012) for the single Rushton turbine configuration. Np represents the power number calculated with the correlation of Bujalski et al. (1987):

$$N_P = 2.5 \left(\frac{x}{D}\right)^{-0.2} \left(\frac{T}{T_0}\right)^{0.065}$$

Where x is the thickness of the impeller and T_0 is a reference tank diameter equal to 1 m.
The following techniques were used by the author to obtain the experimental data:

- the Sauter mean diameter was obtained with a dual optical probe manufactured by *A2 Photonic Sensor*, France;
- the global gas holdup was obtained visually by measuring the difference in height due to the injection of the gas in the solution;
- the local gas fraction was measured by using the dual-probe in a larger tank.

The detailed explanation of these techniques is available in the article of the author himself (Cappello, 2019).

Vsg [m/s]	Gas holdup	Theoretical ε [m^2/s^3]	CFD ε [m^2/s^3]	D_{32}experimental
0.03	0.1078	0.2943	0.0684	0.007498017
0.06	0.155	0.5886	0.1324	0.00759691
0.09	0.1893	0.8829	0.2646	0.00722741
0.16	0.246	1.5696	0.5585	0.007780326
0.25	0.2886	2.4525	0.9540	0.00846781
0.35	0.3318	3.4335	1.3849	0.00854265

Tabella 4 Global holdup, turbulent dissipation rate and Sauter mean diameter for air-demineralized water bubble column (Gemello, 2018)

N [rpm]	Vsg [m/s]	Gas holdup	ε [m^2/s^3]	D32 experimental [m]
600	0,00415	0,0446	1,255	0,003566893
700	0,00415	0,0625	1,993	0,003391729
800	0,00415	0,0769	2,975	0,003467428
900	0,00415	0,0854	4,236	0,003394462
997	0,00415	0,0909	5,758	0,003453516
600	0,0083	0,0506	0,929	0,003839012
700	0,0083	0,0741	1,475	0,003795523
800	0,0083	0,0798	2,202	0,00363392
900	0,0083	0,0991	3,135	0,003794566
997	0,0083	0,1071	4,262	0,003690956
600	0,02075	0,0769	0,725419	0,004529994
700	0,02075	0,1018	1,151939	0,004446879
800	0,02075	0,1124	1,719512	0,004221442
900	0,02075	0,1304	2,448289	0,004167048
997	0,02075	0,1428	3,328286	0,004224071
600	0,0415	0,1304	0,725419	0,004788543
700	0,0415	0,1549	1,151939	0,00476799
800	0,0415	0,1713	1,719512	0,004596376
900	0,0415	0,1848	2,448289	0,00455262
997	0,0415	0,1892	3,328286	0,004588518

Tabella 5 Global holdup, turbulent dissipation rate and Sauter mean diameter for air-demineralized water stirred tank (Cappello, 2019)

For further experimental data see the thesis of the authors themselves (Gemello, 2018; Cappello, 2019).

4.3 Overview of organic liquids' setup

The experiments carried out by Chaumat et al. (2007) in a bubble column filled with cyclohexane, together with the experimental data collected by IFP-NT Vonner Roesler (2018) for hexane at different pressures, have been considered in this work in order to have a view of the use of the analyzed breakage and coalescence models in complex systems.

The following table summarizes the main setup used in the experiments done by Chaumat et al. (2007)(Tab.6) and the data obtained (Tab.7):

Type of vessel	Stainless steel bubble column
Column height [m]	1.6
Column diameter [m]	0.2
Gas sparger	Two concentric perforated torus
Sparger diameter [m]	0.11 & 0.16 with orifice size 0.0001
Gas outlet	Top of the column
Superficial gas velocity [m/s]	0.12 – 0.3

Tabella 6 Experimental setup of nitrogen-cyclohexane bubble column (Chaumat, 2007)

Vsg [m/s]	Gas holdup	Theoretical ε $[m^2/s^3]$	D_{32}experimental
0.032	0.1298	0.3139	0.00475003
0.076	0.2004	0.7456	0.00589175
0.105	0.23	1.03005	0.00630549

Tabella 7 Global holdup, turbulent dissipation rate and Sauter mean diameter for nitrogen-cyclohexane bubble column (Chaumat, 2007)

5.Methodology

As previously mentioned, the main aim of this work is the study of models of coalescence and breakage in gas-liquid systems such as bubble columns and stirred tank reactors, using a 0D approach for the screening and providing suitable models that can predict correctly the bubble size for different operating conditions. In order to reach this goal, a preliminary work has been done by carrying out 0D simulations with VBA in order to test several models and then these models have been implemented in three-dimensional transient Eulerian-Eulerian CFD code (ANSYS Fluent)by using a User-Defined Function (UDF).

5.1 I Part: Modelling work

In order to obtain good prediction of bubble size the Population Balance Model was adopted which is based on the breakage and coalescence phenomena. This zero-dimensional (0D) method has been adopted in order to screen several models in few time, overcoming the issue related to the use of normal three-dimensional transient CFD simulations, which require an extremely high time to carry out many simulations for different operating conditions and thus getting the screening of many models unfeasible.

In the 0D simulations, the continuous and dispersed phases are assumed to be perfectly mixed and also spatial homogeneity has been assumed, leading to very low computational costs (Buffo et al., 2016): in particular, in these simulations a simplified version of the Quadrature method of moments (QMOM) was adopted in order to solve the PBM and test several breakage and coalescence models.

Then, thanks to the experimental database carried out by Gemello (2018) and Cappello (2019), it has been possible to validate sets of kernels capable of predicting correctly the bubble size for a wide range of operating conditions in stirred tanks reactors and bubble columns.

5.1.1 Population Balance Model (PBM)

In dispersed gas-liquid systems, the bubble size distribution (BSD) plays an important role in the phase structure and the interphase forces, which, in turn, determine the multiphase hydrodynamic behaviors, including the spatial profiles of the gas fraction, gas and liquid velocities, and mixing and mass-transfer behaviors. For this reason, it is necessary to consider these influences to get accurate predictions in many different conditions and it is therefore necessary to couple it with the computational fluid dynamics (CFD) simulation. The population balance model (PBM) is an effective method to simulate the bubble size distribution. The PBM was first formulated for chemical engineering purposes by Hulburt and Katz (1964) and has been revealed as a very promising tool from both academic and industrial researches because the size distribution of the dispersed phase can be described by it, in a wide variety of particulate processes (Ramkrishna and Mahoney, 2002).

Before starting with the description of the Population balance equation it is important to say something briefly about another important aspect related to the PBM: the Number-density functions (NDF).

When using an Eulerian approach, the disperse phase is generally described by an NDF. The NDF identifies the entire population of the disperse phase and, in particular, it describes how the population is distributed over the properties of interest inside an infinitesimal control volume (the computational domain), at any instant.

By considering a population of bubbles within an infinitesimal control volume located at the physical point $x=(x_1, x_2, x_3)$ of measure $dx=dx_1\ dx_2\ dx_3$ and the internal-coordinate vector $\xi=(\xi_1, \xi_2,\ldots, \xi_M)$. the NDF $n_\xi(t, x, \xi)$ represents the expected number of entities in the infinitesimal control volume at each instant.

Hence the NDF is an average quantity of the disperse phase.

The quantity $n_\xi(\xi)d\xi$ represents the number density of disperse entities contained in the phase-space volume $d\xi$ and centered at ξ per unit physical volume (Marchisio and Fox, 2013).
Since Ω_ξ represents the internal-coordinate vector, it is possible to integrate the NDF over all its possible values resulting in the total number concentration N(t,x):

$$N = m_{\xi,0} = \int_{\Omega\xi} n_\xi(\xi)d\xi$$

N(t,x) is the total number of entities per unit volume located at time t and at point x, corresponding to the moment of order zero of the density function. In general the kth moment of the NDF can be defined as:

$$m_{\xi,k} = \int_{\Omega\xi} \xi_1^{k1} \dots \xi_M^{kM} n_\xi(\xi)d\xi$$

Where $k=(k_1,\dots, k_M)$ with respect to each of the components of ξ (Marchisio and Fox, 2013).
Now it is possible to consider the evolution of the NDF in time, phase space and physical space. The PBE (population balance equation) is a simple continuity statement written in terms of the NDF and it can be derived as a balance for bubbles in some fixed sub region of computational domain (Ramkrishna, 2000). The advection velocity is assumed to be equal to the local fluid velocity in the continuous phase or directly derivable from this variable. The PBE counts the bubbles belonging to a specific finite volume defined both in physical-space and phase-space. Due to different reasons such as movement of the bubbles in physical space, their velocities, continuous processes and discrete events, the number of elements inside the considered volume changes resulting in the equation showed below (Marchisio and Fox, 2013):

$$\frac{\partial}{\partial t}\left(\int_{\Omega x} dx \int_{\Omega\xi} d\xi\, n_\xi\right) + \int_{\Omega\xi} d\xi \int_{\partial\Omega x} (n_\xi \boldsymbol{u}) \cdot dA_x + \int_{\Omega x} dx \int_{\partial\Omega\xi} (n_\xi \dot{\xi}') \cdot dA_\xi = \int_{\Omega x} dx \int_{\Omega\xi} d\xi\, S_\xi$$

Where **u** is the velocity vector of the bubbles and ξ' is the rate off change of the generic internal coordinate for the bubbles, Ω_x is the finite control volume in physical space, Ω_ξ is the one in phase space and S_ξ takes into account the discrete events (e.g. collision between bubbles, leading to coalescence or breakage and nucleation phenomena).
If the Reynolds-Gauss theorem is applied and in order to be satisfied for any possible control volumes Ω_x and Ω_ξ the following relation must be satisfied:

$$\frac{\partial n_\xi}{\partial t} + \frac{\partial}{\partial x} \cdot (\boldsymbol{u} n_\xi) + \frac{\partial}{\partial \xi} \cdot (\dot{\xi}' n_\xi) = S_\xi$$

Initial conditions for the starting time and boundary conditions for physical and phase space are coupled with the equation above which can be solved through either analytical solutions (available only for few cases) or numerical methods. For a detailed explanation, see Marchisio and Fox (2013).
When the population of bubbles is described by just one internal coordinate (e.g. bubble size L), the PBE is called univariate, whereas it is said to be multivariate when more internal coordinates are needed.
Furthermore, if the bubbles are characterized by their own velocity distribution (namely when part of the internal coordinate vector is equal to the bubble-velocity vector), the PBE becomes the GPBE (generalized population-balance equation) that includes bubble velocity as an internal variable.
The final form of the GPBE is (Marchisio and Fox, 2013):

$$\frac{\partial n_\xi}{\partial t} + \frac{\partial}{\partial x} \cdot (\boldsymbol{u} n_\xi) + \frac{\partial}{\partial \boldsymbol{u}} \cdot (\boldsymbol{u}' n_\xi) + \frac{\partial}{\partial \xi} \cdot (\dot{\xi}' n_\xi) = S_\xi$$

Where **u'** is the continuous rate of change of bubble velocity (i.e. the acceleration) or the force per unit mass acting on the bubbles (e.g. gravity, drag and all the other interfacial forces). The right-hand side S_ξ is the discontinuous jump term that takes into account discontinuous changes in the bubble momentum such as collisions between particles.
If we consider a PBE with only bubble size as the internal coordinate as it is done in this work, the NDF is $n_L(t, x, L)$ and the PBE results in:

$$\frac{\partial n_L}{\partial t} + \frac{\partial}{\partial x} \cdot (\boldsymbol{u} n_L) + \frac{\partial}{\partial L} \cdot (G_L n_L) = S(L)$$

Where G_L represents the continuous rate of change of particle length and S(L) denotes discrete events (for instance it takes into account coalescence and breakage). The bubble velocity is considered as known.
In the case of a population of bubbles that can be described by using only the bubble size as internal coordinate, the kth moment of the length-based NDF can be defined as

$$m_{L,k} = \int_0^\infty n_L(L) L^k dL$$

By applying this moment to the equation above:

$$\frac{\partial m_{L,k}}{\partial t} + \frac{\partial}{\partial x} \cdot \left(\boldsymbol{u}_{L,k} m_{L,k}\right) = k G_{L,k-1} m_{L,k-1} + S_{mk}$$

Where the average rate of change of the kth moment is:

$$G_{L,k} = \frac{\int_0^\infty G_L n_L(L) L^k dL}{\int_0^\infty n_L(L) L^k dL}$$

The growth term will be neglected in this work since the mass transfer in not included.
$\mathbf{u}_{L,k}$ is the average velocity of the kth moment and can be represented as:

$$\boldsymbol{u}_{L,k} = \frac{\int_0^\infty \boldsymbol{u}_L n_L(L) L^k dL}{\int_0^\infty n_L(L) L^k dL}$$

And the source term is:

$$S_{mk} = \int_0^\infty S_L L^k dL$$

This term represents the source term due to discontinuous events and is an unclosed term that depends strongly on the system that is considered. Many closures are available in the literature for the case of gas-liquid systems.
As stated in Marchisio and Fox (2013), this term can be divided into three classes: zero-order processes, in which the rates of the events depend only on the continuous phase (e.g. nucleation); first-order processes, where each event rate depends only on the interaction between continuous phase and an element of disperse phase (e.g. breakage) and second-order processes, where the interactions includes the continuous phase and two elements of the disperse phase. Higher-order processes are usually neglected as interactions among three or more dispersed elements are rare.

5.1.1.1 Source terms of PBM

The source terms represent the right-side of the Population Balance equation. Since the mass transfer is neglected in this work, only breakage and coalescence are considered and hence the source term can be written as the summation of the terms due to breakage and coalescence, where each phenomenon

contributes with two terms: death and birth. In general, the birth terms are summed up, while the coalescence terms are subtracted (Petitti et al., 2010). The terms appearing in the source term are the following:

- Birth term due to breakage, B^B;
- Birth term due to coalescence, B^C;
- Death term due to breakage, D^B;
- Death term due to coalescence, D^C.

Through the phenomenon of breakage there is the formation of daughter bubbles and the birth term can be written as:

$$B^B(L) = \int_L^\infty \beta(L,L')g(L')n_L(L')dL'$$

Where g(L) is the breakage kernel for a bubble L and β(L,L') is the daughter distribution function for a daughter bubble L formed by the breakage of the mother bubble L'.

While, when the coalescence phenomenon occurs, it causes the formation of a new bubble due to the death of two smaller bubbles that collapse together. Therefore, the birth and death terms due to coalescence are, respectively:

$$B^C(L) = \frac{L^2}{2}\int_0^L \frac{h\left((L^3+\lambda^3)^{\frac{1}{3}},\lambda\right)}{(L^3-\lambda^3)^{\frac{2}{3}}} n_L\left((L^3+\lambda^3)^{\frac{1}{3}}\right) n_L(\lambda)d\lambda$$

$$D^C(L) = \int_0^\infty h(L,\lambda)n_L(L)n_L(L)d\lambda$$

Where h(L,L') is the coalescence kernel related to two bubbles of size L and L'.

During the breakage phenomenon, the formation of daughter bubbles is caused by the breakage of a mother bubble, leading to the death term:

$$D^B(L) = g(L)n_L(L)$$

By summing up the birth terms and subtracting the death terms, the explicit form of the source term results in:

$$S(L) = \frac{L^2}{2}\int_0^L \frac{h\left((L^3+\lambda^3)^{\frac{1}{3}},\lambda\right)}{(L^3-\lambda^3)^{\frac{2}{3}}} n_L\left((L^3+\lambda^3)^{\frac{1}{3}}\right) n_L(\lambda)d\lambda - \int_0^\infty h(L,\lambda)n_L(L)n_L(L)d\lambda + \int_L^\infty \beta(L,L')g(L')n_L(L')dL' - g(L)n_L(L)$$

5.1.1.2 Breakage and coalescence kernels

The source terms appearing on the right-hand side of the transport equation include only the breakage and coalescence phenomena since mass-transfer and other phenomena are neglected in this work.

Many bubble coalescence and breakup models have been proposed and are available in the literature as reported in the next paragraphs and in the literature. Comparing several typical bubble coalescence and breakup models, Wang et al. (2005) and other authors showed that different bubble coalescence and breakup models have a distinct influence on the prediction ability of the bubble size distribution by the PBM and, in particular, Wang et al. (2005) showed how, by using proper bubble coalescence and breakup models, the bubble size distribution and regime transition can be well predicted, thus pointing out the importance to take into account the right bubble coalescence and breakup kernels.

Breakage kernels and daughter distribution function

Bubble breakup is determined by the hydrodynamic of the surrounding liquid and the interfacial interactions since gas-liquid flows are characterized by the existence of interfaces between the phases. In particular, the breakup mechanism can be summed up as balance between external stresses on one side and surface stresses of the bubble and viscous stresses on the other side. The former ones come from the continuous phase which attempt to destroy the bubble, while the latter ones restore its form.
As reported in the work of Liao and Lucas (2009), it is possible to divide the breakup mechanism into four categories such as:

1. Breakup due to turbulent fluctuation and collision;
2. Breakup due to viscous shear stress;
3. Breakup due to shearing-off process;
4. Breakup due to interfacial instability.

Breakage due to turbulent fluctuation and collision

Under turbulent conditions, the main reasons of bubble breakup are the turbulent pressure fluctuations along the surface and bubble-eddy collisions. Due to these phenomena, the bubble starts deforming and stretching until it fragments into two or more daughter bubbles. For breakup due to turbulent fluctuations, this mechanism is described through a balance between dynamic pressure difference around the particle acting externally τ_i and its surface stress τ_s (viscous stresses are neglected). The bubble breaks up only depending on the deformation level (namely the Weber number We= τ_i/τ_s) (Liao and Lucas, 2009).
Liao and Lucas (2009) did a further classification about the criterion for breakup based on cases found in the literature:

a. Turbulent kinetic energy of the bubble greater than a critical value;
b. Velocity fluctuation around the bubble surface greater than a critical value;
c. Turbulent kinetic energy of the hitting eddy greater than a critical value;
d. Inertial force of the hitting eddy greater than the interfacial force of the smallest daughter bubble;
e. Combination of the criterion c. and d.

The first model was proposed by Coulaloglou and Tavlarides (1977),referring to the turbulent nature of the liquid-liquid dispersion. The theory under this model states that the drop oscillates anddeforms due to local pressure fluctuations, but it will break only if its kinetic energy Ed is greater than its surface energy Ec. Then their breakup expression results in the following form:

$$g(L) = c_1 L^{-2/3} \varepsilon^{1/3} exp\left[-\frac{c_2 \sigma}{\rho_g \varepsilon^{2/3} L^{5/3}}\right]$$

Accounting for the "damping" effect of droplets on the local turbulent magnitudes at high holdup fractions, the original expression becomes:

$$g(L) = c_1 L^{-2/3} \frac{\varepsilon^{1/3}}{1+\alpha_g} exp\left[-\frac{c_2 \sigma (1+\alpha_g)^2}{\rho_g \varepsilon^{2/3} L^{5/3}}\right]$$

where c1=0.00481 and c2=0.08 are numerical constants.
Prince and Blanch (1990) highlighted in their work that, in the case of gas-liquid systems, the model of Coulaloglou and Tavlarides (1977) predicts very small bubble size compared to the experimental values and the cause could be found in the fact that the density of the gas phase, used for the case of gas-liquid systems, is much lower than that of liquid phase for the liquid-liquid dispersions. Hence, the density of the continuous phase is used in the case of gas-liquid flows (Lasheras et al., 2002):

$$g(L) = c_1 L^{-2/3} \frac{\varepsilon^{1/3}}{1+\alpha_g} exp\left[-\frac{c_2 \sigma (1+\alpha_g)^2}{\rho_l \varepsilon^{2/3} L^{5/3}}\right]$$

Alopaesus et al. (2002a,b) modified the model of Narsimhan and Gupta (1979) by adding to the eddy-drop collision frequency a dependency on turbulent dissipation rate, considering the viscous force of fluid inside the drop (previously neglected).

$$g(L) = c_3 \varepsilon^{1/3} erfc\left(\sqrt{c_4 \frac{\sigma}{\rho_l \varepsilon^{2/3} L^{5/3}} + c_5 \frac{\mu_g}{\sqrt{\rho_g \rho_l} \varepsilon^{1/3} L^{4/3}}}\right)$$

Laakkonen et al. (2006) replaced the viscosity of the dispersed phase with the one of the continuous phase with the idea that viscous stresses that resist the breakage depend on the liquid viscosity surrounding the bubble and not the gas viscosity. So the expression results in:

$$g(L) = c_3 \varepsilon^{1/3} erfc\left(\sqrt{c_4 \frac{\sigma}{\rho_l \varepsilon^{2/3} L^{5/3}} + c_5 \frac{\mu_l}{\sqrt{\rho_g \rho_l} \varepsilon^{1/3} L^{4/3}}}\right)$$

where the constants present in the expression are equal to 4, 0.04 and 0.01, respectively. In particular, the last two constants are obtained by the turbulence theory and are independent from the studied system.

Lehr et al. (2002) proposed a breakup frequency correlation with the idea that the kinetic energy of the eddy overcomes a critical energy which is obtained from the force balance equation (Liao and Lucas, 2009). The authors provided also an analytical solution for the breakup frequency and the daughter size distribution, by expressing the integral as a sum of incomplete gamma-functions.

$$g(L) = 0.5 \frac{L^{5/3} \varepsilon^{19/15} \rho_f^{7/5}}{\sigma^{7/5}} exp\left(-\frac{\sqrt{2}\sigma^{9/5}}{L^3 \rho_f^{9/5} \varepsilon^{6/5}}\right)$$

Since most of the analyzed cases are under turbulent flow, the turbulent fluctuation is assumed arbitrarily as the dominant breakup mechanism and the effects of viscous force, relative velocity and interfacial instability on breakup phenomena are usually neglected.

Breakage due to viscous shear force

A velocity gradient around the interface is caused by viscous shear forces in the continuous phase; thus the bubble will deform and after will breakup. One of the reason of shear stresses could be the wake effect, namely when a trailing bubble has its larger part outside a wake region and due to elongation, bubble surface indentation and necking, the splitting of the wake boundary occurs.

The breakup mechanism that in this case can be expressed as a balance between external viscous stresses τ_v and surface tension forces τ_s, where the force balance is usually expressed in terms of Capillary number ($Ca = \tau_v/\tau_s$). When the capillary number is greater than the critical value, the bubble starts becoming unstable and breakups.

Breakage due to shearing-off process

This additional phenomena occurs when the bubble size starts to increase. In particular the shearing-off process is based on a number of small particles sheared-off from a large one (erosive breakage). However, in the case of air-water flow, it has been showed that the interfacial viscous shear force is negligible due to the low viscosity of water and the shearing-off process is caused by the gas velocity profile inside the cap bubble.

Breakage due to interfacial instability

Even if all the above mechanism depend on the flow dynamic characteristics in the continuous phase, it has been proved that, in the absence of a net flow in the continuous phase, the breakup can be caused by interfacial instabilities when the bubble volume exceeds the maximum stable limit (Liao and Lucas, 2009).

Based on this idea, Carrica and Clausse (1993) proposed an empirical correlation:

$$g(L) = g^* \frac{(L - L_{cr})^m}{(L - L_{cr})^m + L_{cr}^m}$$

With L_{cr} (critical bubble diameter) sets equal to 27 mm, whereas g* and m represent model parameters and are equal to 100 s^{-1} and 6, respectively.

Daughter distribution function

In this work the daughter distribution function of Laakkonen et al. (2006) is the only one considered. In particular, it is based on a common statistical distribution function, the β-function:

$$\beta(L,\lambda) = N_f \left(9 + \frac{33}{2}C + 9C^2 + \frac{3}{2}C^3\right)\left(\frac{L^2}{\lambda^3}\right)\left(\frac{L^3}{\lambda^3}\right)^2\left(1 - \frac{L^3}{\lambda^3}\right)^C$$

Where L and λ are the size of the daughter bubble and the size of the mother bubble, respectively.
N_f is obtained by imposing the following conditions:

$$\int_0^\infty \beta(L,\lambda)dL = N_f$$

$$\int_0^\infty \beta(L,\lambda)L^3 dL = \lambda^3$$

Resulting in: $N_f = \frac{4}{3} + \frac{C}{3}$

Therefore the final expression for the daughter distribution function with C assumed equal to 2 (namely binary breakage) is: $\beta(L,\lambda) = 180\left(\frac{L^2}{\lambda^3}\right)\left(\frac{L^3}{\lambda^3}\right)^2\left(1 - \frac{L^3}{\lambda^3}\right)^2$

Coalescence kernels

The other phenomenon responsible for the evolution of bubble sizes in multiphase flows is coalescence. It involves not only bubbles-surrounding fluid interactions, but also bubble-bubble interactions due to external flow or body forces that bring bubbles together. For this reason, the phenomenon of coalescence is considered more complex then breakage.
Physical models calculated the coalescence kernel by multiplying the collision frequency with the coalescence efficiency. The concept of efficiency (or probability) is introduced since not all collisions lead to coalescence.

$$h(L_1, L_2) = h_0(L_1, L_2)\, \lambda(L_1, L_2)$$

where $h_0(L_1, L_2)$ represents the collision frequency and $\lambda(L_1, L_2)$ the coalescence efficiency.
In general, all the theories proposed for the coalescence process are based on the idea that there must be contact and collision as a premise.
The collision between bubbles is usually caused by their relative velocity and the relative motion, in turbulent flows, may occur due to at least five sources as evidenced by Liao and Lucas (2010):

1. Motion induced by turbulent fluctuations in the surrounding continuous phase;
2. Motion induced by mean-velocity gradients in the flow;
3. Different bubble rise velocities induced by buoyancy or body forces;
4. Bubble capture in an eddy;
5. Wake-entrainment.

Regarding coalescence efficiency, three theories have been proposed:

1. Film-drainage model;
2. Energy model;
3. Critical approach velocity model.

Collision frequency

The collision frequency is normally considered as the sum of the rates due to the different mechanisms that were cited above. Depending on the value of superficial gas velocity, the importance of the different mechanisms vary and some of them become negligible: for example, at medium superficial gas velocities, only the first mechanism is considered, while the others are often neglected; at high superficial gas velocities, the wake-entertainment becomes important since very large bubbles have been formed (Wang et al., 2006).

Collisions due to turbulent fluctuations

The fluctuation of turbulent velocity of the surrounding liquid can cause bubbles collisions. An analogy to the random movement of gas molecules in the kinetic gas theory is done by Kennard (1938) for bubbles in a turbulent flow. In particular, the author considered the collision frequency as the effective volume swept by the moving bubble per unit time: $h_0(L_1, L_2) = S_{12} u_{rel}$

where S_{12} is the collision-sectional area of the colliding bubbles: $S_{12} = \frac{\pi}{4}(L_1 + L_2)^2$

The relative approach velocity u_{rel} is determined by assuming that the colliding bubbles take the velocity of an equal-sized eddy as considered by several authors (Coulaloglou and Tavlarides, 1977; Prince and Blanch, 1990; and others). In particular, a too small eddy has not enough energy to affect bubble motion, whereas very large eddies transport bubbles without effect on the relative motion.

Hence, the relative velocity can be calculated as: $u_{rel} = \sqrt{u_{t1}^2 + u_{t2}^2}$

Where u_{t1} is the velocity of eddy with size L_1 and it can be calculated applying classical turbulent theories and assuming the inertial subrange of isotropic turbulence: $u_{t1} = \sqrt{2}\varepsilon^{1/3} L_1^{1/3}$

The final expression for collision frequency has the following form:

$$h_0(L_1, L_2) = \sqrt{2}\frac{\pi}{4}(L_1 + L_2)^2 \varepsilon^{1/3} \sqrt{L_1^{2/3} + L_2^{2/3}}$$

Prince and Blanch modified the model above: $h_0(L_1, L_2) = C'_1 (L_1 + L_2)^2 \varepsilon^{1/3} \sqrt{L_1^{2/3} + L_2^{2/3}}$

Where the value of the constant C_1' depends on the studied system and it is in the range of values between 0.28 and 1.11.

In more recent works, some corrective factors are proposed; among these modifications, the effect of size ratio between bubbles and eddies has been taken into account (in the previous model equal-sized bubbles and eddies are considered).

As stated by Colin et al. (2004), turbulent collisions occur only in these cases:

$$u_{rel} = \begin{cases} \frac{C_t}{\sqrt{1.61}} \left(\varepsilon \frac{L_1 + L_2}{2}\right)^{1/3} \\ \frac{C_t}{\sqrt{1.61}} (\varepsilon L_1)^{1/3} \end{cases}$$

The first expression is valid when L2<Lt, while the second one when $L_2 > L_t$.

The idea in these cases is that the main mechanism that describes the relative bubble motion is the mean shear of the flow since, if the bubbles are larger than the integral length scale of turbulence, turbulent eddies are not efficient to move the bubbles.

Another corrective factor is γ, which considers the reduction of free space for bubble movement leading to an increase in the collision frequency. As reported by Liao and Lucas (2010), different expression are available in literature for γ proposed by Wu et al. (1998), Hibiki and Ishii (2000), Lehr et al. (2002) and Wang et al. (2005b).

The last corrective factor that is multiplied to the collision frequency expression is represented by π. It is a decreasing factor that takes into account the fact that when the distance between bubbles is larger than the turbulent path length, the collision should not be counted.
In particular, Wu et al. (1998) derived an expression for π, assuming the average size of eddies to be on the same order of the bubble size: $\Pi = \left[1 - exp\left(-C_{\Pi}\frac{\alpha_{max}^{1/3}\alpha_g^{1/3}}{\alpha_{max}^{1/3}-\alpha_g^{1/3}}\right)\right]$
For the case of air-water system, C=3 as it depends on the fluid's properties.
Wang et al. (2005a, b) proposed another correlation for the π factor: $\Pi = exp\left[-\left(\frac{L_{bt,12}}{h_{bt,12}}\right)^6\right]$
Where $l_{bt,12}$ represents the mean relative turbulent path length scale of bubbles with size L_1 and L_2.
The final expression of the collision frequency proposed by Wang et al. (2005b) is:

$$h_0(L_1, L_2) = C'_2\Pi\gamma(L_1 + L_2)^2\varepsilon^{1/3}\sqrt{L_1^{2/3} + L_2^{2/3}}$$

Collisions due to velocity gradient

In general, the mechanism of turbulence is considered the main one among all the different collision theories and all the others are normally neglected.
Anyway, Friedlander (1977) pointed out that collisions in a uniform, laminar shear flow could be caused by velocity gradients.

Collisions due to the capture in a turbulent-eddy

If the bubble size is much smaller than the one of the energy dissipating eddies in a turbulent flow, the collision will be mainly caused by viscous forces, leading to bubble velocities very close to liquid velocity. Hence, the local shear of the flow in turbulent eddies will be the only mean to determine the collision frequency (Chesters, 1991): $h_0(L_1, L_2) = \frac{0.618}{8}(L_1 + L_2)^3\sqrt{\frac{\varepsilon}{\nu}}$
This mechanism of collision becomes important just in the case of very small bubbles.

Buoyancy-induced collisions

Prince and Blanch (1990) stated that the difference in rise velocities of bubbles with different size could lead to bubble collisions.

Collisions due to wake-entrainment

The word wake refers to the liquid that is inevitably carried up and accelerated behind the bubbles during their free-rise through the liquid (Liao and Lucas, 2010). In the wake region, the bubbles can collide with the preceding one (Bilicki and Kestin, 1987).
This mechanism is important for large cap bubbles in fluids sufficiently viscous with laminar wakes (Liao and Lucas, 2010).
Many other models are available in the literature and are presented in the paper of Liao and Lucas (2010).

Coalescence efficiency

Energy model

This model is based on the idea that increasing the energy of collision leads to an increasing number of collisions that result in immediate coalescence. Sovova (1981) developed a model based on this theory where the interfacial energy of bubbles is proportional to the interfacial tension and bubble surface area, whereas the kinetic collision energy is considered proportional to the average volume and relative velocity of two colliding bubbles (Liao and Lucas, 2010).

Critical approach velocity model

Contrarily to what was said regarding the energy model, Doubliez (1991) and Duineveld (1994) demonstrated that gentle collisions lead to more efficient coalescence. Therefore, Lehr et al. (2002) and Lehr and Mewes (1999) proposed a new expression for the coalescence efficiency where the relative velocity u_{rel} can be determined experimentally and, for air-water systems is equal to 0.08 m/s. This correlation shows a problem because, when the relative velocity tends to zero, the coalescence efficiency tends to infinity (obviously erroneous). For this reason the right correlation is the following:$\lambda(L_1, L_2) = min\left(\frac{u_{crit}}{u_{rel}}, 1\right)$

Film drainage model

This model determines the coalescence efficiency by considering two characteristic time scales: the drainage time and the contact time. The former one represents the time required by the liquid film between two particles to drain out, while the latter one is the time that the bubbles stay in contact after the collision. Therefore Coulaloglou (1975) proposed the following expression for the coalescence efficiency: $\lambda(L_1, L_2) = \exp\left(-\frac{t_D}{t_C}\right)$

Based on the rigidity of bubbles and the mobility of the interfaces, it is possible to identifies different regimes of drainage (e.g. non-deformable bubbles or deformable with mobile, partially mobile or fully mobile interfaces).

We talk about rigid bubbles when the viscosity is very high or when the bubble size is smaller than 1 mm (Liao and Lucas, 2010).

However, the assumption of rigid bubbles is only reasonable for very small bubbles, but in most of the applications large bubbles exist and the bubbles are considered deformable during the collision (Simon, 2004).

In the literature it is possible to find several correlations for the coalescence efficiency and, among them, the most common is the one of Coulaloglou and Tavlarides (1977) for the immobile interfaces:

$$\lambda(L_1, L_2) = exp\left[-C''_1 \frac{\mu_l \rho_l \varepsilon}{\sigma^2}\left(\frac{L_1 L_2}{L_1 + L_2}\right)^4\right]$$

In order to consider high gas volume fraction effects, the authors modified the previous expression as:

$$\lambda(L_1, L_2) = exp\left[-C''_1 \frac{\mu_l \rho_l \varepsilon}{\sigma^2\left(1 + \alpha_g\right)^3}\left(\frac{L_1 L_2}{L_1 + L_2}\right)^4\right]$$

Other authors such as Chesters (1991) proposed different expressions for both inertial and viscous collisions and also for different types of interfaces. For example, in the case of inertial collisions with immobile interfaces:$\lambda(L_1, L_2) = \exp\left(-\sqrt{\frac{\rho_l \varepsilon^{2/3} L^{5/3}}{4\sigma}}\right)$

While for viscous collision and immobile interfaces: $\lambda(L_1, L_2) = exp\left(-C"_3 \frac{9\mu_l \rho_l \varepsilon L_{eq}^4}{128\sigma^2 h_f^2}\right)$

Many other correlations have been proposed, available in the literature and collected in the review of Liao and Lucas (2010).

In this work, different set of kernels have been considered in order to find the best one that fitted the experimental results. Of course, it was not possible to analyze all the available models in the literature, hence just few models for breakage and coalescence have been taken into account and these models are those shown above.

5.1.2 Methods to solve PBM

Very different methods have been proposed and developed in order to solve the Population Balance Model. The available approaches can be roughly classified into three groups:

1. Class (or sectional) methods (CM);
2. Monte Carlo methods (MCM);
3. Method of Moments (MOM).

5.1.2.1 Class (or sectional) methods (CM)

Class methods (CM) are based on the discretization of internal coordinates so that the GPBE becomes a set of macroscopic balances (Marchisio and Fox, 2013).
Several authors developed these methods and widely applied for univariate PBE case, whereas in the case of bivariate and multivariate PBE their application is still difficult as it is based on a combination of both the reduction of the number of variables and the extension of univariate methods (Marchisio and Fox, 2013).
With CM, the NDF is often approximated in each interval of the discretized internal coordinate by a low-order polynomial (often a polynomial of order zero) and hence they results in zeroth-order methods. Whereas higher-order methods approximate the NDF in the interval of interest with basic functions (e.g. Dirac Delta functions)or higher-order polynomials.
The so called finite-element methods (FEM) are also part of this group since the sub-domain in which the internal coordinate is discretized is also known as finite element. The FEM are very powerful, but their high computational costs don't let them to be applicable for inhomogeneous systems.
Another class of methods is composed by the ones based on a finite-volume discretization for phase space: their advantage is that is very easy to extend these methods to multivariate PBE (as possible to see in Gunawan et al., 2004), but the drawback is always the high computational cost for the solution of a inhomogeneous PBE.

5.1.2.2 Monte Carlo methods (MCM)

Monte Carlo methods are based on the solution of a set of stochastic differential equations capable of reproducing a finite number of artificial realization of the system behavior (Zhao et al., 2007).

These methods have the inconvenient that they can be used only for simplified simulations since they require very high computational costs when coupled with CFD simulations.

5.1.2.3 Method of moments (MOM)

Hulburt and Katz (1964) introduced the MOM for particulate systems: in their work, the authors solved the PBM in terms of the moments of the NDF and derived the corresponding transport equations.
A closure problem arise from the use of this approach since, for realistic processes, it is not always possible to write the governing equations in terms of the moments themselves (Buffo et al., 2012). To solve this issue, different numerical closures have been proposed (McGraw, 1997 and others).
In particular, the closure proposed by McGraw (1997) is based on a quadrature formula, thus generating a new class of methods: Quadrature-based moment methods (QBMM).
The QBMM consist in the reconstruction of the NDF as a summation of basic functions (e.g. Dirac Delta functions) and, through a Gaussian quadrature, the transport equations of lower-order moments can be written in terms of the lower-order moments themselves (Petitti et al., 2010).

The advantage related to this method is that QMOM is very suitable to be coupled with CFD solvers (Marchisio et al., 2003a; Petitti et al., 2010; Buffo et al, 2012) and it results extremely accurate even with a very low number of nodes (Marchisio et al., 2003; Marchisio and Fox, 2005). For this reason, the QMOM was firstly adopted in this work to solve the Population Balance model.

Quadrature Method of Moments (QMOM)

Quadrature-based moment methods overcome the closure problem by using a quadrature approximation. In particular, the heart of QBMM is the Gaussian quadrature whose theory applies exactly for univariate distribution.

In the univariate case, the weights and nodes are used in the quadrature method of moments (QMOM) to solve moment-transport equations (Marchisio and Fox, 2013).

Using QMOM, the moment equations are solved by estimating the source terms through the quadrature approximation that is determined from a full set of moments by using moment-inversion algorithms (Gemello, 2018).

The way to solve the closure problem (reduced to the following integral) that appears in the QMOM is represented by an interpolation formula:

$$I = \int n(\xi) f(\xi) d\xi \approx \sum_{i=1}^{N} f(\xi_i)\, w_i$$

Wherew_i represents the weights and ξ_i the nodes of the interpolation formula and N is the number of nodes used for the interpolation, while, on the other side, n(ξ) is the unknown NDF, ξ is a generic internal coordinate (e.g. bubble size) and dξ is the integration interval.

Therefore, the closure problem can be overcome by solving the above integral through a numerical scheme capable of calculating the integral itselfand this numerical scheme must be constructed starting from the transported moments of the NDF, since only its moments are known and transported.The Gaussian quadrature represent this kind of scheme (Marchisio and Fox, 2013).

Normally the accuracy of an interpolation formula is quantified by its degree of accuracy. Thanks to this aspect, it is clear why quadrature approximation are so interesting: with the same number of equally spaced nodes,an interpolation formula has a degree of accuracy of N-1, whileGaussian quadrature has a degree of accuracy of 2N-1.

It is possible to say that a Gaussian quadrature is an interpolation formula whose nodes are the roots of the polynomial $P_N(\xi)$ orthogonal to the weight function n(ξ), thus this implies that the quadratureapproximation of order N is exact if the integrand f(ξ) is a polynomial of order equal or less than 2N-1.

A quadrature of order N can be calculated from the first 2N moments. Of course, if the number of nodes is higher, the accuracy increases, but also the computational costs. For this reason and since the QMOM resulted extremely accurate even with a very low number of nodes (Marchisio et al., 2003b; Marchisio and Fox, 2005), a preliminary part of this work was done with QMOM by using N=3 and calculated by tracking the first six moments (from m_0 to m_5) of the BSD. The same number of nodes was also adopted in the works of Petitti et al. (2010) and Gemello (2018).

So, it is necessary to solve six additional moment equations for the gas phase:

$$\frac{\partial}{\partial t}(\rho_g m_k) + \nabla \cdot (\rho_g m_k \boldsymbol{u}_g) = \rho_g S_{mk}$$

Where ρ_g is the gas phase density, u_g is the gas phase average velocity, m_k is the moment of order k of the BSD and S_{mk} is the normalized source term for the k^{th} moment due to breakage and coalescence.

The generic k^{th} moment of the BSD is defined as follow:

$$m_k = \int_0^{\infty} n(L) L^k \, dL \approx \sum_{i=1}^{N=3} w_i L_i^k$$

Where n(L) is the unknown BSD or NDF and w_i and L^k_i represent, respectively, the weights and the nodes of the quadrature approximation.

In order to simplify the implementation, the moment can be normalized with respect to the local bubble volume fraction:

$$m_k = \mu_k \alpha_g$$

Then the moment transport equation becomes:

$$\frac{\partial}{\partial t}(\rho_g \alpha_g \mu_k) + \nabla \cdot (\rho_g \alpha_g \mu_k \boldsymbol{u}_g) = \rho_g S_{mk}$$

The source term that appears in the transport equation above can be calculated by using weights and nodes. For this reason is necessary to use the so called inversion algorithm in order to determine the N quadrature nodes and weights from the 2N moments of the BSD (Gemello, 2018).

As explained by Marchisio and Fox (2013), the roots of the orthogonal polynomials are the nodes of Gaussian quadrature approximation, hence it is possible to employ the recursive relationship for the orthogonal polynomials in order to determine the N weights and nodes.

A set of orthogonal polynomials {Pα(L)} has a recurrence formula relating any three consecutive polynomials as follows:

$$P_{\alpha+1}(L) = (L - a_\alpha) P_\alpha(L) - b_\alpha P_{\alpha-1}(L)$$

With α equal to 0,1,…,N and initial conditions $P_{-1}(L)=0$ and $P_0(L)=1$ and where the coefficients a_α and b_α results in:

$$a_\alpha = \frac{\int L \, n(L) P_\alpha(L) P_\alpha(L) dL}{\int n(L) P_\alpha(L) P_\alpha(L) dL}$$

$$b_\alpha = \frac{\int n(L) P_\alpha(L) P_\alpha(L) dL}{\int n(L) P_{\alpha-1}(L) P_{\alpha-1}(L) dL}$$

Therefore, it is really important to know the recursion coefficients because they allow to compute the zeros of the orthogonal polynomials and with them the quadrature rule.

The recursive formula generates a sequence of orthogonal polynomials with respect to the weight function in the interval of integration.

Knowing the orthogonal polynomials, one can calculate the coefficients a_α and $b_\alpha$and, if the polynomials are explicitly represented and the multiplications are carried out term by term, these coefficient can be written on terms of the moments: for example, it is possible to calculate the coefficients a0, a1 and b1 as showed below:

$$a_0 = \frac{m_1}{m_0}$$

$$a_1 = \frac{m_3 m_0^2 + m_1^3 - 2 m_2 m_1 m_0}{m_2 m_0 + m_1^2 - 2 m_1^2 m_0}$$

$$b_1 = \frac{m_2 m_0 + m_1^2 - 2 m_1^2 m_0}{m_0^2}$$

The sequence of recursive relationship can be interpreted in a matrix form with the roots of $P_N(L)$ (namely the nodes of quadrature approximation) that are the eigenvalues of the tri-diagonal matrix below:

$$L\begin{bmatrix} P_0(L) \\ P_1(L) \\ P_2(L) \\ \vdots \\ P_{N-2}(L) \\ P_{N-1}(L) \end{bmatrix} = \begin{bmatrix} a_0 & 1 & & & & \\ b_1 & a_1 & 1 & & & \\ & b_2 & a_2 & 1 & & \\ & & \ddots & \ddots & \ddots & \\ & & & b_{N-2} & a_{N-2} & 1 \\ & & & & b_{N-1} & a_{N-1} \end{bmatrix} \begin{bmatrix} P_0(L) \\ P_1(L) \\ P_2(L) \\ \vdots \\ P_{N-2}(L) \\ P_{N-1}(L) \end{bmatrix} \begin{bmatrix} 0 \\ 0 \\ 0 \\ \vdots \\ 0 \\ P_N(L) \end{bmatrix}$$

The matrix can be transformed into a symmetric matrix known as Jacobi matrix by using a diagonal similarity transformation, by preserving the eigenvalues at the same time (Marchisio and Fox, 2013):

$$J = \begin{bmatrix} a_0 & \sqrt{b_1} & & & & \\ \sqrt{b_1} & a_1 & \sqrt{b_2} & & & \\ & \sqrt{b_2} & a_2 & \sqrt{b_3} & & \\ & & \ddots & \ddots & \ddots & \\ & & & \sqrt{b_{N-2}} & a_{N-2} & \sqrt{b_{N-1}} \\ & & & & \sqrt{b_{N-1}} & a_{N-1} \end{bmatrix}$$

By mean of this procedure, the problem of finding the roots of a polynomial is overcome through the problem of finding eigenvalues and eigenvectors of the matrix. Furthermore,the N weights can be calculated as wα = m0 j2α1 where jα1 is the first component of the αth eigenvector jα of the Jacobi matrix (Marchisio and Fox, 2013).

The coefficients aα and bα of the recursive formula can be computed by means of the orthogonality condition and by using the moments.

The Product-Difference algorithm developed by Gordon (1968) and the Wheeler algorithm by Wheeler (1974) are two efficient methods capable to carry out these calculations.

The product-difference (PD) algorithm

The product-difference (PD) algorithm is based on the theory of continued fractions of Stieltjes and was developed by Gordon (1968). Firstly, it is necessary to construct a matrix P with components $P_{\alpha,\beta}$ starting from the moments of the weight function (Marchisio and Fox, 2013). The matrix is composed as:

- First column: Pα,1 = δ α,1 for α = 1,…, 2N+1 where δ α,1 is the Kronecker delta;
- Second column: Pα,2 = (-1)α -1 m α-1 for α = 1,…, 2N;
- Remaining components: Pα,β = P1,β-1 Pα+1,β-2 – P1,β-2 Pα+1,β-1 for β = 3,…, 2N+1 and α = 1,…, 2N+2-j.

To determine the coefficients of the recursive relation, it necessary to set equal to zero the first element of the coefficients of the continued fraction (namely ζ_1=0) and then computing the others as following:

$$\zeta_\alpha = \frac{P_{1,\alpha+1}}{P_{1,\alpha}P_{1,\alpha-1}}$$

Where α=2,…, 2N.

Resulting in:

$$a_\alpha = \zeta_{2\alpha} + \zeta_{2\alpha-1}$$

$$b_\alpha = -\sqrt{\zeta_{2\alpha+1} + \zeta_{2\alpha}}$$

Where α=1,…, N.

The PD algorithm is generally quite efficient in several practical cases, but it becomes less stable as N increases (typically problems can be expected when N>10). The other issue related to the PD

algorithm is that it blows up for distributions with mean equal to zero, since a division by zero is performed when ζ_α are computed (Marchisio and Fox, 2013).
The Wheeler algorithm described below does not suffer from these problems.

The Wheeler algorithm

Wheeler (1974) developed an efficient algorithm to calculate the coefficients of the Jacobi matrix.
The approach of Sack and Donovan (1971) uses a different set of basic functions πα(L) to represent the orthogonal polynomials, instead of the usual powers of L. This new polynomial basis leads to an improved stability due to its ability of better sample the interval of integration.
Hence, the coefficients are calculated from the modified moments defined as:

$$\nu_k = \int \pi_k(L) n(L) dL$$

Where k=0,…, 2N-1.
The basic functions $\pi_k(L)$ satisfies the following condition:

$$\pi_{-1}(L) = 0$$

$$\pi_0(L) = 1$$

$$\pi_{\alpha+1}(L) = (L - a'_\alpha)\pi_\alpha(L) - b'_\alpha \pi_{\alpha-1}(L)$$

Where the coefficients a'α and b'α have to be known explicitly.
Hence, from this findings, Wheeler (1974) developed an algorithm capable of calculating the coefficients of the Jacobi matrix through the quantities:

$$\sigma_{\alpha,\beta} = \int n(L)\pi_\alpha(L)\pi_\beta(L)dL$$

With α,β≥ -1.
The initialization conditions, that let these quantities be calculated, are:

$$\sigma_{-1,\alpha} = 0$$

With α = 1,…, 2N-2.

$$\sigma_{0,\alpha} = \nu_\alpha$$

With α = 0,…, 2N-1.

$$a_0 = a'_0 + \frac{\nu_1}{\nu_0}$$

$$b_0 = 0$$

Then the following equation is obtained:

$$\sigma_{\alpha,\beta} = \sigma_{\alpha-1,\beta+1} - (a_{k-1} - a'_\beta)\sigma_{\alpha-1,\beta} - b_{\beta-1}\sigma_{\alpha-2,\beta} + b'_{\beta-1}\sigma_{\alpha-1,\beta-1}$$

Where β = α,…, 2N-α-1.
And the coefficients for the Jacobi matrix are computed as follows:

$$a_\alpha = a'_\alpha - \frac{\sigma_{\alpha-1,\alpha}}{\sigma_{\alpha-1,\alpha-1}} + \frac{\sigma_{\alpha,\alpha+1}}{\sigma_{\alpha,\alpha}}$$

$$b_\alpha = \frac{\sigma_{\alpha,\alpha}}{\sigma_{\alpha-1,\alpha-1}}$$

The Wheeler algorithm has higher stability than PD algorithm and can be applied for the calculation of higher-order quadrature approximations. Another advantage is that it is able to calculate the coefficients of the Jacobi matrix even in the case of distributions with mean equal to zero (namely, e.g. $m_1=0$).
In practice, the Wheeler algorithm returns a set of weights and nodes for a realizable moment set. In the case of unrealizable moment sets it will fail, hence an adaptive version of the algorithm proposed by Yuan and Fox (2011) can be used.

Consistency of a moment set and correction algorithms

Very often happens that, during the simulation, the moments could be corrupted, forming an unrealizable or inconsistent moment set (Gemello, 2018). An unrealizable moment set is no longer representative of physical BSDs. The creation of the corrupted moment sets is accompanied by the loss of numerical stability in the simulation (Petitti et al., 2010) reaching a complete divergence.
For this reason, different authors proposed their methods for recovering a corrupted moment set when it is encountered.
McGraw (1997) proposed the so called Minimum Square Algorithm that consists in a iterative method based on the idea of identifying and correcting only the moment which, after adjustment, maximizes the smoothness of its logarithmic function, through a minimization procedure. In particular, the method can identify quickly the moments that ought to be corrected and the corrected value of the moment that results in a valid set (Petitti et al., 2010).
Sometimes this method does not succeed in the correction of the moment set in an acceptable number of iterations, and hence it is required a second correction procedure.
This is the method proposed by Wright (2007) that restores the corrupted moment sequence with the moments calculated as the arithmetic mean of two log-normal distributions. From the first four moments of the set that must be corrected, it is possible to evaluate these distributions, keeping fixed the moments of order zero and three.
Both the algorithms of McGraw (1997) and Wright (2007) allow the correction of the unphysical results of moment corruption and the removal of the associated stability problems. These correction algorithms mainly modify the higher-order moments. It is important to highlight that these corrections do not affect largely the final results, only leading to higher stability to the code.
Petitti et al. (2010) proposed this approach that was tested under different operating conditions and played a crucial role both in terms of the numerical stability of the simulation and the physical consistency of the results.

Source term in the QMOM

As previously mentioned, the term appearing on the right-side of the moment transport equation is the source term. By considering only breakage and coalescence, neglecting the mass-transfer and applying the quadrature formula with three nodes, the source term results in:

$$S_{mk} = \frac{L^2}{2}\int_0^L \frac{h\left((L^3+\lambda^3)^{\frac{1}{3}},\lambda\right)}{(L^3-\lambda^3)^{\frac{2}{3}}} n_L\left((L^3+\lambda^3)^{\frac{1}{3}}\right) n_L(\lambda)d\lambda - \int_0^\infty h(L,\lambda)n_L(L)n_L(L)d\lambda$$
$$+ \int_L^\infty \beta(L,L')g(L')n_L(L')dL' - g(L)n_L(L)$$
$$\approx \frac{1}{2}\sum_{i=1}^{N=3} w_i \sum_{i=1}^{N=3} w_i\, h_{ij}\left[(L^3+\lambda^3)^{\frac{k}{3}} - L_i^k - L_j^k\right] + \sum_{i=1}^{N=3} w_i\, g_i(b_i^k - L_i^k)$$

Where:

- L_i and L_j are the nodes of the quadrature approximation;
- w_i and w_j are the weights of the quadrature approximation;
- $h_{ij}= h(L_i, L_j)$ is the coalescence kernel generated by the interaction between bubbles of size L_i and L_j;
- $g_i=g(L_i)$ is the breakage kernel depending on bubble size L_i;
- b^k_i is the kth moment of the daughter distribution function of the daughter bubble L, generated by the mother bubble L_i. It can be represented as:

$$b_i^k = \int_{Lmin}^{Lmax} \beta(L, L_i) L^k dL$$

Where the daughter bubble has L_{min} equal to zero and L_{max} equal to the mother bubble size (L_i).
By restoring to the quadrature approximation defined through its weights wi and nodes Li, the closure problem is overcome. Thus the source term results in:

$$S_{mk} = \approx \frac{1}{2}\sum_{i=1}^{N=3} w_i \sum_{i=1}^{N=3} w_i\, h_{ij} \left[(L^3 + \lambda^3)^{\frac{k}{3}} - L_i^k - L_j^k\right] + \sum_{i=1}^{N=3} w_i\, g_i((\int_0^{L_i} \beta(L, L_i) L^k dL) - L_i^k)$$

An analytical solution exists in the case of binary break up, starting with the daughter distribution function of Laakkonen et al. (2007) as showed in the work of Petitti et al. (2010):

$$b_i^k = \int_0^{Li} (180(\frac{L^2}{L_i^3})\left(\frac{L^3}{L_i^3}\right)^2 (1 - \frac{L^3}{L_i^3})^2)\, L^k dL = \frac{3240 L_i^k}{(k+9)(k+12)(k+15)}$$

Besides the binary breakage, other values were tested, but in these cases a numerical integration must be carried out. In particular, it is possible to resort to a quadrature formula (for example, Newton-Cotes) or to a quadrature approximation such as Gauss-Legendre and the latter method showed better accuracy.

Simplified QMOM

As already said previously, the QMOM with three nodes is calculated by tracking the first six moments, but the idea applied in this work is that only one average bubble diameter is sufficient to describe the effect of breakage and coalescence on m2. In fact the working hypothesis is to solve only the moment transport equation for the second-order moment in order to calculate the Sauter mean diameter ($d_{32} = m_3/m_2$) as m_3 is linked to the gas holdup (this one is known). In this case only one diameter L is considered for the calculation (i=j=1), hence the source term results in the following form:

$$S_{m2} = \frac{6\alpha}{\pi L}[\frac{3\alpha}{\pi L^3} h(L, L)\left(2^{\frac{2}{3}} - 2\right) + g(L)\left(\frac{b^2}{L^2} - 1\right)]$$

As mentioned before, this approximation of the BSD to a homogeneous flow with a single diameter is sufficient to describe the effect of breakage and coalescence on gas/liquid area (m_2). Furthermore, as it will be showed in the following parts (Fig.5-8) that this approximation is reasonable since the difference in the prediction of the Sauter mean diameter between the QMOM and the m2 equation is only around 2.5%. Thanks to these finding, the calculation of the Sauter mean diameter through this method are much faster and simpler (just one equation is solved instead of five as it is done with the QMOM), therefore this approximation has been applied in the numerical simulations done in this work of thesis.

5.1.3 Modelling work: Results and discussion

5.1.3.1 Air-Water systems

The idea was to study different breakage and coalescence kernels with the lowest computational costs in order to find the best models capable of fitting the experimental data for a particular gas-liquid system. For this reason, as mentioned before, a preliminary work was done on Microsoft Excel, by using a VBA code. A zero-dimensional (0D) approach have been adopted to obtain preliminary results as, by using normal three-dimensional transient CFD simulations, the time required is extremely high to carry out many simulationsfor different operating conditions.

As explained by Buffo et al. 2016, in 0D models the continuous and dispersed phases are assumed to be perfect mixedand also spatial homogeneity, leading to very low computational costs.

Initially,the Quadrature method of moments (QMOM) was adopted to do these simulations.

The adopted method is iterative, namely the value of the moment calculated in the previous iteration is used to calculate the new value.The same approach is applied to the bubble size: the value of the previous iteration is used to calculate the breakage and coalescence terms that constitute the source term used to calculate the moment that, in turn, allows to calculate the new bubble size. The number of iterations is chosen in order to be sure to obtain a final bubble size that is the one at the steady-state.

In particular, as known from the work ofGemello (2018), the best set of kernels (both the breakage and coalescence one)in the case of bubble columns under heterogeneous regime seemed to be the model proposed by Laakkonen et al.(2006) for the breakage, the daughter distribution function proposed by Laakkonen et al. (2007), the collision frequency proposed by Wang et al.(2005b) (except for a modified coefficient) and the coalescence efficiency proposed by Lehr et al.(2002) based on the critical approach velocity model.

Consequently, the first simulations have been done in order to investigate whether this set of kernels was able to fit also the experimental data carried out by Cappello (2019) for air-water stirred tank reactors; perhaps by modifying the constant inside the collision frequency model proposed by Wang et al.(2005b).

If the outcome had been positive, it would have meant that this set of kernels has a wider range of validity.

In general, the idea is to find a correlation whose use is not limited to geometry and operating condition similar to those experimentally observed, but that is valid for a wider range of those and for different geometries.

The results obtained from this preliminary work showed that these models are not able to describe in the right way the experimental data, as done in the case of bubble columns. In fact, it is possible to notice from the graphs below(Fig.8-9)that the effect of Vsg is not the same as in the experimental case: in the latter case the effects of Vsg and ε are less pronounced and the Sauter mean diameter profiles are almost flat, while with the QMOM the slope is greater and the trend suggests a stronger increase of Sauter mean diameter while varying the Vsg. This trend leads to an underestimation of the Sauter mean diameter at low values of Superficial gas velocity and an overestimation of it at high values of Superficial gas velocity.

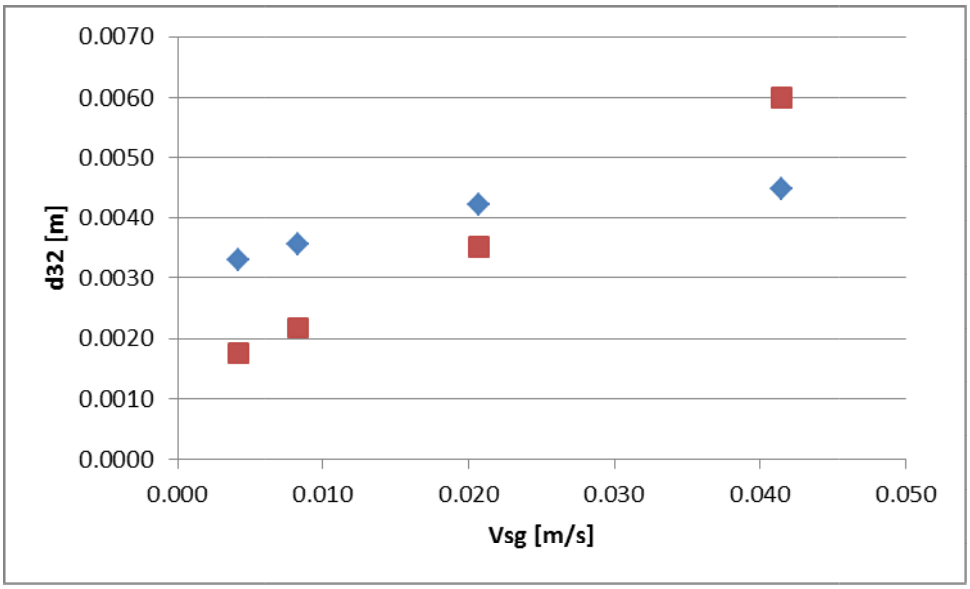

Figura 8 Sauter mean diameter versus Superficial gas velocity: experimental data (□), results obtained with 0D simulation (◊)

a. N=600 rpm

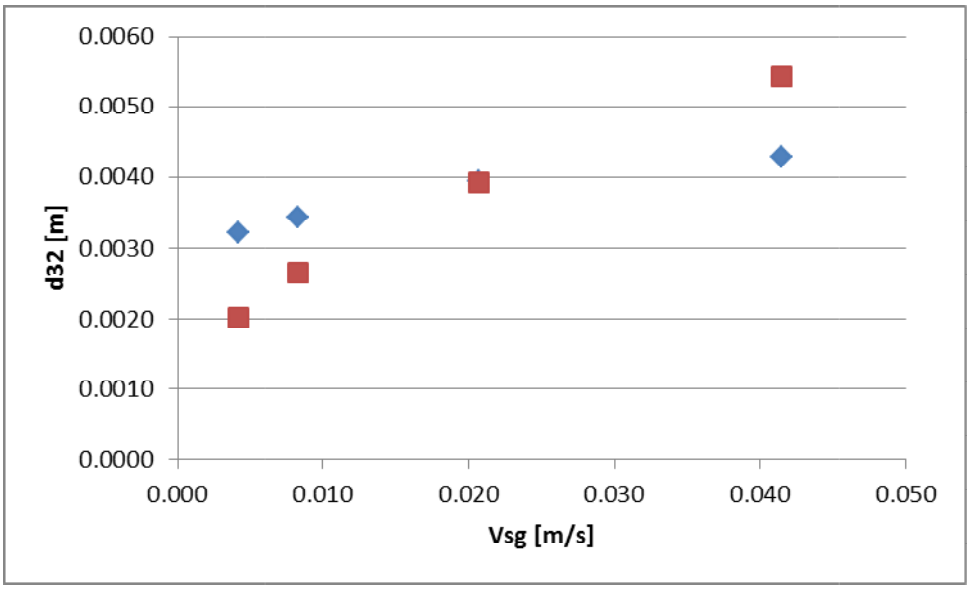

Figura 9 Sauter mean diameter versus Superficial gas velocity: experimental data (□), results obtained with 0D simulation (◊)

b. N=997 rpm

Even changing the value of the multiplicative constant within the model of Wang et al.(2005b), the curve trends were still wrong. This is a further confirmation of the fact that this set of kernels is not able to correctly describe the experimental data taken in analysis.

In order to find the best set of kernels that fits the experimental data of stirred tank reactors, different models for breakage and coalescence are tested.

As showed in the reviews of Liao and Lucas (2009, 2010), several authors proposed their models based on different mechanisms that are available in the Literature; therefore, this leads to many different combinations that have to be tested and a faster way to screen the population balance kernels is necessary.

The idea of screening kernels is feasible through the use of a simple 0D approach based on average gas holdup (α_g) and turbulent dissipation rate (ε) and, as previously mentioned, in this work a QMOM with a number of nodes of the quadrature approximation equal to three was adopted and calculated by tracking the first six moments of the BSD (six equation are solved).
By knowing that only one average bubble diameter is sufficient to describe the effect of breakage and coalescence, a simplified approach had been adopted based on the knowledge that the calculation of m2 is sufficient to recalculate the Sauter mean diameter (calculated as the ratio of m3 and m2),as m3 is linked to the gas holdup known from experimental data.
So, the working hypothesis for this step include to solve only transport equation related to the moment of second order with only one size of bubbles, that means only one node of the quadrature approximation and only one equation has to be solved.
Since this approach is only a simplification of the QMOM, it remains an iterative method that consider the values of the 2nd-order moment and bubble size of the previous iteration to calculate the new ones.
This idea was already proposed by Lane et al.(2005) who suggested to use a "single diameter" model.
Thanks to this shortcut method, the computational time is greatly reduced making model screening easier.
It is possible to show that this simplification is legit, because the results obtained by solving only the m2 transport equation differ only by a value less than 3% compared to the results obtained with the QMOM (see Fig.10-13).

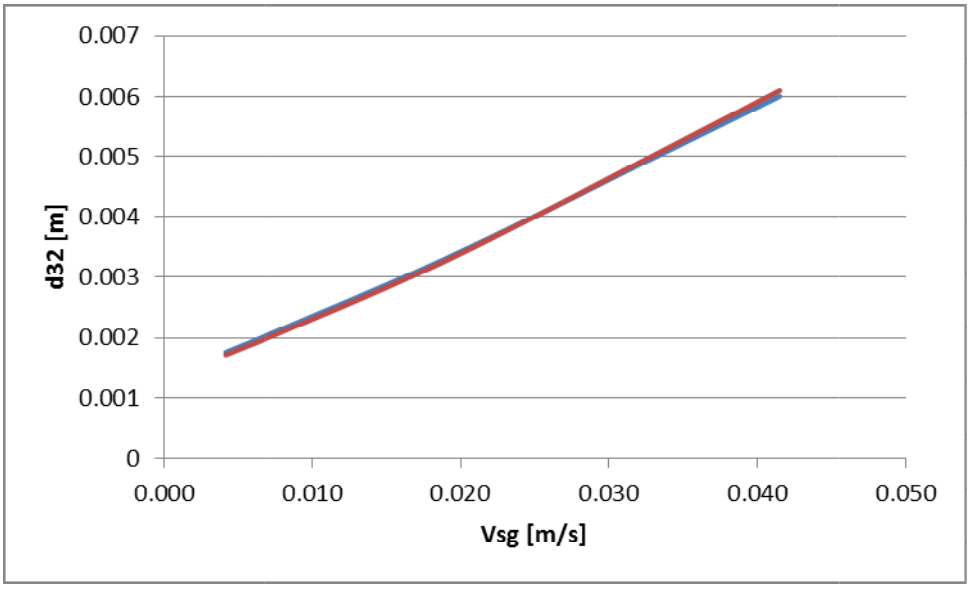

Figura 10 Comparison Sauter mean diameter predicted by QMOM and Simplified QMOM (set of kernels found by Gemello, 2018)

a. N=600 rpm

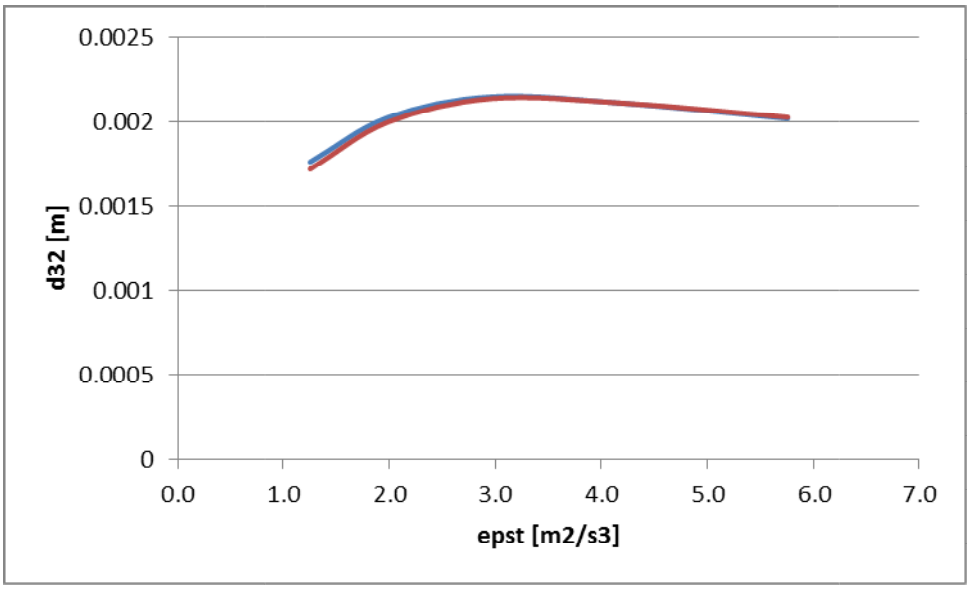

Figura 11 Comparison Sauter mean diameter predicted by QMOM and Simplified QMOM (set of kernels found by Gemello, 2018)

b. N=997 rpm

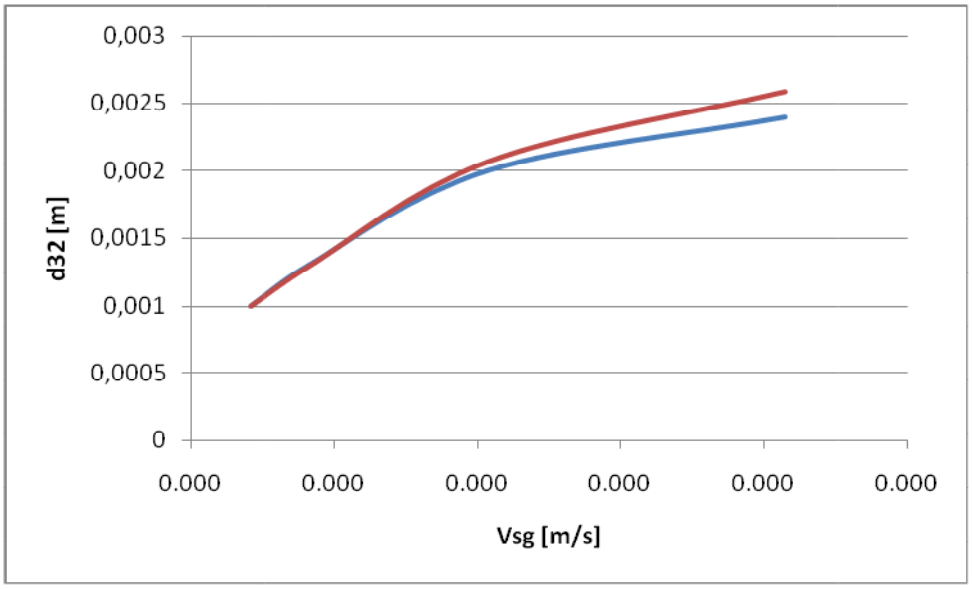

Figura 12 Comparison Sauter mean diameter predicted by QMOM and Simplified QMOM (set of kernels composed by BM: Laakkonen et al., 2006; CF: Lehr et al., 2002; CE: Coulaloglou and Tavlarides, 1977)

a. N=600 rpm

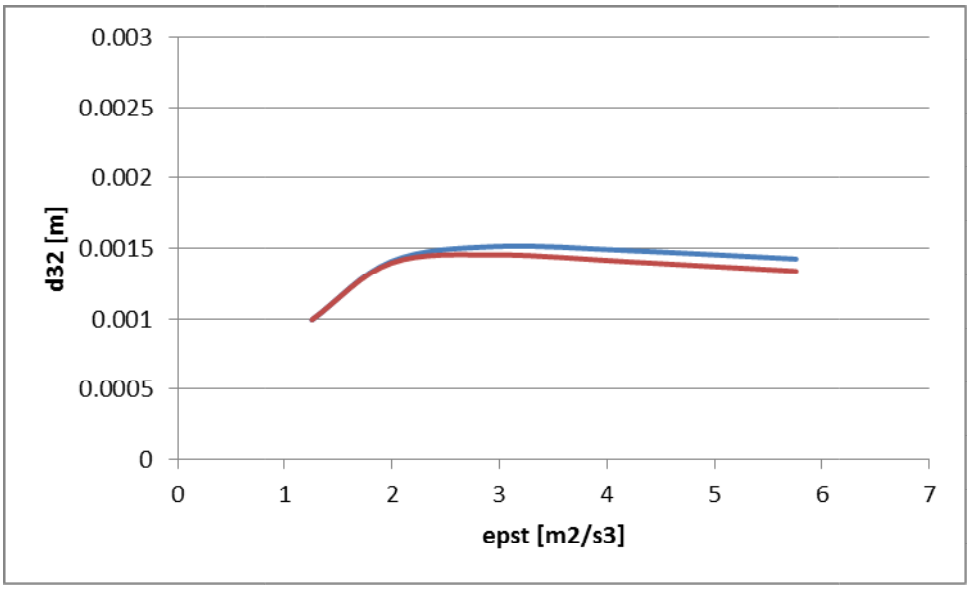

Figura 13 Comparison Sauter mean diameter predicted by QMOM and Simplified QMOM (set of kernels composed by BM: Laakkonen et al., 2006; CF: Lehr et al., 2002; CE: Coulaloglou and Tavlarides, 1977)

b. N=997 rpm

Hence, the successive step was the implementation of a VBA code in Excel to do an automatic screening in order to test all the different possible combinations of kernels and find one that perfectly fits the experimental results.

As a first step, a screening of the different set of kernels was done for the case of bubble columns containing air and water as dispersed and continuous phases, and, for this system, the dissipation rate was calculated through the theoretical expression (ε=Vsg*g), due to the fact that the values of dissipation rate taken from the thesis of Gemello et al. (2018) derive from CFD simulations and so it is not possible to know the rightness of these values as it is not possible to measure experimentally the turbulent dissipation rate.

For this kind of equipment the aim of the screening was to see whether or not there were other sets of models equivalent to the one found by Gemello et al.(2018) in his work.

Then, the screening of kernels was applied also to stirred tank reactors in order to find one (or more) fitting combinations to describe the experimental results obtained by Cappello (2019) for the case of air-water systems.

The results obtained from this initial screening, showed how several model combinations furnished good trends of Sauter mean diameter (d32) vs. turbulent dissipation rate (ε), but the range of magnitude was far from the experimental one: in fact, many models gave underestimated or overestimated values of the bubbles diameter. For example, in the case of bubble columns, the different combinations of kernels, considering the model of Laakkonen et al. (2007) as breakage model, gave the following trends (Fig.14):

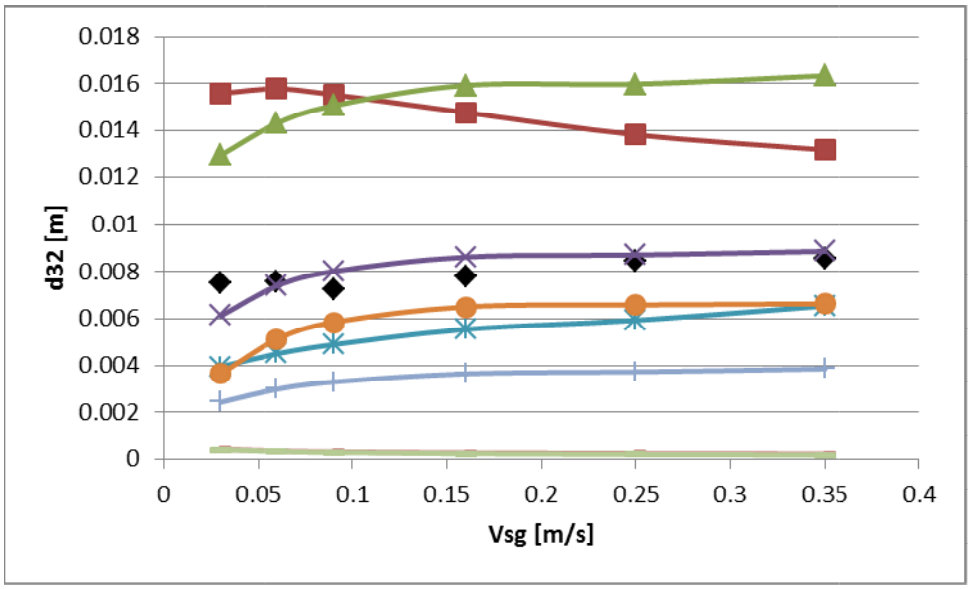

Figura 14 Sauter mean diameter predicted by different set of kernels considering the model of Laakkone et al. (2006) as breakage model; comparison with experimental results (◊)

In general, the reason for this behavior (namely overestimation and underestimation of Sauter mean diameter) was attributed to coalescence term as it was thought to be necessary to weigh it up in order to obtain the right range of magnitude of d32 centered on the average experimental value. To do this, a corrective factor was added to the coalescence term.

The corrective factor is represented by a simple ratio between the average experimental Sauter diameter and the average calculated one. So, this means that a value of the corrective factor higher than one is obtained for the models underestimating the bubbles diameter and a value in between zero and one for the models overpredicting the results.

$$corr_{factor}^{n} = corr_{factor}^{n-1} * \frac{L_{exp}}{L_{0D}}$$

This is an iterative method that takes into account also the value of the previous iterations in order to know exactly the value of the multiplicative constant required to center the results on the average experimental value.

By weighting the coalescence term with the corrective factor, the following results are obtained (divided into different breakage model).

Concerning bubble columns, the first graph (Fig.15) shows the curves of the predicted Sauter mean diameter by the different set of kernels considering the Coulaloglou and Tavlarides (1977) model for breakage. In this case, the trend of the Sauter mean diameter versus the superficial gas velocity is plotted. The comparison among the experimental curve and the obtained ones highlights how curves profiles are in the right range of magnitude but they have a too pronounced trends that means a stronger effect of Vsg is predicted by this breakage model. In fact, the simulated curves show an increasing behavior by increasing the superficial gas velocity, whereas the experimental profile is almost flat. Anyway, the results obtained are not that far from the experimental ones, in fact the deviation is always equal or less than 20%. In particular, a mean error of approximation equal to 14% has been obtained by applying the sets of kernels considering this breakage model, the collision frequency of Prince and Blanch (1990) and the coalescence efficiency of Chesters (1991) (squared dots) or that proposed by Lehr et al. (2002) (triangular dots) (Fig.16). The curves profiles suggest that these two sets of models predict both bubble size and effect of Vsg that are close to the real ones, perhaps slightly modifying the effect of Vsg could lead to an improved agreement with experimental results.

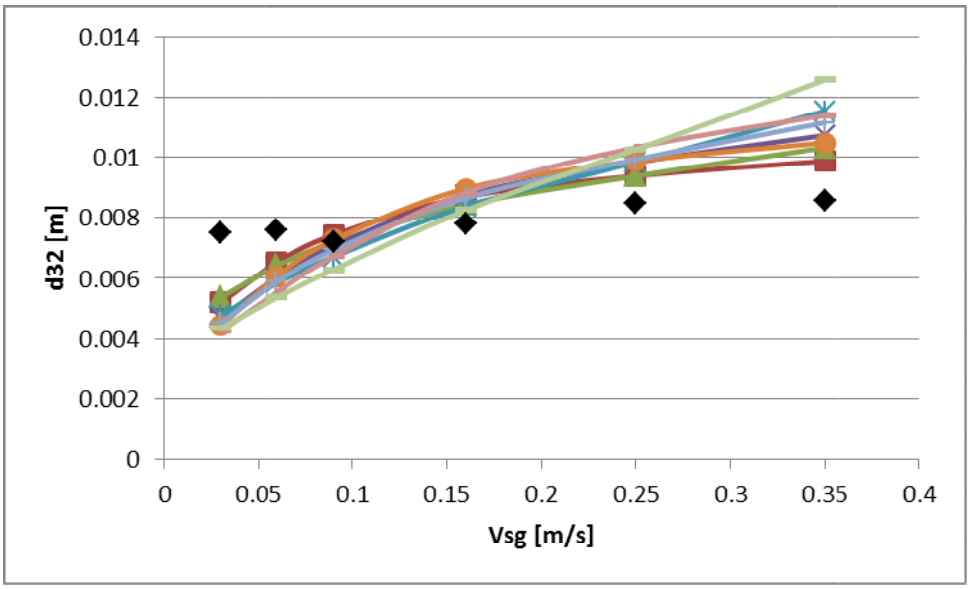

Figura 15 Sauter mean diameter predicted by different set of kernels considering the model of Coulaloglou and Tavlarides (1977) as breakage model; comparison with experimental results (◊)

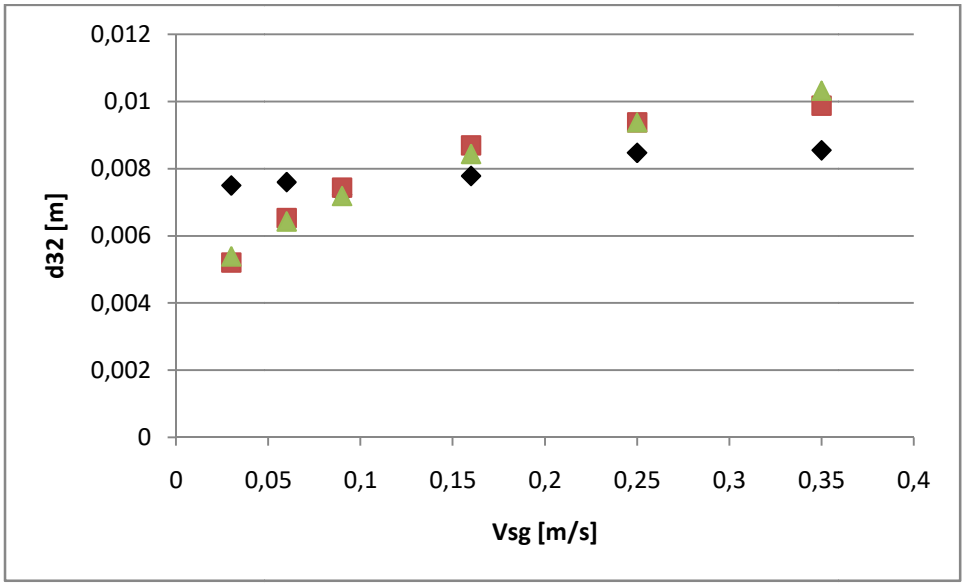

Figura 16 Sauter mean diameter versus Vsgobtained experimentally (◊) and by the sets of kernels considering BM: Coulaloglou and Tavlarides (1977), CF: Prince and Blanch (1990), CE: Chesters (1991) (□) and Lehr et al. (2002) (Δ)

Also the breakage model of Prince and Blanch (1990) was tested (Fig.17) and it is possible to notice two different common curves profiles: all sets of kernels that used the model of Chesters (1991) as coalescence efficiency showed a trend similar to the experimental one except at lower values of Vsg where the models predicted a smaller value of the Sauter mean diameter; on the other side, all the combinations considering the model of Lehr et al. (2002) for coalescence efficiency predicted very small bubbles size that could mean that breakage is the dominant phenomenon. So, we can conclude that the critical approach velocity model of Lehr et al. (2002) is not the right way to describe the coalescence when coupled with this breakage kernel.

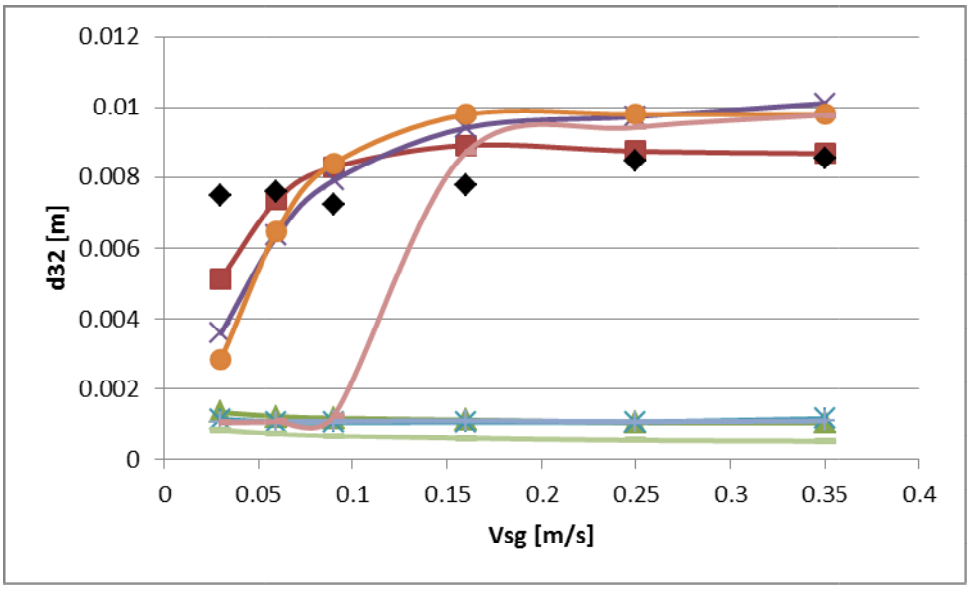

Figura 17 Sauter mean diameter predicted by different set of kernels considering the model of Prince and Blanch (1990) as breakage model; comparison with experimental results (◊)

The breakage models of Alopaesus et al. (2002) and Laakkonen et al. (2006) were also investigated and showed the same results since, in the latter kernel, the author substituted the gas viscosity with the viscosity of the continuous phase , but in the considered system of air-water the viscosities of the two phases are almost the same. The results obtained in these cases (Fig.18-19) showed that all the different combination have almost the same effect of Vsg as the experimental results: the average error of approximation is always lower than 15% that means these breakage model well describe the heterogeneous flow regime, in accordance with the results obtained by Gemello (2018). In particular, the best agreement was obtained with the sets of kernels that combined this breakage model to the collision frequency of Prince and Blanch (1990) and the coalescence efficiency of Chesters (1991) (squared dots) or the one proposed by Lehr et al. (2002) (triangular dots), leading to an error of approximation equal to 5% and 7%, respectively(Fig.20). This result lets us conclude that the set of kernels found by Gemello (2018) is not the only one suitable to describe the bubble size within a bubble column, but also the one that consider the coalescence efficiency of Chesters (1991).

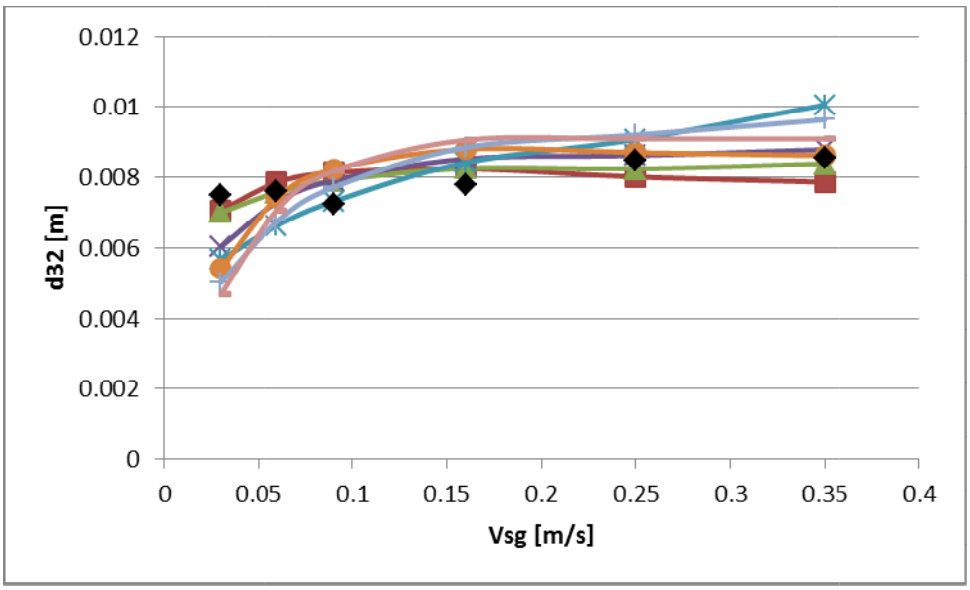

Figura 18 Sauter mean diameter predicted by different set of kernels considering the model of Alopaesus et al. (2002) as breakage model; comparison with experimental results (◊)

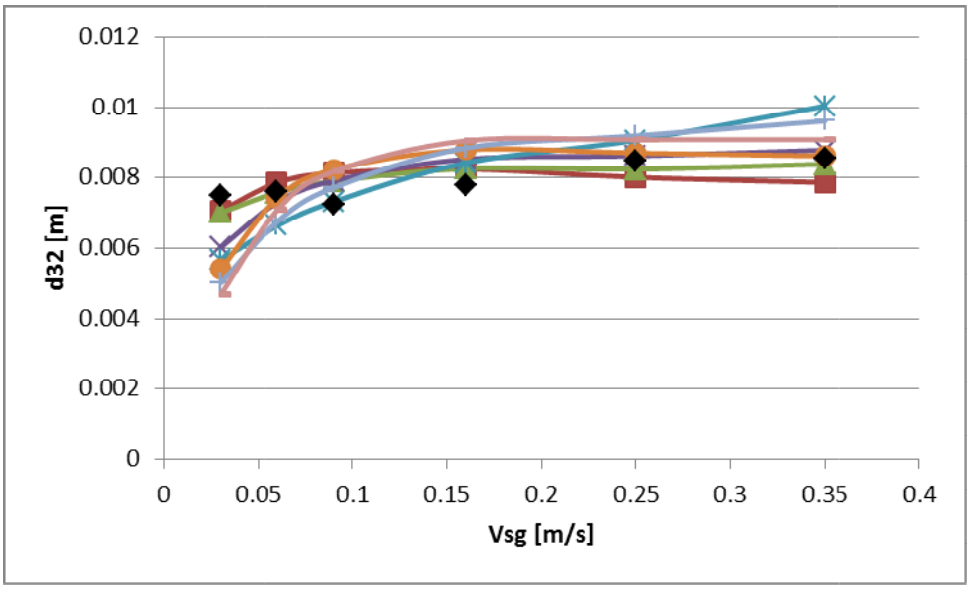

Figura 19 Sauter mean diameter predicted by different set of kernels considering the model of Laakkonen et al. (2006) as breakage model; comparison with experimental results (◊)

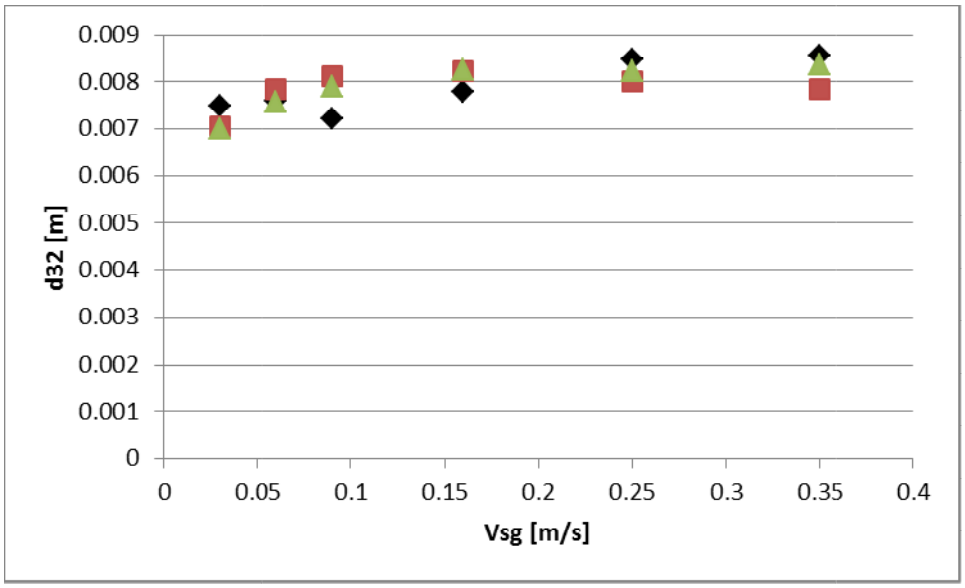

Figura 20 Figure 1Sauter mean diameter versus Vsg obtained experimentally (◊) and by the sets of kernels considering BM: Laakkonen et al. (2006), CF: Prince and Blanch (1990), CE: Chesters (1991) (□) and Lehr et al. (2002) (Δ)

Another aspect can be highlighted from these results: since the different combination of kernels gave almost the same results and since the terms of collision frequency are almost the same except for the corrective factor pi and gamma, this could lead to doubt the utility of these factors (putting one or another of the suggested corrective factor does not change a lot the results).

Among several breakage kernels, also the model of Lehr et al. (2002) was taken into account for the screening(Fig.21) and all the different set of kernels considering this one as the breakage model failed to predict the bubble size: the experimental observation showed a slight influence of Vsg on the Sauter mean diameter and the curve profile is almost flat, whereas the curves obtained with this model showed a decreasing trend for increasing superficial gas velocity values. This result leads to think that increasing the Vsg, the breakage phenomenon becomes the predominant one, which is contrary to the experimental observation.

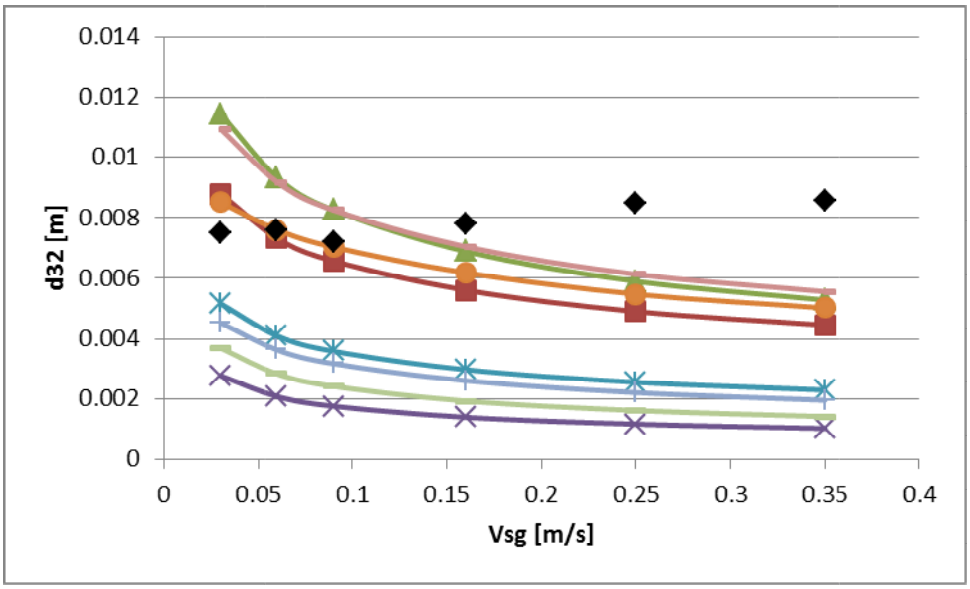

Figura 21 Sauter mean diameter predicted by different set of kernels considering the model of Lehr et al. (2002) as breakage model; comparison with experimental results (◊)

The last breakage model analyzed was the one of Carrica and Clausse (1993) that considered breakage due to interfacial instability; in this case the results were completely wrong, leading to a strong disagreement with the experimental data.

After comparing several possible sets of kernel and adding a corrective factor in order to center the results in the right range of magnitude, the following conclusions are done for the case of bubble columns:

- the best set of kernels that seems to be able to simulate heterogeneous bubble columns is the one that consider the breakage kernel proposed by Laakkonen et al. (2006), the daughter distribution function proposed by Laakkonen et al. (2007), the modified collision frequency proposed by Prince and Blanch (1990) and the coalescence efficiency proposed by Lehr et al. (2002) based on the critical approach velocity model. These kernels together gave only a 5% mean error of approximation of experimental results. This result is almost the same obtained by Gemello (2018) in his PhD thesis as the only difference is the model of collision frequency considered: in fact, the author found that the modified model proposed by Wang et al. (2005b) fitted better the results, while in this work the model of Prince and Blanch seems to give better agreement with the experimental data. The reason for this slight disagreement is due to the fact that, as mentioned above, Gemello (2018) used the turbulent dissipation rate (ε) derived from his CFD simulations, while in this case epsilon has been calculated through the theoretical correlation (ε=Vsg*g) and therefore we have different starting values for this parameter that bring to slightly different results.
- Alternatively, the set of kernels considering the Laakkonen et al. (2006) model as breakage frequency, the daughter distribution function proposed by Laakkonen et al. (2007), the collision frequency model of Prince and Blanch (1990) (modified by the correction factor) and the film-drainage model for coalescence efficiency proposed by Chesters et al. (1991) considering only inertial collisions was still coherent with the experimental data; in fact, the mean error of approximation is about 7%. This result is interesting because it lets say that also the kernel of coalescence efficiency based on the film drainage model are suitable to describe the bubble size within a bubble column as an alternative to the set of models found by Gemello (2018).

- In general, by observing the graphs above, it is possible to notice that, after adding the correction factor to the coalescence term, several combinations tested showed errors lower than 20%. Therefore, just by adding a correction factor that depends on the gas holdup, it could be possible to adjust the trend of these curves, leading to a better agreement with experimental data.

The tables below summarize the two set of kernels fitting the experimental data in bubble columns:

Breakage Model	$g(L) = c_3\varepsilon^{1/3} erfc\left(\sqrt{c_4\frac{\sigma}{\rho_l\varepsilon^{2/3}L^{5/3}} + c_5\frac{\mu_l}{\sqrt{\rho_g\rho_l}\varepsilon^{1/3}L^{4/3}}}\right)$	c3=4; c4=0.04; c5=0.01
Collision Frequency	$h_0(L_1,L_2) = C'_1(L_1+L_2)^2\varepsilon^{1/3}\sqrt{L_1^{2/3}+L_2^{2/3}}$	c'1=0.23
Coalescence Efficiency	$\lambda(L_1,L_2) = min\left(\frac{u_{crit}}{u_{rel}},1\right)$	—

Tabella 8 set of kernels suitable for bubble columns

Breakage Model	$g(L) = c_3\varepsilon^{1/3} erfc\left(\sqrt{c_4\frac{\sigma}{\rho_l\varepsilon^{2/3}L^{5/3}} + c_5\frac{\mu_l}{\sqrt{\rho_g\rho_l}\varepsilon^{1/3}L^{4/3}}}\right)$	c3=4; c4=0.04; c5=0.01
Collision Frequency	$h_0(L_1,L_2) = C'_1(L_1+L_2)^2\varepsilon^{1/3}\sqrt{L_1^{2/3}+L_2^{2/3}}$	c'1=0.38
Coalescence Efficiency	$\lambda(L_1,L_2) = \exp\left(-\sqrt{\frac{\rho_l\varepsilon^{2/3}L^{5/3}}{4\sigma}}\right)$	—

Tabella 9 set of kernels suitable for bubble columns

The same work has been done for stirred tank reactors and the same models have been considered. After a preliminary screening, some models showed curve profile in slight agreement with the experimental trend: for example, some sets of kernels considering the breakage model of Coulaloglou and Tavlarides (1977) slightly underestimated the results, but the effect of turbulent dissipation rate seemed to be well predicted, leading to mean errors around 20% (Fig.22-23 below).

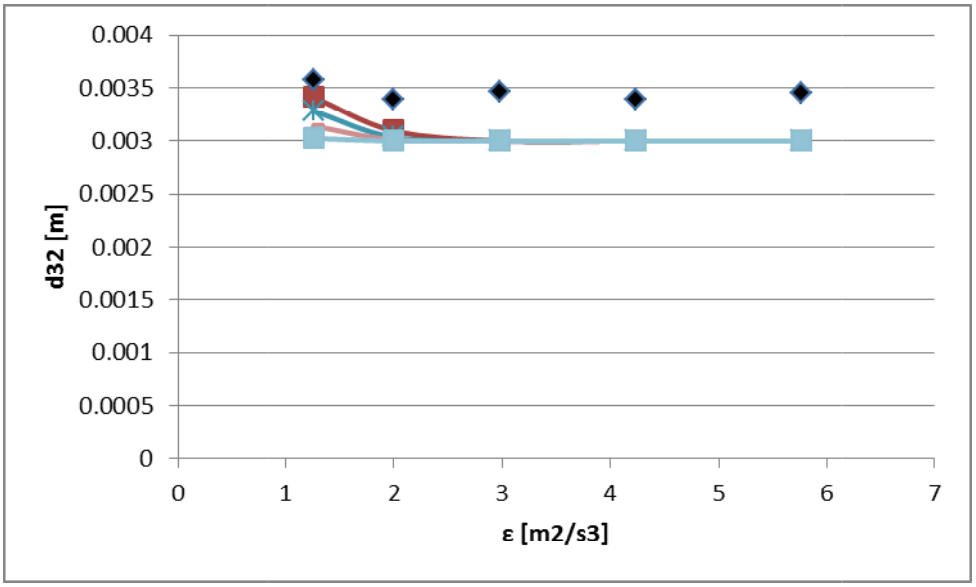

Figura 22 Sauter mean diameter versus turbulent dissipation rate predicted by sets of kernels considering BM: Coulaloglou and Tavlarides (1977), CE: Coulaloglou and Tavlarides (1977), CF: Prince and Blanch (1990) (□ red), Wang et al. (2005b) (x), Lehr et al. (2002) (-) and Chesters (1991) (□ light blue); comparison with experimental results (◊)

a. Vsg= 0.00415 m/s

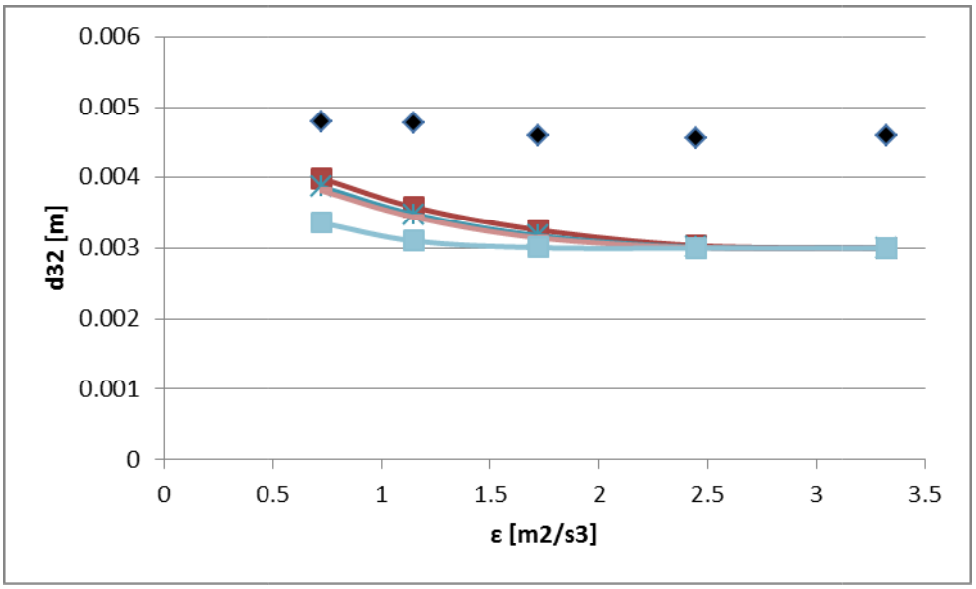

Figura 23 Sauter mean diameter versus turbulent dissipation rate predicted by sets of kernels considering BM: Coulaloglou and Tavlarides (1977), CE: Coulaloglou and Tavlarides (1977), CF: Prince and Blanch (1990) (□ red), Wang et al. (2005b) (x), Lehr et al. (2002) (-) and Chesters (1991) (□ light blue); comparison with experimental results (◊)

b. Vsg= 0.0415 m/s

On the other side, some models showed both results in the wrong range of magnitude and completely wrong curve profile, maybe due both to a wrong effect of gas holdup and turbulent dissipation rate. For example, all the set of kernels considering the model of Lehr et al. (2002) showed a more pronounced effect of turbulent dissipation rate, leading to smaller bubble size at high values of turbulent dissipation rate(Fig.24-25). The same behavior have already been observed in the case of bubble column as shown above, leading to think that the breakage phenomenon prevails at higher values of turbulent dissipation rate (Fig.16).

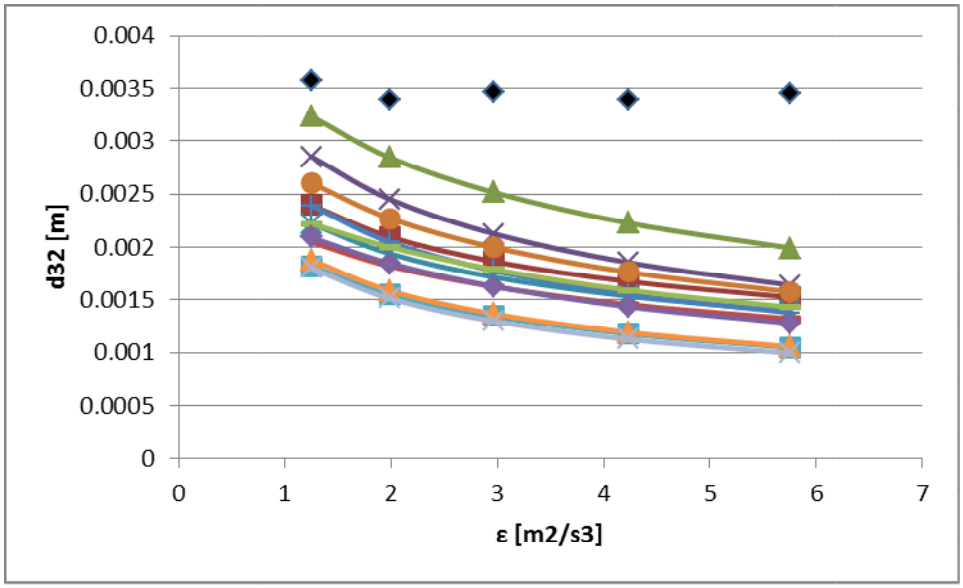

Figura 24 Sauter mean diameter predicted by different set of kernels considering the model of Lehr et al. (2002) as breakage model; comparison with experimental results (◊)

a. Vsg= 0.00415 m/s

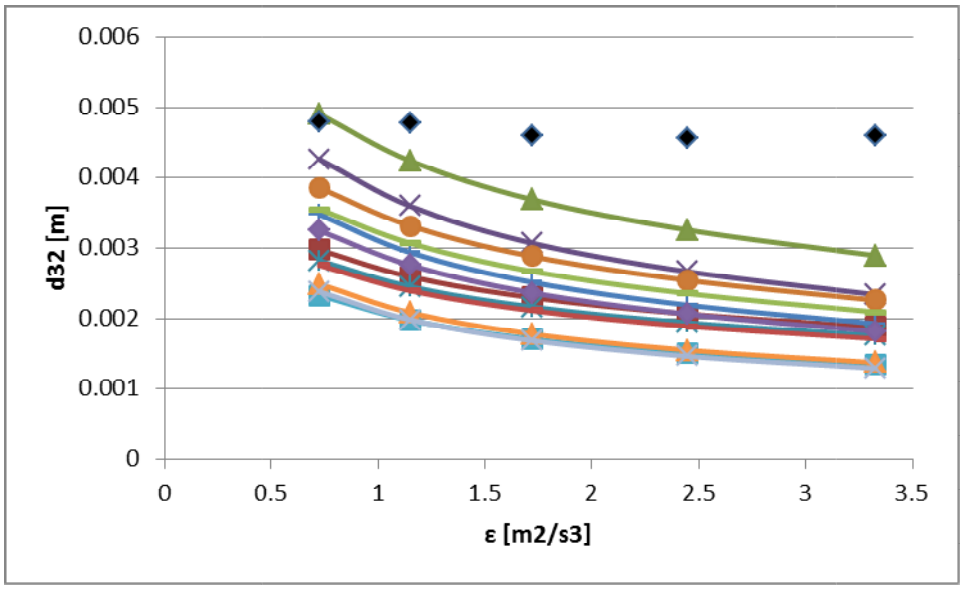

Figura 25 Sauter mean diameter predicted by different set of kernels considering the model of Lehr et al. (2002) as breakage model; comparison with experimental results (◊)

b. Vsg= 0.0415 m/s

Regarding the other sets of kernels analyzed, several models described a wrong effect of gas holdup since at the low values of αg the model predicted underestimated results, while at higher values of this parameter the results where overestimated as shown in Fig.26-27 for the set of kernels considering the breakage model proposed by Laakkonen et al. (2006), the collision frequency by Wang et al. (2005b) and the coalescence efficiency model for inertial collisions by Chesters (1991).

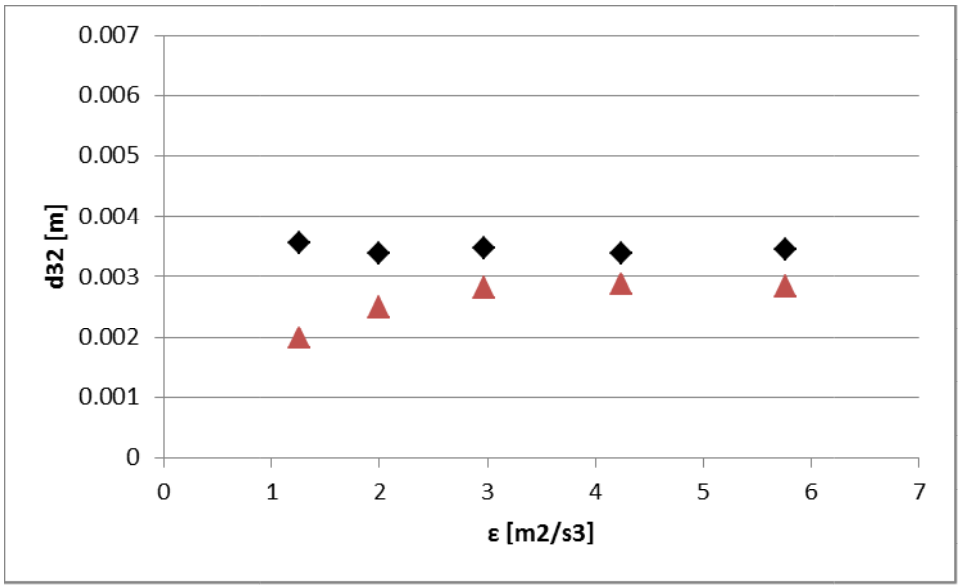

Figura 26 Sauter mean diameter versus turbulent dissipation rate: comparison experimental (◊) versus results obteined with BM: Laakkonen et al. (2006), CF: Wang et al. (2005b), CE: Chesters (1991) (Δ)

a. Vsg= 0.00415 m/s

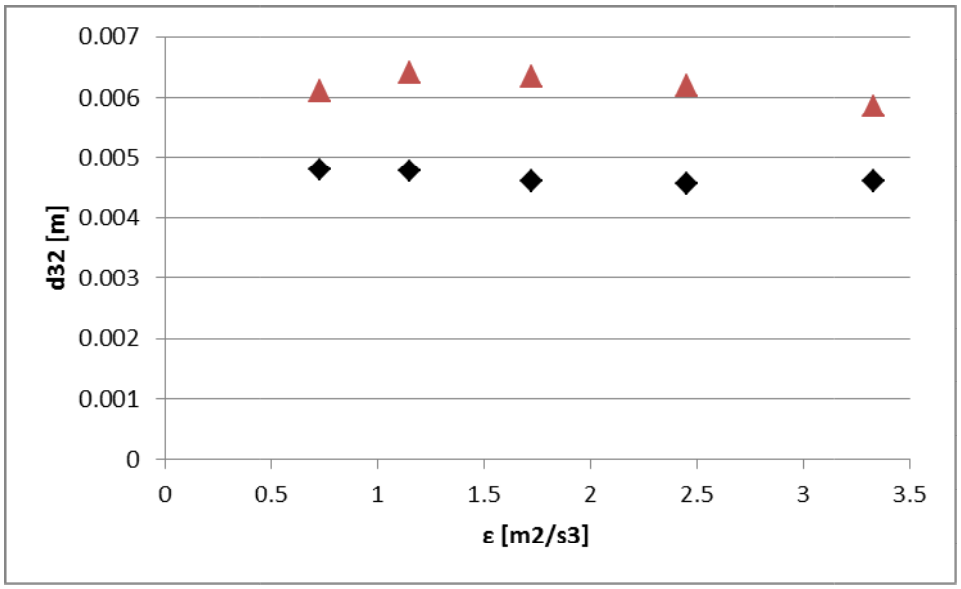

Figura 27 Sauter mean diameter versus turbulent dissipation rate: comparison experimental (◊) versus results obteined with BM: Laakkonen et al. (2006), CF: Wang et al. (2005b), CE: Chesters (1991) (Δ)

b. Vsg= 0.0415 m/s

Since the results obtained were still not satisfactory, the same approach adopted in the case of bubble column wad applied to stirred tank reactor and a correction factor was used in order to weight the coalescence term. By applying the correction factor, some curve profiles have improved and are better suited to experimental results.

For example, all the combination of kernels considering the breakage model of Coulaloglou and Tavlarides (1977) and the coalescence efficiency of Chesters (1991) or Lehr et al. (2002) successfully predict the Sauter mean bubble size and the mean error is lower than 10% (Fig.28-29); whereas the other combinations considering the same breakage model but the coalescence efficiency of Coulaloglou and Tavlarides (1977) showed a slightly pronounced decreasing trend of Sauter mean diameter compared to the experimental trend, leading to a mean error of about 20%.

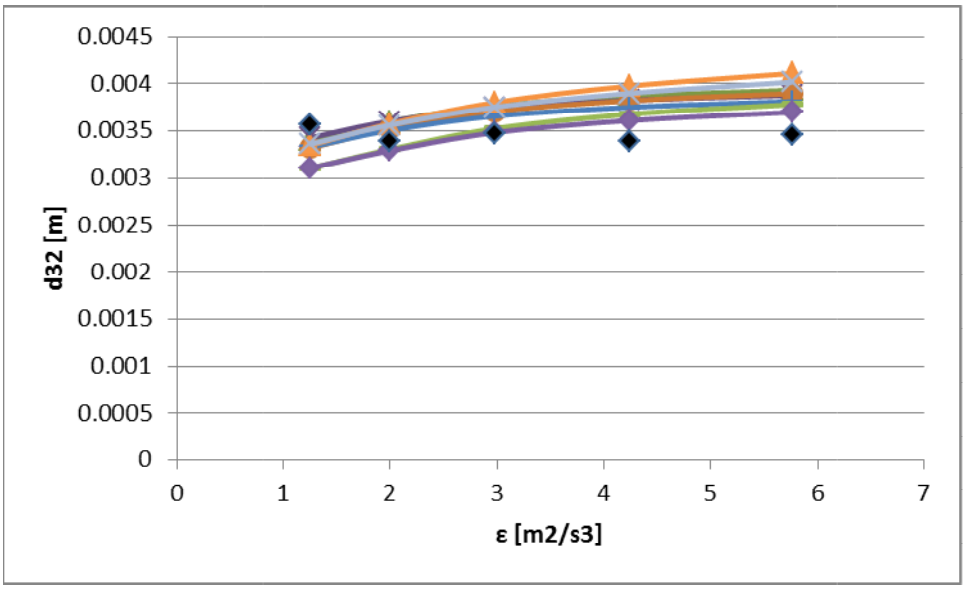

Figura 28 Sauter mean diameter predicted by different set of kernels considering the model of Coulaloglou and Tavlarides (1977) as breakage model; comparison with experimental results (◊)

a. Vsg= 0.00415 m/s

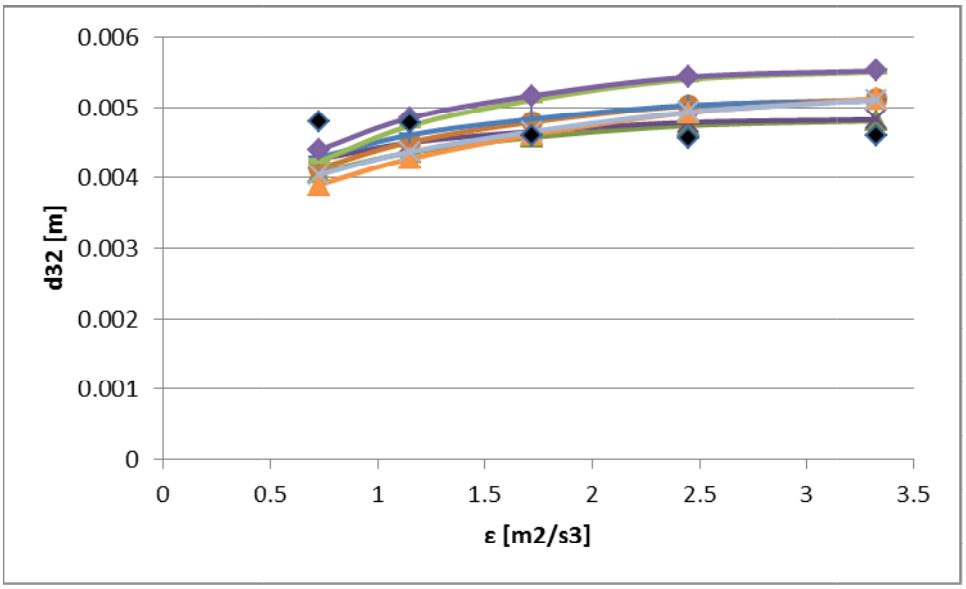

Figura 29 Sauter mean diameter predicted by different set of kernels considering the model of Coulaloglou and Tavlarides (1977) as breakage model; comparison with experimental results (◊)

b. Vsg= 0.0415 m/s

Other combinations that showed acceptable results considered the breakage model of Laakkonen et al. (2006) and the coalescence efficiency of Coulaloglou and Tavlarides (1977), leading to a mean error equal to 14%. In this case, the Sauter mean diameter calculated by these models slightly decreased at high values of turbulent dissipation rate, while the experimental trend was less pronounced(Fig.27-28). On the other side, considering the coalescence efficiency model for inertial collisions proposed by Chesters (1991) and maintaining the same breakage model, the predicted bubble size was still close to the experimental data with a mean error of approximation again equal to 14% and a slight different effect of superficial gas velocity (Fig.30-31).

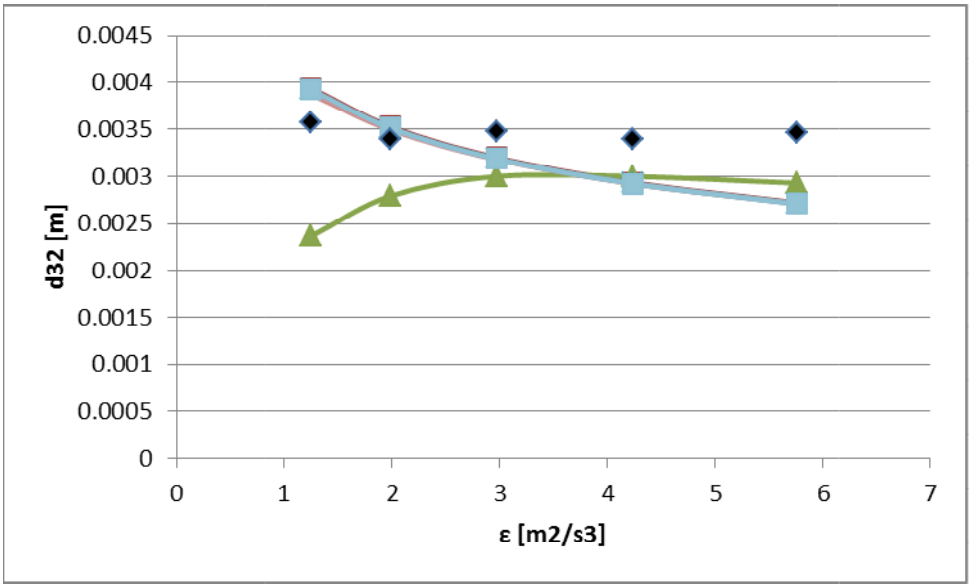

Figura 30 Sauter mean diameter versus Turbulent dissipation rate predicted by experiments (◊) and by the sets of kernles considering BM: Laakkonen et al. (2006), CF: Prince and Blanch (1990), CE: Coulaloglou and Tavlarides (1977) (□) and Chesters (1991) (Δ)

a. Vsg= 0.00415 m/s

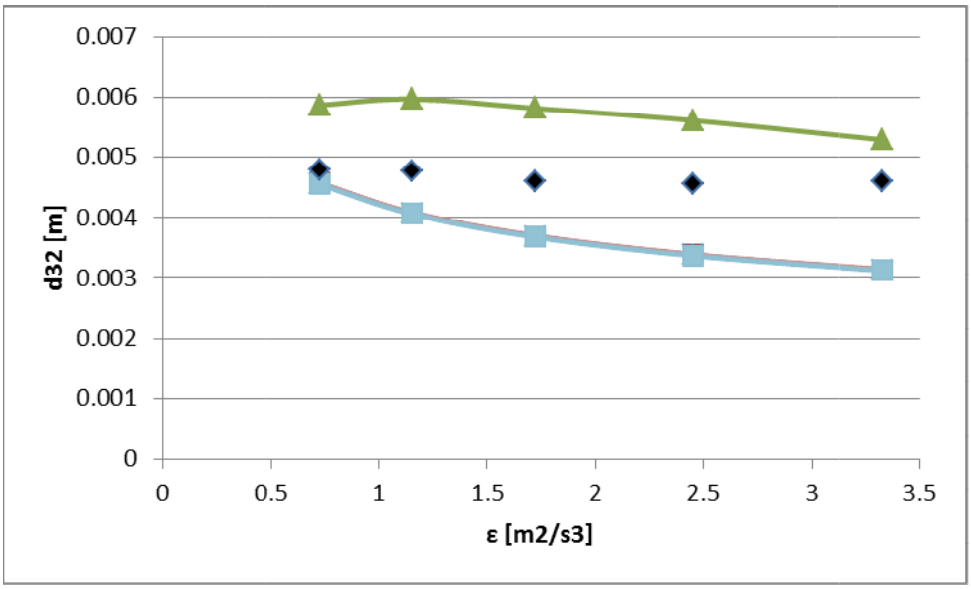

Figura 31 Sauter mean diameter versus Turbulent dissipation rate predicted by experiments (◊) and by the sets of kernles considering BM: Laakkonen et al. (2006), CF: Prince and Blanch (1990), CE: Coulaloglou and Tavlarides (1977) (□) and Chesters (1991) (Δ)

b. Vsg= 0.0415 m/s

After modifying the coalescence term by adding the correction factor, some models seemed to be promising (low mean error of approximation), but they were still not perfect since they predicted a different effect of the gas hold up or turbulent dissipation rate, as shown in the graphs above. Therefore, in order to obtain results that could be as much as possible in accordance with the experimental data, a new type of modification was introduced in the coalescence term. The new corrective factor consisted of a function of the only gas holdup ($\pi=f(\alpha_g)$) and it was introduced in order to modify the effect of gas holdup itself of the models. Therefore, many expressions of this function have been tried empirically to find a good shape one that could lead a model to fit perfectly the experimental data.

In particular, this correction function was applied to the set of kernels found by Gemello (2018) for bubble columns in order to see whether or not these models were also capable of fitting the experimental results of stirred tanks measured by Cappello (2019), just by modifying the effect of gas holdup of the coalescence kernel.

Although different expressions for the corrective function have been tried, none of those has been able to provide good results. Hence, another approach was tried.

Since the set of kernels that considers the breakage model of Laakkonen et al. (2006), the collision frequency proposed by Prince and Blanch (1990) and the coalescence efficiency of Coulaloglou and Tavlarides (1977) seemed promising, we tried to change the value of the constant within the Coulaloglou and Tavlarides (1977) model in order to see the effect.

As possible to notice from the graphs below, good results have been obtained by using a constant equal to $1.5*10^8$,leadin to a mean error of approximation equal to 5% (Fig.32-35).

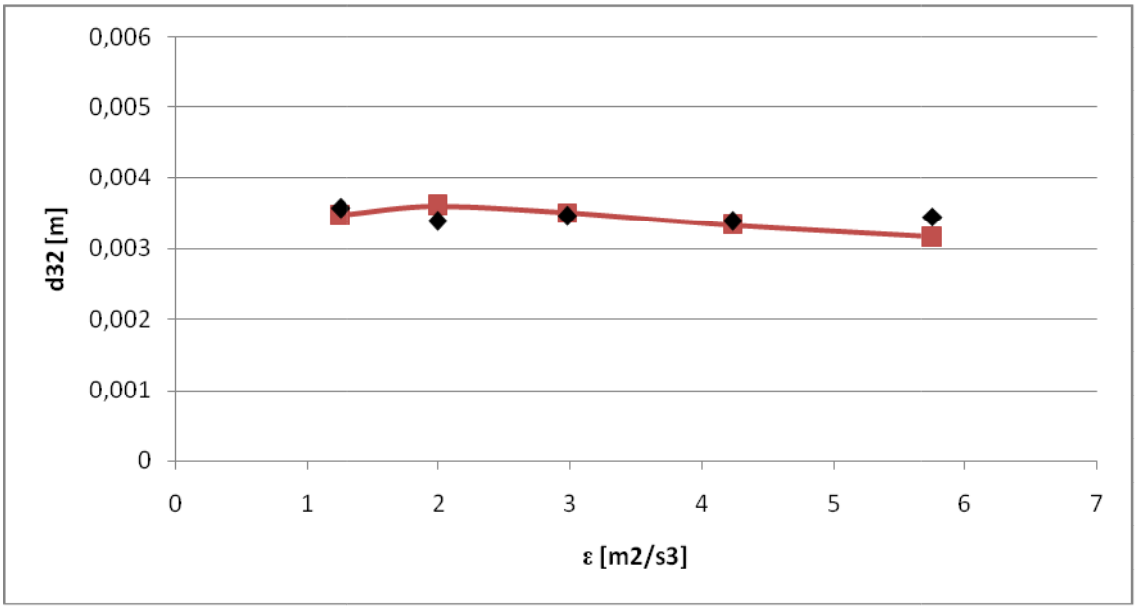

Figura 32 Sauter mean diameter versus Turbulent dissipation rate predicted by experiments (◊) and by the set of kernles considering BM: Laakkonen et al. (2006), CF: Prince and Blanch (1990), CE: modified Coulaloglou and Tavlarides (1977) (□)

a. Vsg= 0.00415 m/s

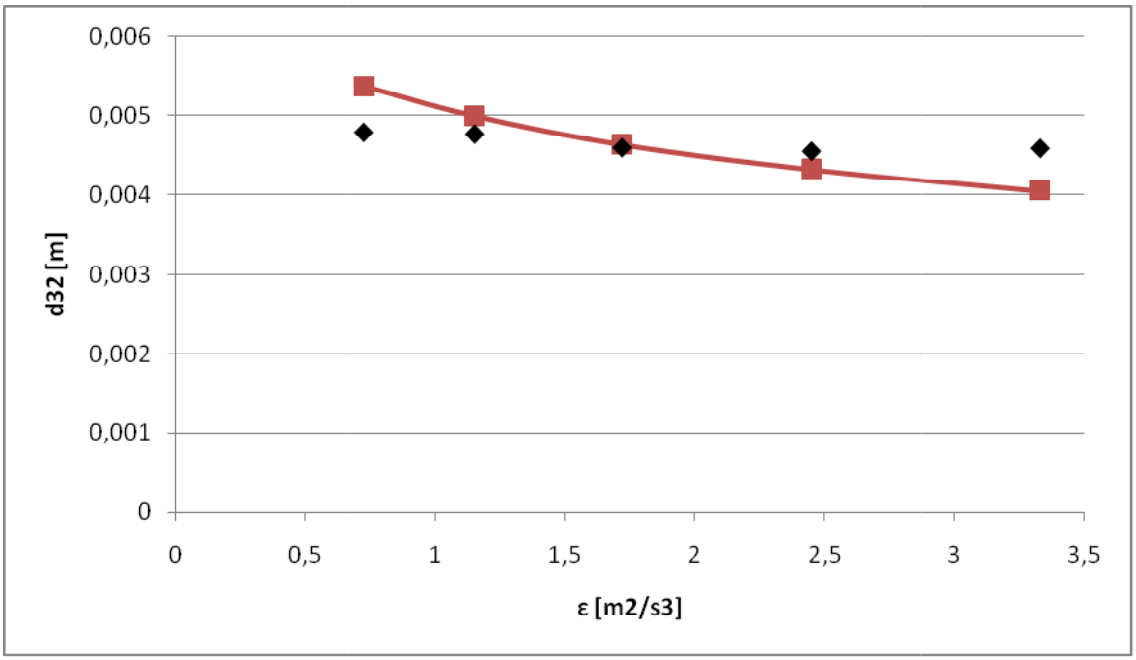

Figura 33 Sauter mean diameter versus Turbulent dissipation rate predicted by experiments (◊) and by the set of kernles considering BM: Laakkonen et al. (2006), CF: Prince and Blanch (1990), CE: modified Coulaloglou and Tavlarides (1977) (□)

b. Vsg= 0.0415 m/s

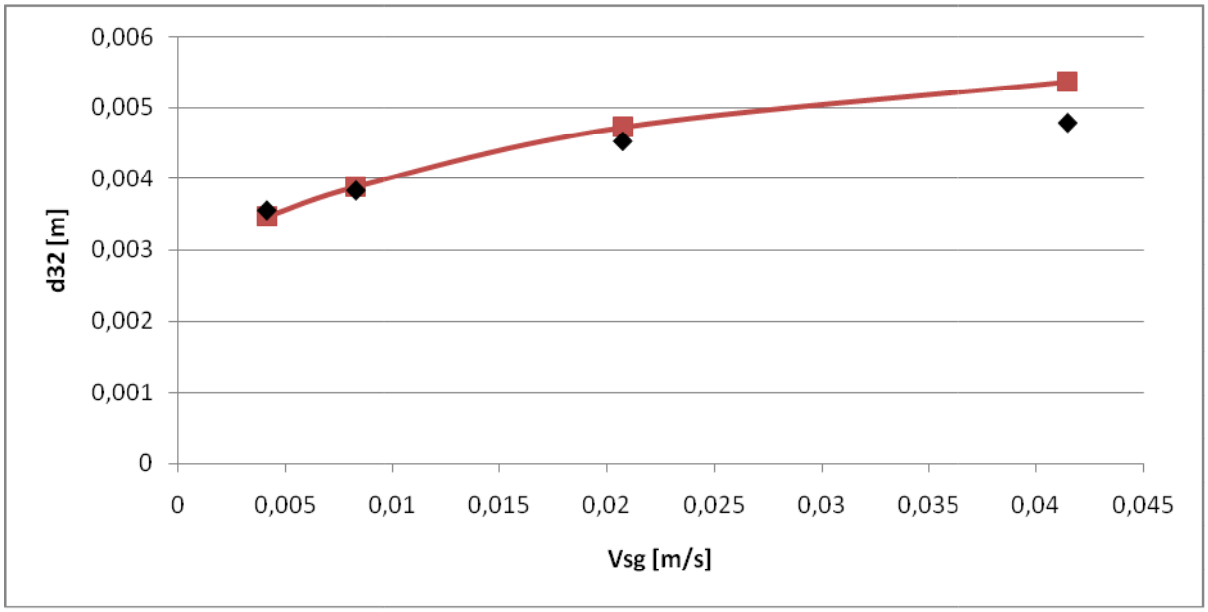

Figura 34 Sauter mean diameter versus superficial gas velocity predicted by experiments (◊) and by the set of kernles considering BM: Laakkonen et al. (2006), CF: Prince and Blanch (1990), CE: modified Coulaloglou and Tavlarides (1977) (□)

a. N= 600 rpm

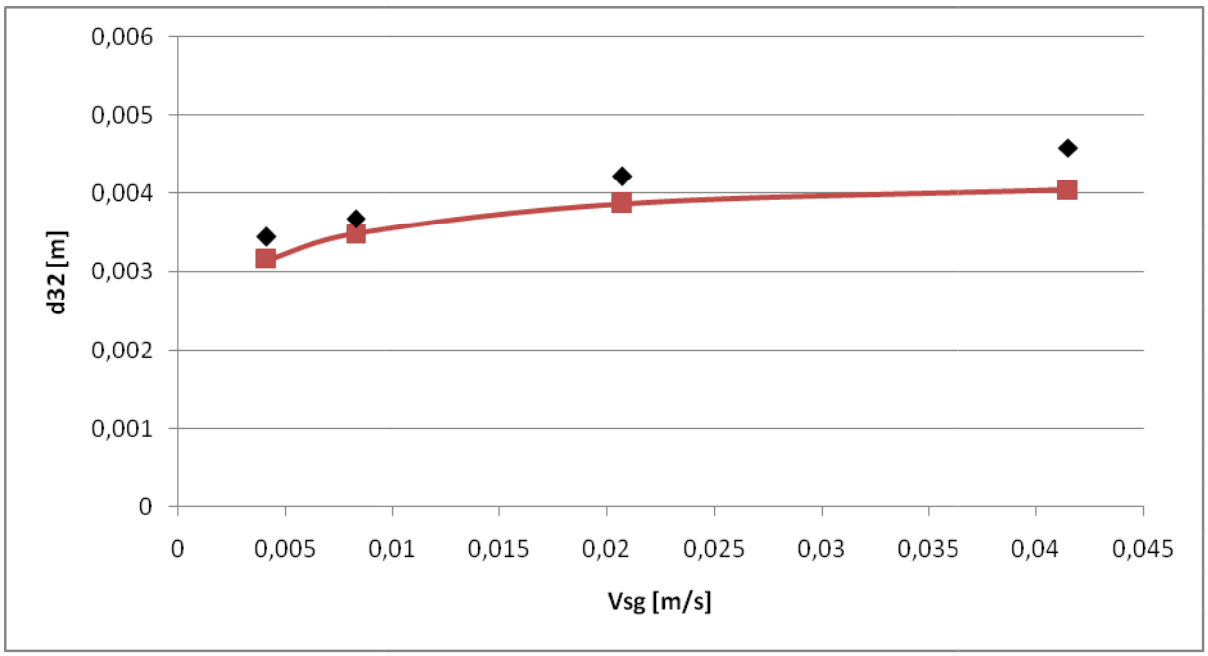

Figura 35 Sauter mean diameter versus superficial gas velocity predicted by experiments (◊) and by the set of kernles considering BM: Laakkonen et al. (2006), CF: Prince and Blanch (1990), CE: modified Coulaloglou and Tavlarides (1977) (□)

b. N= 997 rpm

The following table summarize the set of kernels capable of reproducing the experimental data in stirred tanks:

Breakage Model	$g(L) = c_3\varepsilon^{1/3} erfc\left(\sqrt{c_4\frac{\sigma}{\rho_l\varepsilon^{2/3}L^{5/3}} + c_5\frac{\mu_l}{\sqrt{\rho_g\rho_l}\varepsilon^{1/3}L^{4/3}}}\right)$	c3=4; c4=0.04; c5=0.01

Collision Frequency	$h_0(L_1,L_2) = C'_1(L_1+L_2)^2\varepsilon^{1/3}\sqrt{L_1^{2/3}+L_2^{2/3}}$	c'1=0.24
Coalescence Efficiency	$\lambda(L_1,L_2) = exp\left[-C''_1\frac{\mu_l\rho_l\varepsilon}{\sigma^2}\left(\frac{L_1L_2}{L_1+L_2}\right)^4\right]$	c''1=1.5e^8

Tabella 10 set of kernels suitable for stirred tanks

The same results could be obtained by considering the coalescence efficiency model of Chesters (1991) for viscous collisions, instead of the kernel of Coulaloglou and Tavlarides (1977) as these two models have almost the same expression.

After finding out the right models capable of predicting the Sauter mean diameter in each gas-liquid system (both bubble columns and stirred tanks), the idea was to find a common set of kernel that could describe both the systems. Therefore, all the models that seemed to be promising after a first screening were tested in order to find the right one. In particular, for this part of the work, we tested the set of kernels found by Gemello (2018) for bubble columns, the one found in this work for stirred tank reactors and also the set of kernels composed by the breakage model of Laakkonen et al. (2006), the modified collision frequency of Prince and Blanch (1990) and the coalescence efficiency for inertial collisions proposed by Chesters (1991). The latter model was taken into account since it considers an effect of the turbulent dissipation rate that is in between the coalescence efficiency of Coulaloglou and Tavlarides (1977) and the one proposed by Lehr et al. (2002) that have been found to be valid for stirred tanks and bubble columns, respectively.

In order to fit the results of both the systems, different modifications of the coalescence terms have been tried: by adding a correction factor, by modifying the constant inside the models or by adding a corrective function as described above.

The following graphs (Fig.36-38) show the results obtained by applying the set of kernels found by Gemello (2018); in this case the mean error of approximation is about 18%. Regarding stirred tanks plots, it is possible to notice that the set of kernels is still not able to predict exactly the same bubble size that is obtained with the experimental results, in fact the curve profile is too pronounced and a modification that considers a different effect of Vsg should be applied.

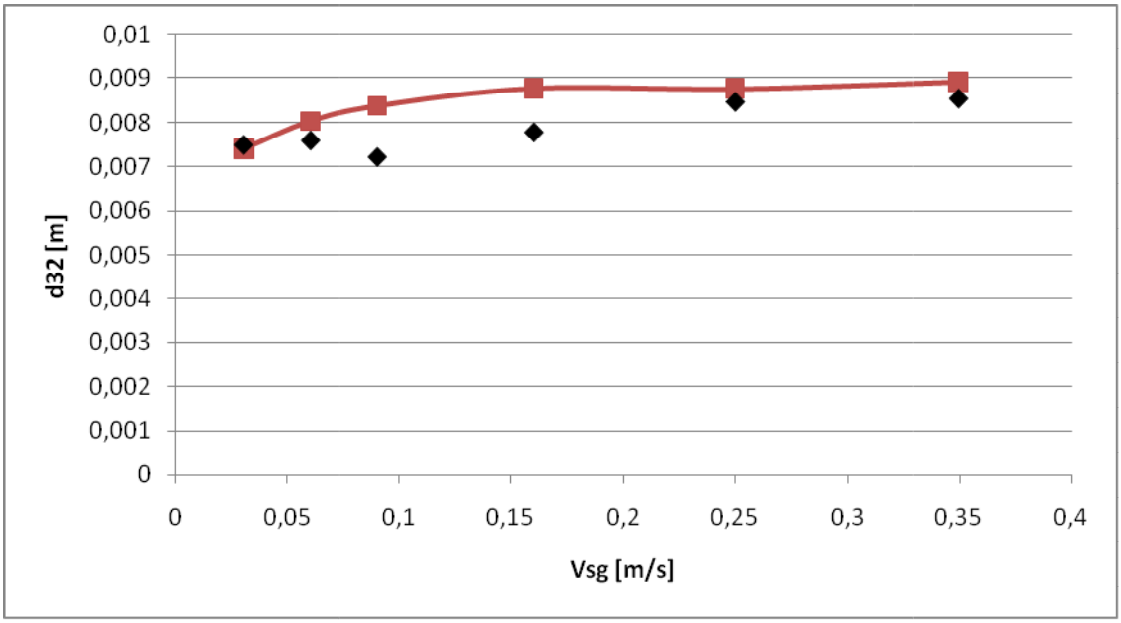

Figura 36 Sauter mean diameter versus superficial gas velocity predicted by experiments (◊) and by the set of kernles considering BM: Laakkonen et al. (2006), CF: Wang et al. (2005b), CE: Lehr et al. (2002) (□) for bubblecolumns

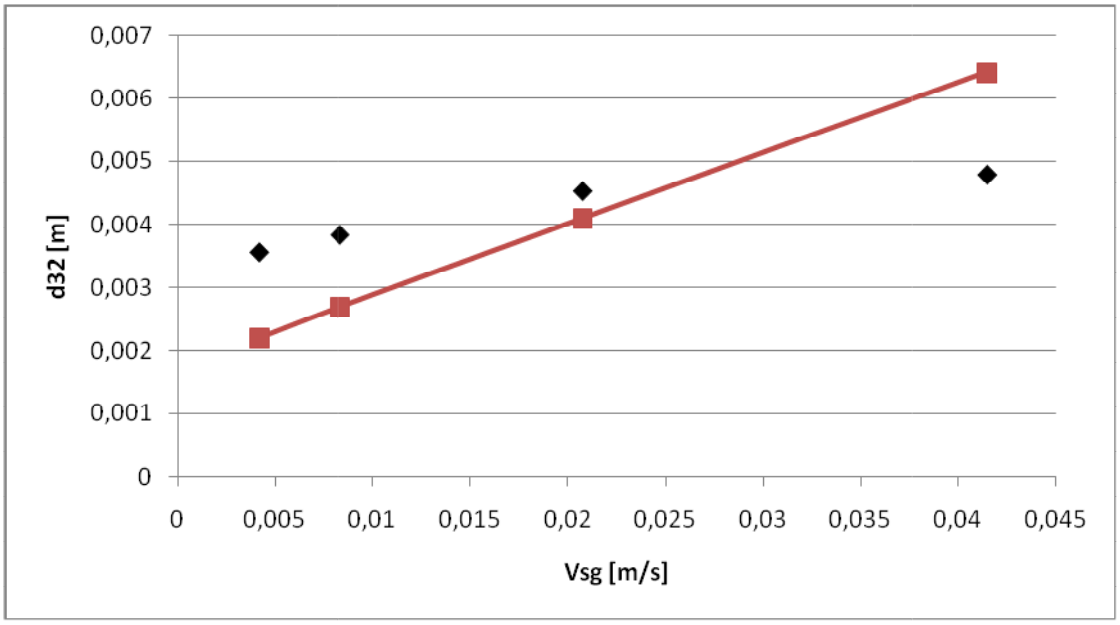

Figura 37 Sauter mean diameter versus superficial gas velocity predicted by experiments (◊) and by the set of kernles considering BM: Laakkonen et al. (2006), CF: Wang et al. (2005b), CE: Lehr et al. (2002) (□) for stirred tanks

a. N= 600 rpm

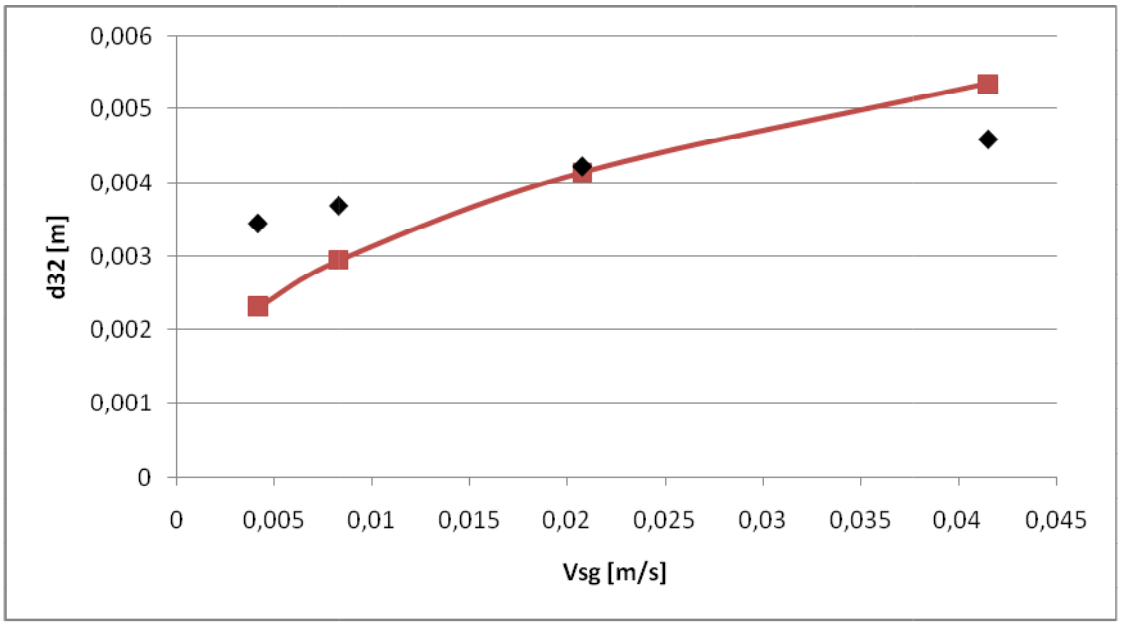

Figura 38 Sauter mean diameter versus superficial gas velocity predicted by experiments (◊) and by the set of kernles considering BM: Laakkonen et al. (2006), CF: Wang et al. (2005b), CE: Lehr et al. (2002) (□) for stirred tanks

b. N= 997 rpm

Regarding the set of kernels found in this work for stirred tanks (breakage kernel of Laakkonen et al. (2006), collision frequency by Prince and Blanch (1990) and coalescence efficiency of Coulaloglou and Tavlarides (1977)), we tried to modify the constant inside the efficiency model in order to fit the experimental data of both the systems, leading to a mean error of 15% by using a constant equal to $2*10^7$; with these models the curves profiles are still not in perfect agreement with the experimental trends: too pronounced effect of Vsg predicted by the model for the case of bubble columns, whereas a decreasing trend is obtained for bubble columns, as possible to notice in the graphs below (Fig.39-41).

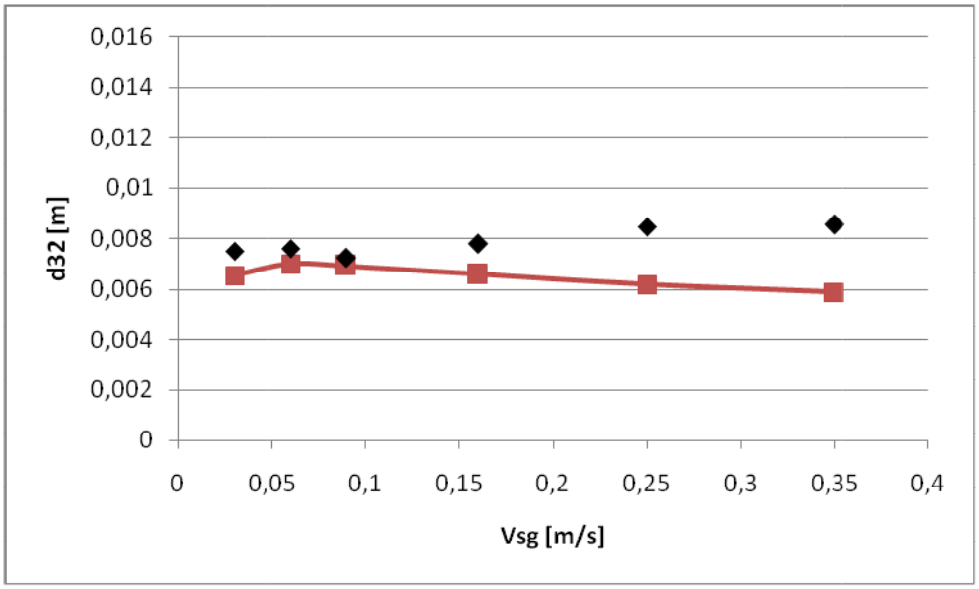

Figura 39 Sauter mean diameter versus superficial gas velocity predicted by experiments (◊) and by the set of kernles considering BM: Laakkonen et al. (2006), CF: Prince and Blanch (1990), CE: modified Coulaloglou and Tavlarides (1977) (□) for bubble columns

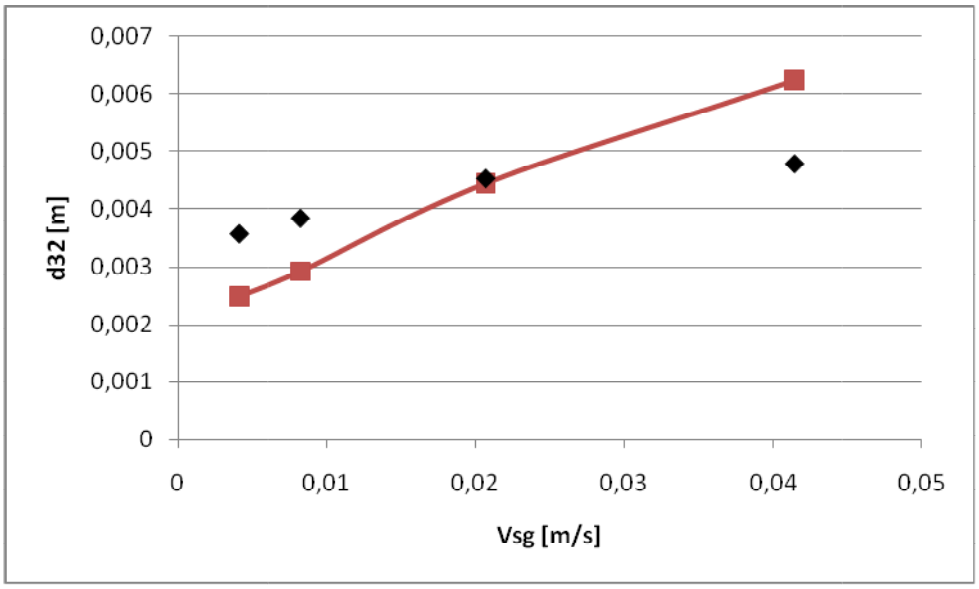

Figura 40 Sauter mean diameter versus superficial gas velocity predicted by experiments (◊) and by the set of kernles considering BM: Laakkonen et al. (2006), CF: Prince and Blanch (1990), CE: modified Coulaloglou and Tavlarides (1977) (□) for stirred tanks

a. N=600 rpm

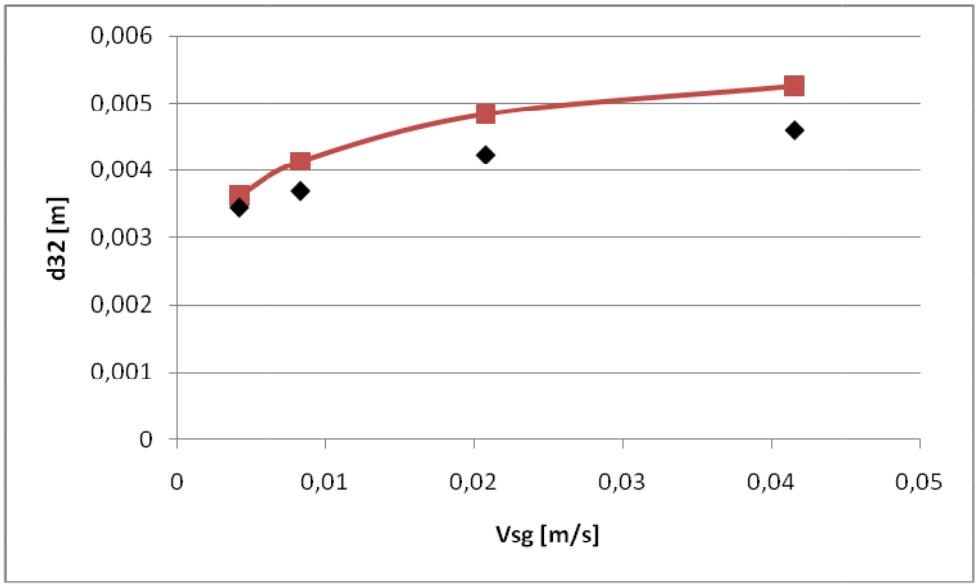

Figura 41 Sauter mean diameter versus superficial gas velocity predicted by experiments (◊) and by the set of kernles considering BM: Laakkonen et al. (2006), CF: Prince and Blanch (1990), CE: modified Coulaloglou and Tavlarides (1977) (□) for stirred tanks

b. N=997 rpm

The set of kernels mentioned above that consider the coalescence efficiency by Chesters (1991) for inertial collision seemed to give the best agreement with experimental results relatively to the models analyzed (mean error of approximation equal to 13%). In fact, by looking at the graphs (Fig.42-44) it is possible to notice that the curves are close to the experimental profile for both the systems, even if the slope of the curve is too pronounced for the case of stirred tanks.

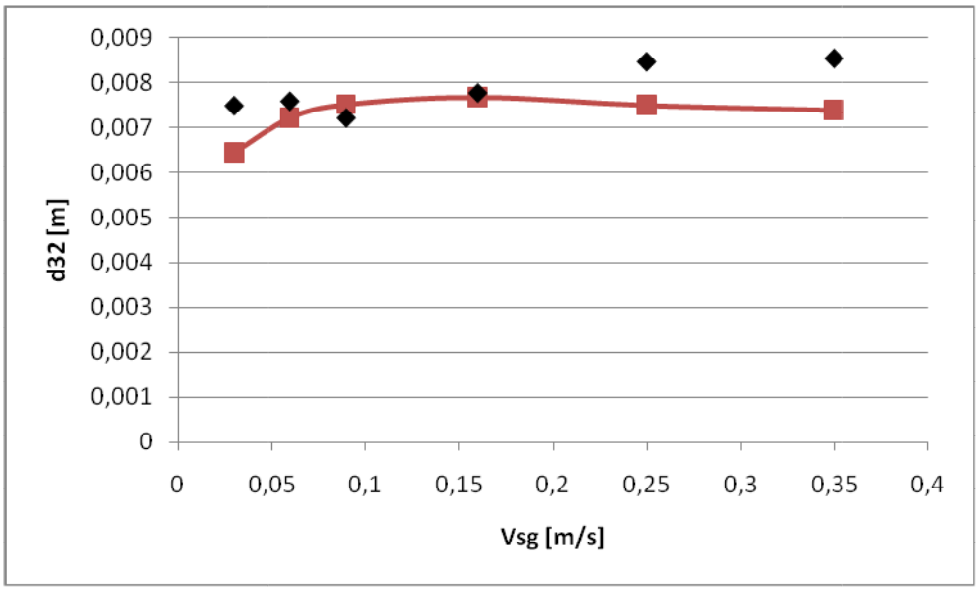

Figura 42 Sauter mean diameter versus superficial gas velocity predicted by experiments (◊) and by the set of kernles considering BM: Laakkonen et al. (2006), CF: Prince and Blanch (1990), CE: Chesters (1991) (□) for bubble columns

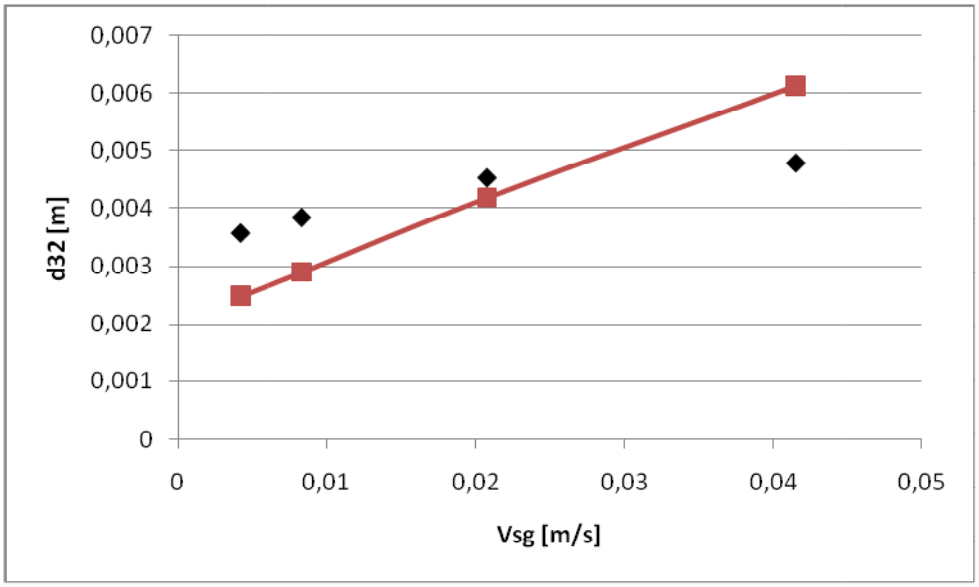

Figura 43 Sauter mean diameter versus superficial gas velocity predicted by experiments (◊) and by the set of kernles considering BM: Laakkonen et al. (2006), CF: Prince and Blanch (1990), CE: Chesters (1991) (□) for stirred tanks

a. N= 600 rpm

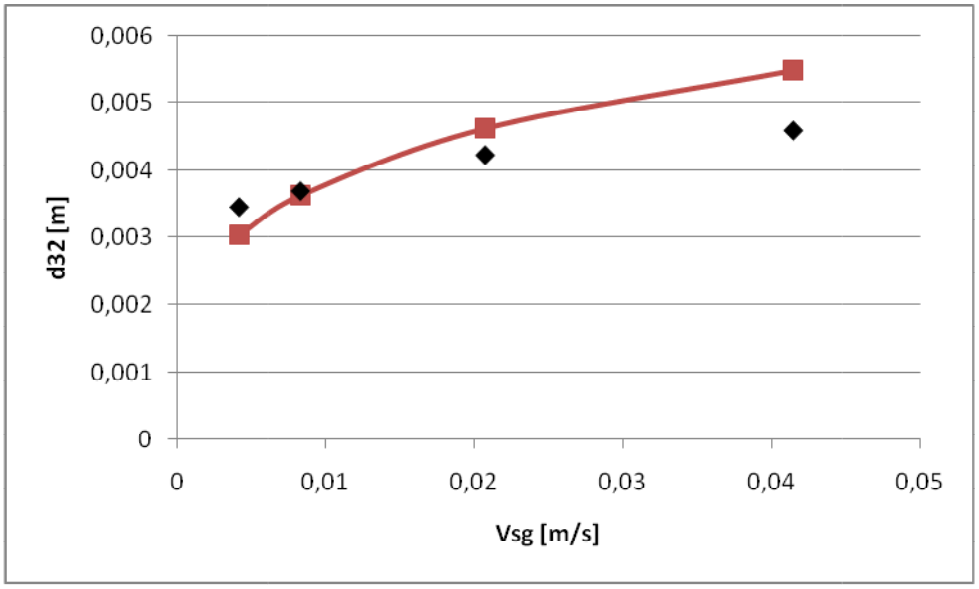

Figura 44 Sauter mean diameter versus superficial gas velocity predicted by experiments (◊) and by the set of kernles considering BM: Laakkonen et al. (2006), CF: Prince and Blanch (1990), CE: Chesters (1991) (□) for stirred tanks

b. N= 997 rpm

Other sets of kernels have also been tested, but those did not give interesting results and for this reason they have not been showed.

The study done above allows to make some conclusions about the common model: as previously stated, the set of kernels that consider the coalescence efficiency by Chesters (1991) for inertial collision seemed to give the best agreement with experimental results compared to the other models analyzed. This behavior could be explained by the fact that the effect of the turbulent dissipation rate considered by the model is in between the effect considered by the coalescence efficiency of Coulaloglou and Tavlarides (1977) and the one of Lehr et al. (2002) which have been found to describe very well stirred tanks and bubble columns, respectively. For this reason, to obtain better

results, it could be possible trying other coalescence efficiency kernels that consider a different effect of turbulent dissipation rate.
The following table summarize the set of kernels that describes quite well both the systems:

Breakage Model	$g(L) = c_3 \varepsilon^{1/3} erfc\left(\sqrt{c_4 \frac{\sigma}{\rho_l \varepsilon^{2/3} L^{5/3}} + c_5 \frac{\mu_l}{\sqrt{\rho_g \rho_l} \varepsilon^{1/3} L^{4/3}}}\right)$	c3=4; c4=0.04; c5=0.01
Collision Frequency	$h_0(L_1, L_2) = C'_1 (L_1 + L_2)^2 \varepsilon^{1/3} \sqrt{L_1^{2/3} + L_2^{2/3}}$	c'1=0.2
Coalescence Efficiency	$\lambda(L_1, L_2) = \exp\left(-\sqrt{\frac{\rho_l \varepsilon^{2/3} L^{5/3}}{4\sigma}}\right)$	—

Tabella 11 common set of kernels for either the systems

5.1.3.2 Gas-liquid flows with complex physical properties

After testing and validating breakage and coalescence models in air-water systems, we tried to have a view of their use in complex systems of organic type. In particular, the idea was to verify whether or not the set of kernels that has been validated for the case of air-water bubble columns, was still valid for other flows with different physical properties. If the response had been positive, it would have meant that these kernels are universal models capable of describing a wide range of operating conditions, physical properties and kind of fluids.

Therefore, we applied the set of kernels found by Gemello (2018) to two different organic liquids: heptane at different pressures andcyclohexane. The experimental results obtained by Chaumat et al. (2007) and by IFP-NT VonnerRoesler (2018) respectively for cyclohexane and heptane have been used as a database for model validation.

In the following table (Tab. 12) the main physical properties of the gas-liquid flows are reported in order to see easily the differences with air-water system and understand the results.

Gas-liquid flow	Pressure [atm]	Liquid density [kg/m3]	Gas density [kg/m3]	Superficial tension [N/m]	Liquid viscosity [Pa s]
Air-water	1	999	1.18	0.072	1.00e-3
Nitrogen-heptane	1	686	1.17	0.02	3.91e-4
Nitrogen-heptane	9	686	10.8	0.021	3.94e-4
Nitrogen-cyclohexane	1	779	1.18	0.02495	1.02e-3

Tabella 12 physical properties of the analyzed gas-liquid flows

The results showed that the set of kernel that gave good fitting of air-water experimental data, did not give the same agreement with the other liquids. In fact, as reported in the graphs below (Fig.45-46) for the case of heptane at different pressures, the models were not able to fit the experimental results, leading to a completely wrong trend. The kernels, in fact, predicted too small bubbles size at low superficial gas velocity and too big bubbles size at high Vsg, but it was not possible to understand from these simulations whether this behavior is due to the coalescence or the breakage phenomena.

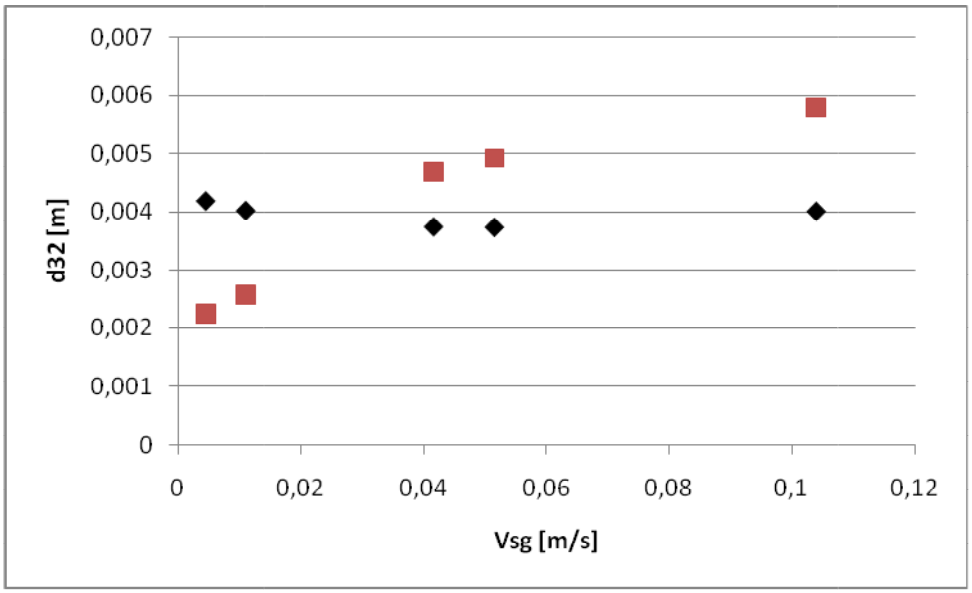

Figura 45 Sauter mean diameter versus superficial gas velocity predicted by experiments (◊) and by the set of kernles considering BM: Laakkonen et al. (2006), CF: Wang et al. (2005b), CE: Lehr et al. (2002) (□) for gas-liquid system with heptane at 1 atm as liquid phase

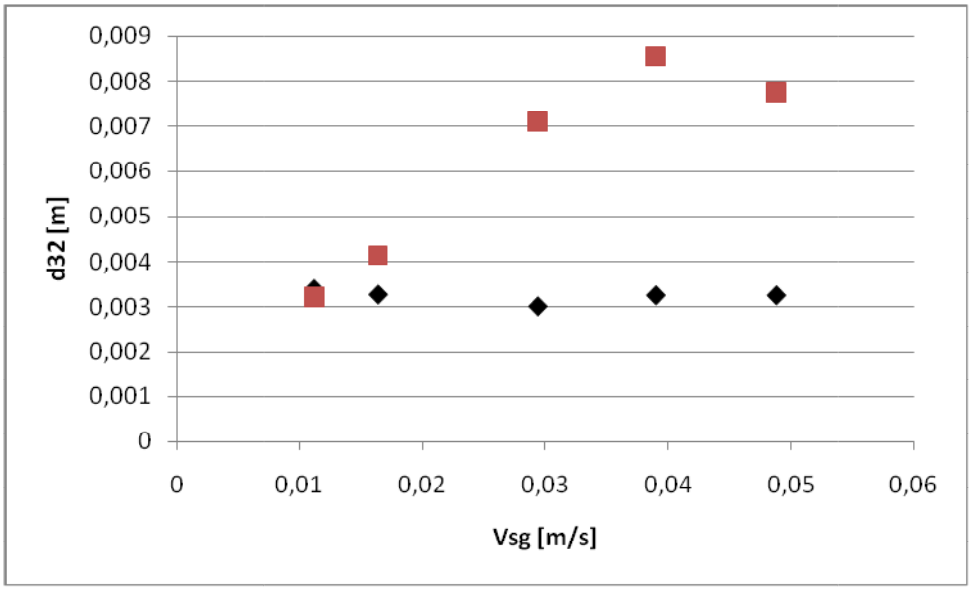

Figura 46 Sauter mean diameter versus superficial gas velocity predicted by experiments (◊) and by the set of kernles considering BM: Laakkonen et al. (2006), CF: Wang et al. (2005b), CE: Lehr et al. (2002) (□) for gas-liquid system with heptane at 9 atm as liquid phase

In order to understand the reason of this behavior, we focused our attention on the breakage term since it is the only one that takes into account the different physical properties (the coalescence term does not). The breakage model here used is the one proposed by Laakkonen et al. (2007) and it is possible to distinguish two terms inside the model itself: one considers the effect of superficial tension and the other takes into account the liquid phase viscosity. Hence the two terms were plotted separately and compared to the values obtained with the air-water system in order to understand why this set of kernels applied very well to this system and not to the organic liquids(Fig.47-48).

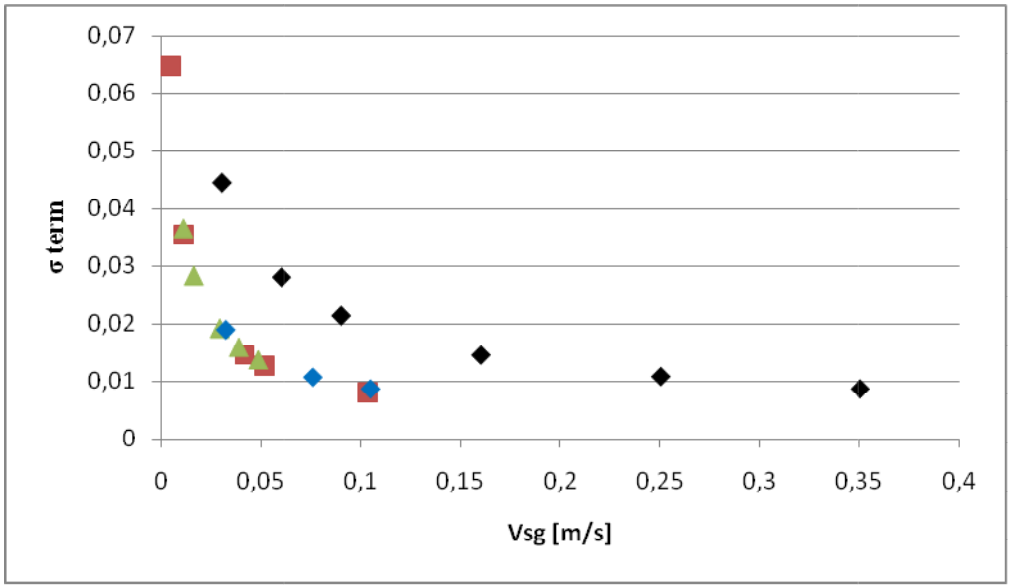

Figura 47 term that considers the superficial tension versus Vsg for water (black ◊), cyclohexane (blue ◊), heptane at 1 atm (□) and heptane at 9 atm (Δ)

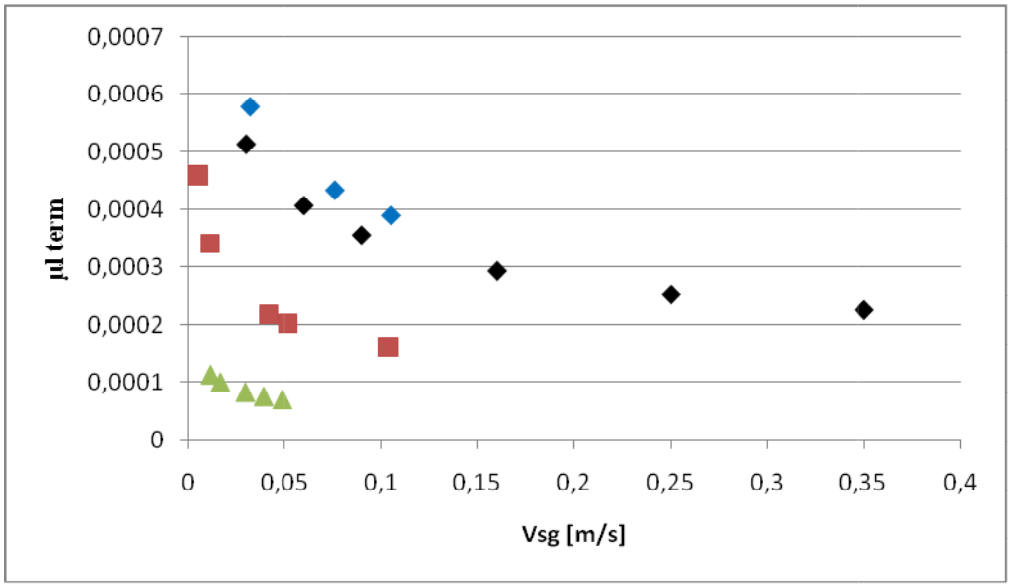

Figure 2 term that considers the liquid phase viscosity versus Vsg for water (black ◊), cyclohexane (blue ◊), heptane at 1 atm (□) and heptane at 9 atm (Δ)

As it is possible to notice, in both the cases the term that takes into account the superficial term is dominant, but compared to the values of water, the values for the organic liquids are almost one order of magnitude lower, and this means that the breakage term of water is smaller than the one of organic liquids, leading to bigger bubbles in accordance with the experimental observation (see Fig.48 below):

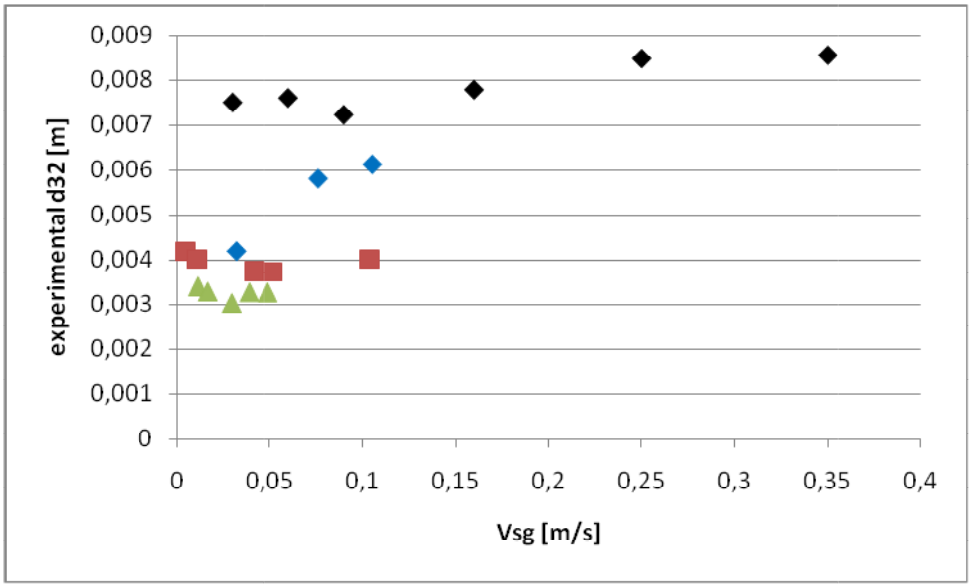

Figura 48 experimental observations of d32 versus Vsg for water (black ◊), cyclohexane (blue ◊), heptane at 1 atm (□) and heptane at 9 atm (Δ)

Anyway, this analysis is still not able to explain why the analyzed set of kernels is not able to include the effect of more complex physical properties and, in order to fit the experimental results, it is necessary to modify the value of the constants inside the breakage model of Laakkonen et al. (2007).Modifying the fitting constants means that the model found by Gemello for air-water systems is not universal as we hoped, because for each system the value of the constants is different.
Therefore, a more in-depth study is required to understand better this behavior and find a set of kernels capable of predict the bubble size for a wider range of physical properties and gas-liquid flows, perhaps by doing experiments on these system and investigating breakage and coalescence phenomena

separately. In fact, a future work could be focused initially only on the breakage phenomena and then the study of the coalescence could done using coalescing and non-coalescing systems.

5.2 II Part: CFD Simulations

After testing the models by 0D simulations, the set of kernel that gave the best agreement with the experimental results have been implemented in a CFD code (Ansys Fluent).

The stirred tank reactor used in this part of the work is the one simulated by Cappello (2019) as presented in his PhD thesis; geometry, meshes and all the other models used by the author itself to study the hydrodynamic within the vessel have been unchanged. That means an Euler-Euler approach have been adopted for describing the fluid-dynamics in the reactor instead of the Euler-Lagrange approach.

The latter one is also known as Discrete bubble model and is based on the theory that the liquid phase represents the continuous phase, while the gas phase is the discontinuous one. In particular, the continuous phase is treated by solving the time-averaged Navier-Stokes equations, while the equation of motion Newton for the dispersed phase is solved for each particle individually by tracking explicitly the particles themselves. The gas phase as dispersed phase can exchange momentum, mass and also energy with the liquid phase. The problem related to this approach is that the gas phase is described by tracing several inclusions, through the solution of a motion equation, but the number of inclusions that could be tracked is limited. Hence this approach is appropriate just for cases of small tanks or for conditions of low gas volume fraction (<10-15%). Since in this work wedeal also with higher values of gas volume fraction, this approach is discharged and the Euler-Euler approach is applied for this analysis.

In the theory of the Euler-Euler model, both the continuous and the dispersed phases are considered as interpenetrating continua and the concept of volume fractions for each phase is introduced since the volume of a phase cannot be occupied by the others. For each phase conservation equations are solved: the continuity equation that represents the local conservation of mass and the Navier-Stokes equation for the local conservation of momentum (assuming no mass transfer between the phases) (Petitti et al., 2010):

$$\frac{\partial \rho}{\partial t} + \nabla \rho \boldsymbol{u} = 0$$

$$\frac{\partial (\rho \boldsymbol{u})}{\partial t} + \nabla \cdot (\rho \boldsymbol{u}\boldsymbol{u}) + \nabla p = \nabla \cdot \boldsymbol{T} + \boldsymbol{g} + \boldsymbol{F}$$

Where **u** is the averaged velocity of the phase and can be calculated by solving the momentum balance equation. **g** represents the gravitational acceleration, **F** is the interfacial forces term and **T** is the viscous stress tensor and is equal to:

$$\boldsymbol{T} = \mu \left[\nabla \boldsymbol{u} + (\nabla \boldsymbol{u})^T - \frac{2}{3} \nabla \cdot \boldsymbol{u} \boldsymbol{I} \right]$$

Where **I** is the identity matrix and μ represents the viscosity and is the sum of the turbulent and the molecular viscosities.

The Euler-Euler approach includes three different multiphase models:

1. The volume of fluid (VOF) model, which tracks the surface of a fixed Eulerian mesh. In this model, a unique set of momentum equations is shared by the fluids and the volume fraction of each phase is tracked throughout the domain in each computational cell;
2. The Mixture model, which solves for the mixture momentum equation and prescribes relative velocities to describe the dispersed phase;
3. The Eulerian model, that solves a set of n conservation equations for each phase, while a single pressure is shared by the phases.

The Eulerian model is the one used in this work. The advantage of this model is that the number of secondary phases is just limited by memory requirements or convergence behavior.
As previously mentioned, with this approach the concept of phasic volume fractions α_q has to be introduced and represents the space occupied by each phase in the vessel.
The volume of the phase q is defined as:

$$V_q = \int_V \alpha_q dV$$

Where

$$\sum_{q=1}^{n} \alpha_q = 1$$

The conservation equations that define fluid flows are calculated for each phase separately and are represented as follows.
The continuity equation for the phase q is:

$$\frac{\partial(\alpha_q \rho_q)}{\partial t} + \nabla \cdot \left(\alpha_q \rho_q \boldsymbol{u}_q\right) = \sum_{p=1}^{n} (\dot{m}_{pq} - \dot{m}_{qp})$$

Where $\mathbf{u}_q$ is the velocity of the phase q and $\dot{m}_{pq}$ represents the mass transfer from the phase p to the phase q.
The equation for momentum conservation for the phase q is:

$$\frac{\partial(\alpha_q \rho_q \boldsymbol{u}_q)}{\partial t} + \nabla \cdot \left(\alpha_q \rho_q \boldsymbol{u}_q \boldsymbol{u}_q\right) = -\alpha_q \nabla p + \nabla \cdot \left(\alpha_q \boldsymbol{\tau}_q\right) + \alpha_q \rho_q \boldsymbol{g} + \sum_{p=1}^{n} \left(\dot{m}_{pq} \boldsymbol{u}_{pq} - \dot{m}_{qp} \boldsymbol{u}_{qp}\right) + \boldsymbol{F}$$

Where τ_q is the stress-strain tensor for the phase q.
If $\dot{m}_{pq}>0$ (namely phase p mass is being transferred to phase q), $\mathbf{u}_{pq}=u_p$; while if $\dot{m}_{pq}<0$ (phase q mass is transferred to phase p), $\mathbf{u}_{pq}=u_q$. Likewise for the case of $\dot{m}_{qp}$.
The interphase forces term **F** includes all the different forces that can appear in a gas-liquid system.

Interfacial forces

Dispersed gas-liquid systems are characterized by interfacial forces between the two phases and, for reason, they must be studied. Among these forces we can find:

- Drag force;
- Lift force;
- Virtual mass force;
- Turbulent Dispersion force;
- Wall Lubrication force.

The drag force is considered to be the controlling one in this kind of systems and usually the others are neglected.
The Lift force acts on a bubble mainly due to velocity gradients in the continuous phase flow field, since the dispersed phase is affected by a force acting perpendicularly to the flow direction.
Whether or not including the Lift force in CFD simulations of gas-liquid systems under heterogeneous regime is still an open question as many different opinions and results are available in the literature about this topic. For this reason, in general the Lift force is neglected as done in this work.
Another interfacial force is the Virtual mass force that occurs when there is a relative acceleration between the two phases. The liquid phase mass exerts a virtual force on the bubbles that accelerate

relative to the continuous phase (Gemello et al., 2018). The Virtual mass force becomes important when the difference between the densities of the two phases increases. In this work, a constant virtual mass force coefficient is considered in order to simplify the CFD code.
The Wall Lubrication force acts in the direction normal to the wall and pushes the secondary phases away from walls. Likewise the previous forces, the Wall Lubrication force has been neglected in this work.
The last force included in the interphase forces term is the Turbulent Dispersion force which accounts for the interphase turbulent momentum transfer and it is obtained by averaging the instantaneous drag over time. This force acts as a turbulent diffusion in the dispersed flows.
Since Turbulent Dispersion force acts as a turbulent diffusion in dispersed flows, the option "diffusion in vof" was adopted in this work.

Drag force

In several works this force is considered as the main contribution to the interfacial force term, while the other forces presented above are often neglected.
The drag force represents the resistance force caused by the rising motion of the bubble through the liquid. It is opposed to the buoyancy force when bubbles go upwards vertically within the stirred tank reactor. This force influences the relative velocity of the bubbles and also the gas volume fraction.
Since this is a two fluid system (liquid as continuous phase, while gas as dispersed phase), the drag force can be calculated as:

$$F_{D,q} = K_{pq}(\boldsymbol{u}_p - \boldsymbol{u}_q)$$

Where p is the dispersed phase and q the continuous one. The term K_{pq} represent the exchange coefficient between the two phases and can be written in the following general form:

$$K_{pq} = \frac{C_D Re_b A_i \mu_q}{8 d_p}$$

Where C_D represents the drag coefficient and it is defined in different ways for the different exchange-coefficient models available in literature; A_i is the interfacial area between phases per unit mixture volume and the Reynolds number for bubbles takes into account the relative velocity between the bubble and the surrounding liquid:

$$Re_b = \frac{\rho_q(\boldsymbol{u}_p - \boldsymbol{u}_q)d_p}{\mu_q}$$

Different drag models are available in the literature for different operating conditions, different shapes of the bubbles (spherical or deformed) and also drag laws that consider the effect of water contamination. Among all these drag laws, the software ANSYS Fluent (used in this work to run the CFD simulations) provides the following ones.
The default model, acceptable for general use, is the one proposed by Schiller and Naumann (1935) and can be expressed as:

$$C_D = \begin{cases} \frac{24}{Re_b}\left(1 + 0.15\, {Re_b}^{0.687}\right) \\ 0.44 \end{cases}$$

Where the first part of the equation is valid for $Re_b \leq 1000$, while a constant value is considered for $Re_b \geq 1000$.
The model of Morsi and Alexander (1972) is also available and is the most complete since it adjusts the C_D definition over a large range of Reynolds numbers, but it could lead to less stable calculations.
The symmetric model uses values of density and viscosity calculated from volume averaged properties and is recommended for systems where the secondary phase in one region of the domain becomes the primary one in another

Another one is the Grace et al. (1978) model which is used in case of gas-liquid flows where the bubbles can have a range of shapes (to see the equations of this and the previous models, refer to the theory guide of ANSYS Fluent).
The model of Tomiyama (1998) is one of the most common drag laws and, similarly to the Grace et al. (1978) model, it is suitable for both spherical and ellipsoidal bubbles, in the case of slightly contaminated air-water systems:

$$C_D = max\left(min\left(\frac{24}{Re}(1 + 0.15Re^{0.687}), \frac{72}{Re}\right), \frac{8}{3}\frac{E_O}{E_O + 4}\right)$$

Where EO is the Eötvös number and is calculated as follows:

$$E_O = \frac{g(\rho_q - \rho_p)d_p^2}{\sigma}$$

The model of Tomiyama (1998) is referred to isolated bubble.
The model of Ishii (1979) is suitable only for boiling flows and the drag coefficient is the minimum value between the one of the viscous regime and the one of the distorted regime.
The last models available are the Universal Drag Laws which have a wider range of validity as they are suitable for the calculation of the drag coefficients in several gas-liquid flow regimes. It is important to notice that the universal drag models are suitable for two-phase systems where the characteristic length of the flow domain is much larger than the averaged size of the bubbles. Depending on the flow regime, different expressions for the drag coefficient are considered:

- In the viscous regime:

$$C_D = C_{D_{vis}} = \frac{24}{Re}(1 + 0.1\,Re^{0.75})$$

- In the distorted bubble regime:

$$C_D = C_{D_{dis}} = \frac{2}{3}\left(\frac{d_p}{\lambda_{RT}}\right)\left\{\frac{1 + 17.67\,f^{*6/7}}{18.67\,f^*}\right\}^2$$

  Where $f^*=(1-\alpha_p)^{1.5}$.

- In the strongly deformed, capped bubble regime:

$$C_D = C_{D_{cap}} = \frac{8}{3}(1 - \alpha_p)^2$$

The universal drag law was compared to the model of Grace et al. (1978) and they showed similar results when applied to the 0.1 m diameter tank. For this reason, the CFD simulations of this work used the Grace et al. (1978) model as drag law.

Turbulence models

Turbulence is an important aspect and must be taken into account since it enhances both heat and mass transfer rates and influences bubbles coalescence and breakup.
In order to simulate turbulent flows, it is possible to use different approaches such as DNS, LES and RANS. The DNS approach (Direct Numerical Simulation) consists of resolving directly the Navier-Stokes equations without turbulence models; this implies huge computational costs even if it gives more accurate results. Likewise, the LES approach (Large-Eddy Simulation) requires high computational costs, but it allows using coarser meshes than DNS. The LES approach resolves momentum equation only where the flow presents the largest eddies. Hence, due to its reasonable computational costs, the RANS model is adopted: the Reynolds-averaged Navier-Stokes equations (RANS) are obtained by averaging over time both pressure and velocity (in continuity and momentum equations) through Reynolds decomposition. The idea is to describe separately fluctuating part and mean time independent part of instantaneous variables.
If the mass transfer is neglected, the RANS equations can be written in the following form:

$$\frac{\partial(\alpha_q\rho_q)}{\partial t} + \nabla\cdot\left(\alpha_q\rho_q\langle\boldsymbol{u}_q\rangle\right) = 0$$

$$\frac{\partial\left(\alpha_q\rho_q\langle u_q\rangle\right)}{\partial t} + \nabla\cdot\left(\alpha_q\rho_q\left(\langle u_q\rangle\langle u_q\rangle\right)\right) + \alpha_q\nabla\langle p\rangle = \alpha_q\rho_q\left(\nabla^2\langle u_q\rangle\right) + \alpha_q\rho_q\boldsymbol{g}_q - \nabla\cdot\left(\alpha_q\rho_q\langle\boldsymbol{u'}_q\boldsymbol{u'}_q\rangle\right) + \boldsymbol{F}$$

Where $\boldsymbol{\tau}"_q=\rho_q\langle u'_q u'_q\rangle$ represents an unknown symmetric second-order tensor that has to be modelled to close the problem since each time we try to derive an equation to solve an unknown term, it will yield to another equation that contains another unknown term and so on.
In order to close the problem, the Boussinesq approximation consider the Reynolds Stress Tensor (RST) proportional to the mean velocity gradients and introduces the turbulent viscosity (Andersson et al. 2012).

$$\boldsymbol{\tau}"_q = \rho_q\langle\boldsymbol{u'}_q\boldsymbol{u'}_q\rangle = -\frac{2}{3}\left(\rho_q k_q + \mu_{t,q}\nabla\cdot\langle\boldsymbol{u}_q\rangle\right)\boldsymbol{I} + \mu_{t,q}\left(\nabla\cdot\langle\boldsymbol{u}_q\rangle + \nabla\cdot\langle\boldsymbol{u}_q\rangle^T\right)$$

Three options exist in order to adapt the two-equations turbulence models studied for a single-phase system to multiphase systems (Buffo and Marchisio, 2014): Dispersed turbulence model, Mixture turbulence model and Per-phase model.
In this work, only the Dispersed turbulence model was adopted since the ratio between the two phases is high. This model calculates the turbulence only for the continuous phase and further terms are involved in the primary-phase turbulence equations that consider the turbulence induced by the dispersed phase.
Different turbulence models are available in the literature and are already implemented in ANSYS Fluent: standard k-ε, realizable k-ε, RNG k-ε and k-ω models. These models were tested and it was observed that standard k-ε and realizable k-ε models give almost the same results (acceptable computational costs and stability), whereas RNG k-ε had some problem of convergence. For this reason, the realizable k-ε turbulence model was adopted in this work.

Realizable k-ε model

This turbulence model satisfies certain mathematical constraints on the Reynolds Stress tensor and it is consistent with the physics of turbulent flows. The Realizable k-ε model contains a different formulation for the turbulent viscosity and a modified transport equation for the dissipation rate derived from the transport equation of the mean-square vorticity fluctuation.
By adopting the Dispersed turbulence model, the turbulence kinetic energy for multiphase flows is:

$$\frac{\partial(\alpha_q\rho_q k_q)}{\partial t} + \nabla\cdot\left(\alpha_q\rho_q k_q\langle\boldsymbol{u}_q\rangle\right) = \nabla\cdot\left[\alpha_q\left(\mu_q + \frac{\mu_{t,q}}{\sigma_k}\right)\nabla k_q\right] + \alpha_q\left(G_{k,q} + G_{b,q} - \rho_q\varepsilon_q\right) + \alpha_q\rho_q S_{k,q}$$

And the equation for turbulence dissipation rate is:

$$\frac{\partial(\alpha_q\rho_q\varepsilon_q)}{\partial t} + +\nabla\cdot\left(\alpha_q\rho_q\varepsilon_q\langle\boldsymbol{u}_q\rangle\right) = \nabla\cdot\left[\alpha_q\left(\mu_q + \frac{\mu_{t,q}}{\sigma_\varepsilon}\right)\nabla\varepsilon_q\right] + \alpha_q\varepsilon_q\left(C_1\rho_q S + C_{1\varepsilon}C_{3\varepsilon}\frac{G_{b,q}}{k_q} - C_2\rho_q\frac{\varepsilon_q}{k_q + \sqrt{\nu_q\varepsilon_q}}\right) + \alpha_q\rho_q S_{\varepsilon,q}$$

$$C_1 = max\left(0.43, \frac{\eta}{\eta+5}\right)$$

$$\eta = S\frac{k_q}{\varepsilon_q}$$

$$S = (2\langle \boldsymbol{S} \rangle \langle \boldsymbol{S} \rangle)^{\frac{1}{2}}$$

Where ‹**S**› is the mean strain rate tensor, while $G_{b,q}$ is the generation term of the kinetic energy due to buoyancy and it is null as, in this case, the temperature gradient is zero and the dispersed phase density is constant (hence the constant $C_{3\varepsilon}$ does not need to be defined. $G_{k,q}$ is the generation term of the kinetic energy due to gradients of mean velocity. C_1, $C_{1\varepsilon}$, C_2 are constants. σ_k and σ_ε are the turbulent Prandtl numbers, while $S_{k,q}$ and $S_{\varepsilon,q}$ are production terms of k and ε, respectively.
The values of the model constants are calculated in order to ensure good performance and accuracy for different kind of flow.

Moving reference frame

In this work the CFD simulations represented a stirred tank reactor, involving moving part such as rotating blades and impeller. By default ANSYS Fluent solves motion equations in an inertial reference frame, but this approach could lead to instability when applied to moving parts. Therefore, in this work the equations have been solved in a moving reference frame (MRF) in order to take into account the impeller motion. The tank has been divided in two zones: the moving part, containing the impeller and the surrounding fluid (namely the rotor) and the steady-state one, considering the wall of the reactor and the remaining fluid (the stator). With MRF, the impeller and the shaft do not move, but its reference frame rotates with angular speed equal to 2πN. Forces, such as Coriolis force, are generated by the motion of the reference frame and are included in the Navier-Stokes equation. Besides the MRF method, the Sliding mesh is another approach that let account for the impeller motion; however, since the computational costs of the latter method are much higher compared to the ones of MRF method, this method has been applied in the CFD simulations of this work, allowing good predictions of stationary behavior of STR.

5.2.1 CFD-PBM coupling

To help convergence the CFD simulations, initially it has been decided to run the simulations decoupling the population balance from the calculations of hydrodynamics (one-way coupling) and to solve the population balance model coupled with the flow field (two-way coupling) only in a second step.
Starting from the geometry and the meshes used by Cappello (2019)in his work, the flow field has been calculated (assuming constant and fixed bubble size), leading to converged and fully developed simulations. Then the population balance model was implemented in the CFD simulation via udf (user-defined function).
As previously mentioned, a one-way coupling approach was adopted in this former case by using a constant and fixed bubble size as initialization value; the discrete phase pattern was predicted by considering the influence of a fixed continuous phase flow field on the discrete phase itself. This initial step was done in order to see whether the set of kernels was able to predict the bubble size distribution (BSD) inside the reactor without any problem. After verifying that there were not problems and the convergence was reached, the next step was to incorporate the effect of the discrete phase on the liquid phase by coupling the population balance model with the CFD simulations. In this way, the assumption of a constant and fixed bubble size was replaced by considering the bubble size

distribution in order to calculate the hydrodynamics, as it is well known that these parameters (turbulent dissipation rate ε, gas holdup α_g, flow field) depend on the bubble size.
In fact, as shown in the article of Wang et al. (2007), the CFD two-fluid model and the Population balance model are linked each other: the flow field, gas holdup and turbulent energy dissipation rate calculated by CFD are used to solve the Population balance model (PBM) and the BSD calculated from the PBM is used to identify the flow regime, and calculate the interphase forces and turbulence modification in order to close the two-fluid model.
It is really important to take into account the bubble size distribution when the hydrodynamics have to be calculated, because the assumption of a fixed bubble diameter represents a significant limitation to the description of gas-liquid reactors.
Therefore, the PBM was implemented and compiled in the CFD simulations via User-Defined Function (UDF), making the CFD simulations more predictive. In particular, as previously mentioned, the PBM was solved through the simplified Quadrature Method of Moments where only the transport equation of the second-order moment have been solved (simplified QMOM).
Together with the UDF, one User-Defined Scalar (UDS) for the gas phase have been added. The User-Defined Scalar (UDS) in this work is represented by the second-order moment normalized with respect to the local bubble volume fraction:

$$\mu_2 = \frac{m_2}{\alpha_g}$$

Moreover, eight User-Defined Memories (UDM) have been added in order to check the different parameters and values obtained by the m2 method (e.g. the Sauter mean diameter, the breakage and coalescence kernels, etc.).
The subroutine "Adjust" defined in the UDF have been hooked and the location of the subroutine for the calculation of the source term for the moment was specified.
The scalar of the moment was initialized at the inlet boundary with a log-normal distribution centered on a mean bubble size and with a fixed variance of 15%, in accordance to the work of Pettiti et al. (2010); furthermore, the UDS has been initialized in the entire volume at the boundary value through patch operation.

Test case and CFD simulations setup

A stirred tank reactor has been simulated in three-dimensional CFD Eulerian-Eulerian simulations carried out with ANSYS Fluent 2019 R2, under different operating conditions. In particular, the stirring rate ranged from 600 rpm to 997 rpm with a size step of 100 rpm, whereas the superficial gas velocity varied from 0.00415 m/s to 0.0415 m/s.
The stirred tank simulated has a diameter of 0.1 m, a six-blade Rushton turbine with a diameter D=T/3 was placed at a distance h_D=T/3 from the bottom of the vessel, it was also equipped with four equispaced baffleswith a 0.06 m diameter ring sparger that was used to introduce gas into the vessel.
In order to minimize grid size, since multiphase calculations can take a very long time, the geometry represented in the CFD simulations was a section of the real tank and consisted of 1/6 of the entire vessel, containing just one impeller blade and one baffle. Periodicity has been assumed in the azimuthal direction. This configuration leaded to a uniform grid of 621200 cells that is fine enough for the three-dimensional transient simulations (Fig.49).

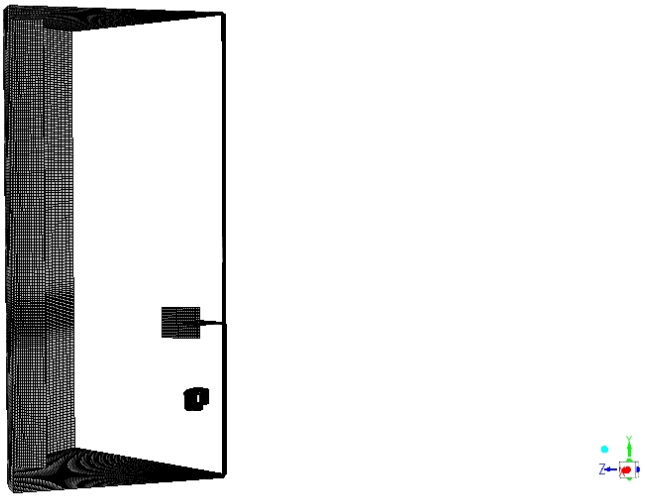

Figura 49 geometry and mesh of the stirred tank's section simulated with ANSYS Fluent

At the inlet sparger the gas fraction was set equal to one to simulate just a gaseous flow entering the tank, while within the vessel the gas fraction was initialized to 6% and the remaining part was made up of water. Regarding the inlet conditions, a turbulent intensity was imposed equal to 3% and an hydraulic diameter equal to 0.01 m.A degassing condition has been used as outlet of the tank. This boundary condition consider the outlet wall as a free surface through which is seen as outlet by the dispersed gas phase that escapes and as a no slip wall by the continuous phase which does not go out.
Regarding the solution methods, a coupled scheme has been adopted for the pressure-velocity coupling, while the adopted methods of spatial discretization are the following:Least Squares Cell based for the gradient, PRESTO! for pressure, Second order Upwind for Momentum, User-defined scalar, Turbulent kinetic energy and Turbulent dissipation rate, whereas First order Upwind for volume fraction. Under-relaxation factors are set equal to 1 for density, body forces and turbulent viscosity, 0.5 for volume fraction, 0.8 for Turbulent kinetic energy and Turbulent dissipation rate, whereas 0.1 for User-defined scalar. The residuals of all the quantitieshave been monitored and used as criterion for convergence; they are all imposed equal to 1e-6, except for the one of the UDS set equal to 1e-9. All the simulations have been done in transient mode and the time step size was determined by imposing that the Courant-Friedrichs-Lewy number (CFL) lower than unity. Hence, the time step size has been imposed equal to 0.001 for almost all the cases.

5.2.2 CFD Simulations: Results and discussion

One-way coupling

As a first step, the simulations have been run decoupling the population balance from the calculations of hydrodynamics (one-way coupling).
The Population balance model was implemented via UDF (User-Defined function) in a fully converged CFD simulation where the flow field was previously calculated assuming constant and fixed bubble size.
By adopting a one-way coupling approach, the discrete phase pattern has been predicted considering the influence of a fixed continuous phase flow field on the discrete phase itself. Different operating conditions were simulated (the same ones tested for 0D simulations) and preliminary results have been obtained.
In particular, for these initial simulations, a fixed value for the bubble size equal to 3 mm have been adopted as initialization value, leading to the following results (Fig.50-51). As shown by the parity

plots below, the Sauter mean diameter predicted by the CFD code are in good agreement with both the experimental observations and the results obtained with the 0D approach, resulting in a deviation always less than 15%. This constitutes an important achievement since it confirms that the shortcut 0D approach is valid also for stirred tanks reactors and represents a useful tool for models investigation.

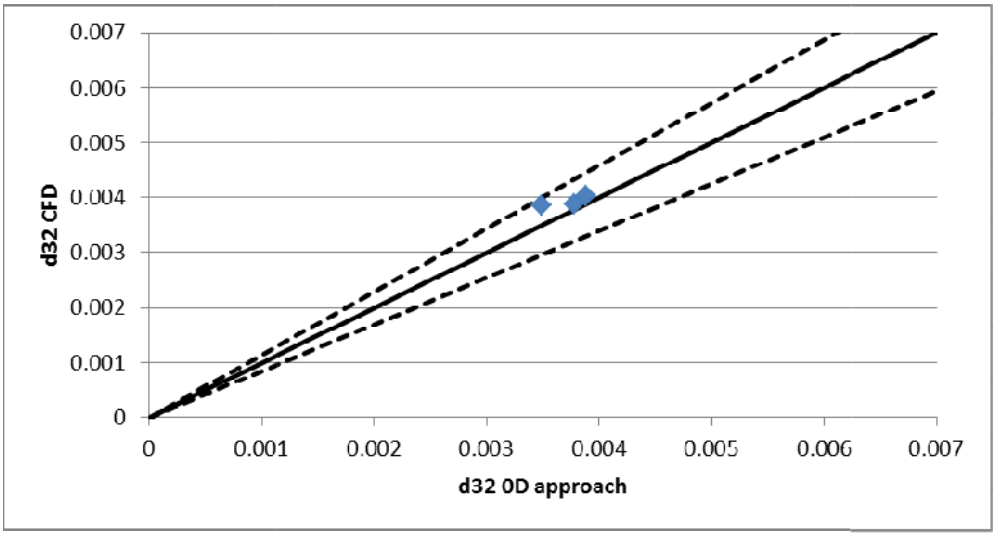

Figura 50 parity plot of d32: comparison results obtained with 0D approach and CFD simulations (dashed lines: 15% of deviation)

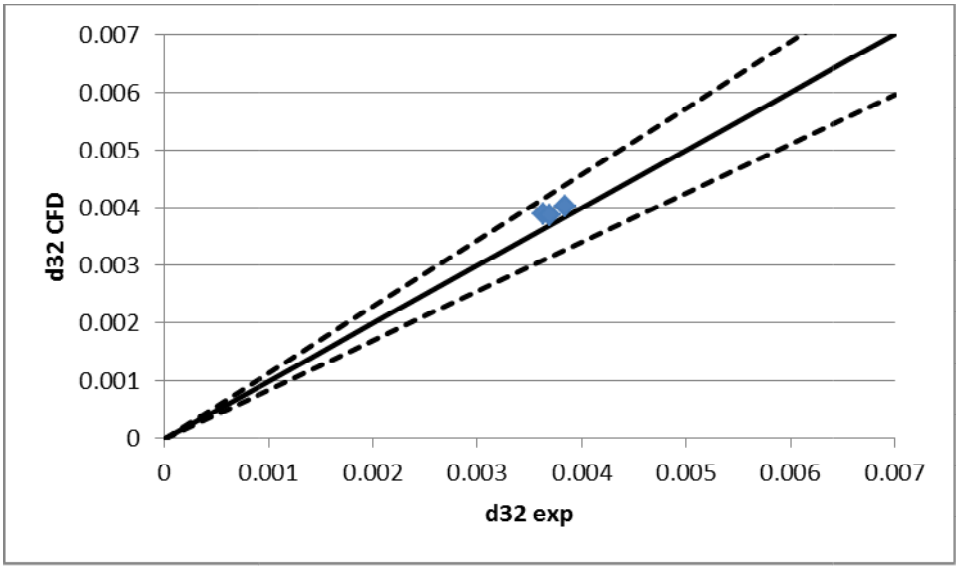

Figura 51 parity plot of d32: comparison CFD simulations and experimental results , varying N (dashed lines: 15% of deviation)

Vsg [m/s]	N [rpm]	d32 experimental [m]	d32 0D simulations [m]	d32 CFD simulations [m]
0.004	800	0.003467	0.003509	0.003979
0.008	800	0.003633	0.003777	0.003889
0.020	800	0.004221	0.004305	0.003917
0.008	600	0.003839	0.003882	0.004028
0.008	997	0.003690	0.003488	0.003854

Tabella 13 Comparison experimental, 0D and CFD simulations results of Sauter mean diameter

Furthermore, these CFD simulations not only predicted results close to the experimental ones, but they were also able to describe the right effect of both superficial gas velocity and impeller speed and thus providing curve profilein high agreement with experimental observations (Fig.52).

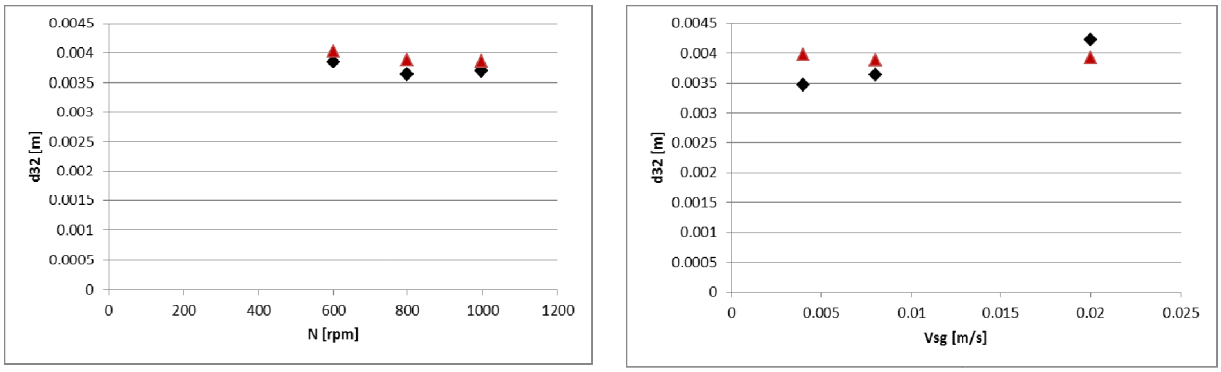

Figura 52 Suater mean diameter observed experimentally (◊) and predicted with CFD-PBM one-way coupling (Δ)

Effect of initial bubble size

The inlet bubble size can influence on the prediction of the final bubble size. For this reason, different initialization values have been tested and the contour plots of the Sauter mean diameter has been reported in order to analyze the effects of this variation.

Three different inlet bubble sizes have been considered (2, 3 and 5 mm) and the corresponding contour plots of Sauter mean diameter are shown below (Fig.53-56).

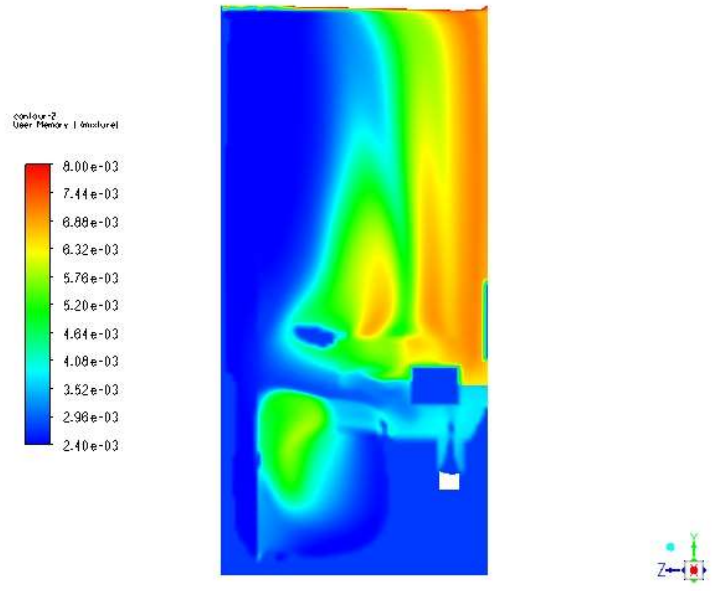

Figura 53 contour plot of local d32 with initial bubble size equal to 3 mm

The Fig.49above show the contour obtained by adopting 3 mm as initialization value for the bubble size. It could be expected to find the smallest bubbles in the impeller region, where turbulence intensity is the highest. On the contrary, the smallest bubbles are localized in the bottom (in particular, in the region under the impeller). A similar behavior was obtained by Venneker et al. (2002). An explanation for this behavior could be that not all the bubbles that cross the impeller are broken and, consequently, the minimum local value of Sauter mean diameter is not found at the outlet of the impeller. However, the bubbles that do not break up in the impeller region rise up through the tank and their d32 increases due to coalescence phenomenon with increasing height. Besides, as observed also by Venneker et al. (2002) in their experiments, at the height where the impeller outflow reaches the wall of the tank, the flow is divided into two circulation loops: the largest bubbles are mainly carried away with the upper loop, while the smallest ones go in both of them. In the lower loop it is possible

to notice the presence of large bubbles; this behavior could be explained by taking a look at the local value of gas volume fraction in that region. In fact, as reported in the figure below (Fig.54)representing the contour plot of the gas holdup, in the lower loop the gas volume fraction is higher compared to the surrounding region (a local accumulation is shown, in accordance with that usually observed experimentally) that means the coalescence phenomenon prevails, leading to a larger d32 (the higher the gas holdup, the more is dominant the coalescence phenomena at constant value of turbulent dissipation rate). A similar local distribution of the Sauter mean diameter was obtained by Petitti et al. (2010), except for the impeller outflow region where the authors observed the smallest bubbles, as reasonable to think sincein this region the turbulence is higher and the effect of breakup is more intense.

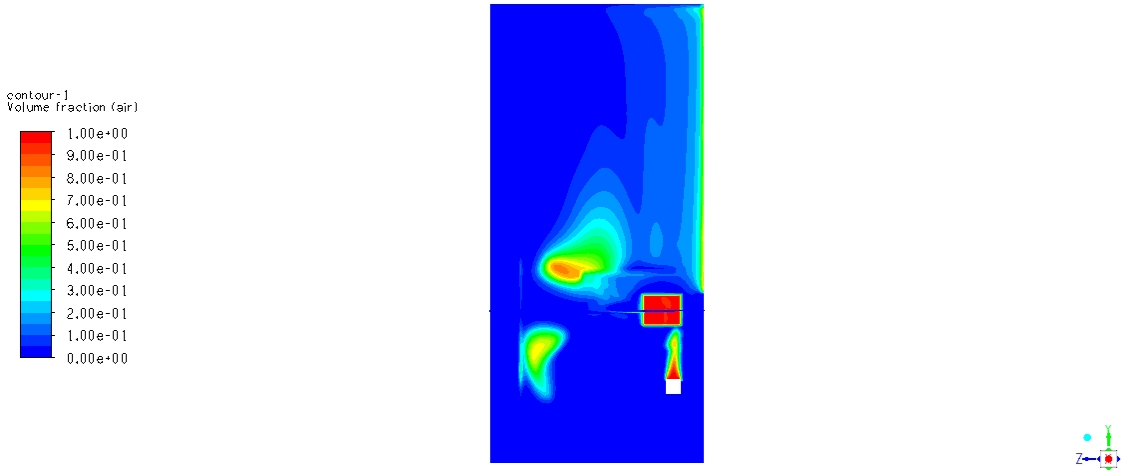

Figura 54 contour plot of gas volume fraction

Then, as mentioned before, a smaller initial bubble size (2 mm) have been applied in order to see the effect of this parameter on the final bubble size. The contour plot reported below (Fig.55) shows that reducing the initial bubble size does not influence significantly the results: almost the same local bubble size distributions is obtained, except for the size of the smallest bubbles which is slightly lowered (1.7 mm instead of 2.4 mm). The latter trend can be explained by considering that, since the initial size of the bubbles is smaller, when these are subjected to the phenomenon of breakage they obviously become even smaller,leading to the local values of d32 observed.

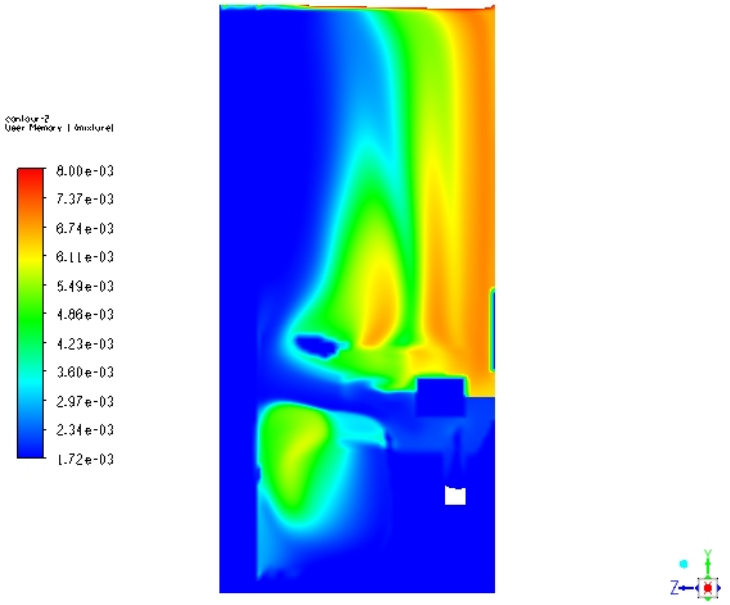

Figura 55 contour plot of local d32 with initial bubble size equal to 2 mm

After analyzing the effect of a smaller initial bubble size, we tried also to see the effect in the opposite direction: hence, we simulated the stirred tank starting with an inlet bubble size higher than the expected final values. A different behavior has been observed in this latter case(Fig. 56) compared to the previous ones. In fact the contour plot highlighted how, in this case, the smallest bubbles are not localized in the region under the impeller, but are situated in the upper part near the wall where the gas phase is almost absentand the coalescence is negligible (see gas volume fraction contour plot, Fig.54). On the contrary, the largest ones are situated in the recirculation zones where coalescence prevails due to an higher presence of gas phase, above and below the impeller and near the impeller shaft where there is low dissipation rate.

Since the regions where there are larger bubbles are wider than the ones with smaller bubbles, the predicted volume-averaged value of d32 in this case is slightly overestimated respect to the experimental result.

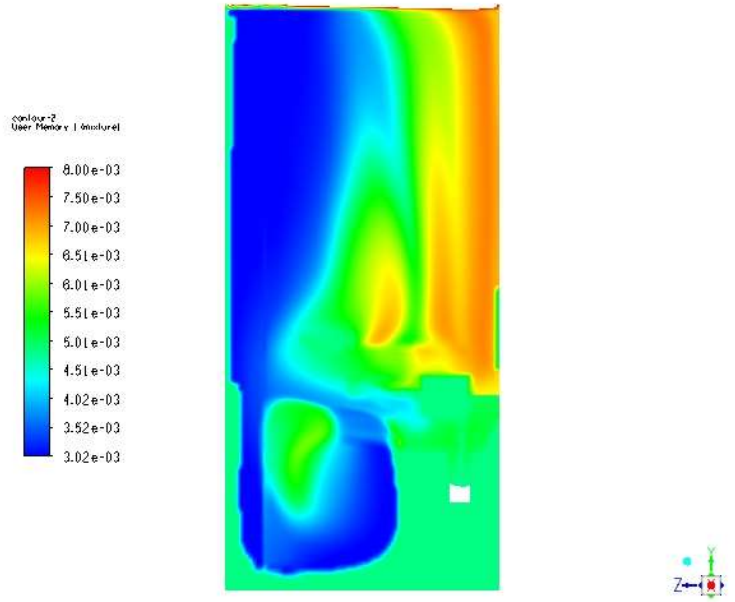

Figura 56 contour plot of local d32 with initial bubble size equal to 5 mm

The following table (Tab.14) summarizes the volume-averaged Sauter mean diameter obtained with different initial bubble size.

Initial bubble size [m]	Vsg [m/s]	N [rpm]	d32 predicted [m]	Mean error of approximation
0.002	0.008	800	0.003319	8.6%
0.003	0.008	800	0.003889	7%
0.005	0.008	800	0.004515	24%

Tabella 14 Effect of initial bubble size on final bubble size

The following parity plot shows what has been reported in the Tab 7 in order to have a better idea of the deviation of the results respect to the experimental observation(Fig.57).

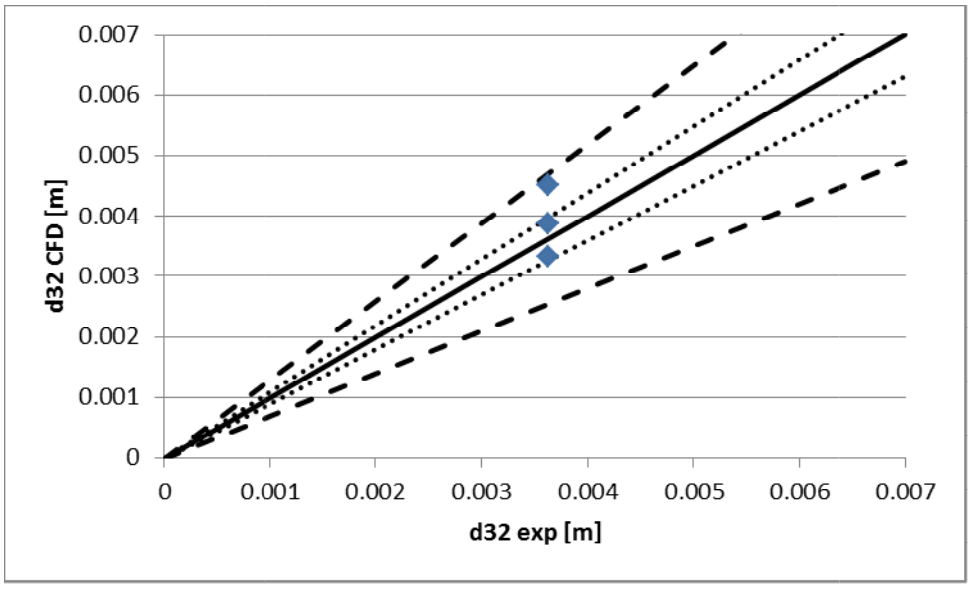

Figura 57 parity plot of final bubble size obtainedstarting with different initial values

The given results let us conclude that an initial bubble size close or slightly smallerthan the mean expected value of the final diameter leads to results that have a better fitting with the experimental observations. On the contrary, choosing an initial bubble size bigger than the mean experimental observation leads to a slight overestimation of the final bubble size(mean error of approximation equal to 24%). For this reason, an initial value of 3 mm has been adopted in the simulations.

Stable Sauter mean diameter

The evaluation of the rightness of results calculated by the CFD simulations is another important aspect. In particular we wanted to investigate how far was the CFD prediction of the Sauter mean diameter from the stable value. Therefore, the experimental data of Cappello (2019) have been used in order to find an empirical correlation of the stable Sauter mean diameter. In this correlation d32 depends on the turbulent dissipation rate and the gas holdup with the following form:

$$d_{32} = a\varepsilon^{b}\alpha_g^{c}$$

The constant a,b and c were found though optimization and are respectively a= 0.0076, b= -0.212 and c=0.214.

This analysis has been done at three different operating condition such as N=600/800/997 rpm and Vsg=0.0083 m/s.

Since in the stirred tank there are some regions with low or without gas phase, the stable Sauter mean diameter has been calculated considering the volume-averaged values of turbulent dissipation rate and gas holdup (even if the best way to calculate d32 it is by applyingthe Favre-like average).The results obtained highlighted that the d32 predicted by the CFD simulations is close to the stable value, leading to a deviation of less than 23%. The following parity plot shows what has been obtained (Fig.58).

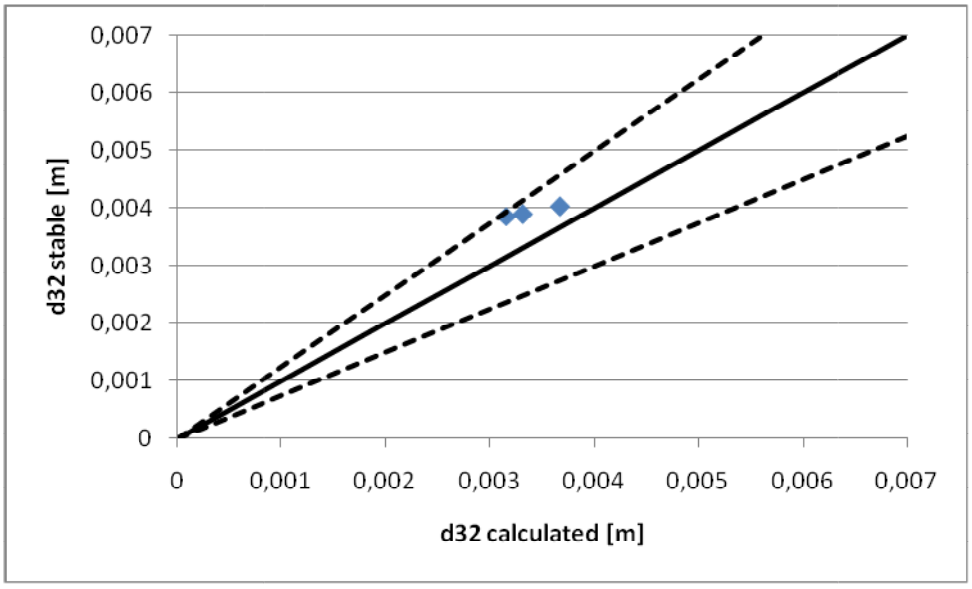

Figura 58 parity plot of stable Sauter mean diameter compared to the Sauter mean diameter obtained with a volume average

N [rpm]	Vsg [m/s]	Experimental d32 [m]	d32 calculated [m]	Stable d32 [m]	Deviation
600	0.0083	0.003839	0.0040283	0.0036716	10%
800	0.0083	0.003633	0.0038894	0.0033195	17%
997	0.0083	0.003690	0.0038542	0.0031554	22%

Tabella 15 Comparison stable diameter vs. Sauter mean diameter calculated by CFD simulations

6.Concluding remarks and future perspectives

The aim of this work was the use of a 0D approach to study several models of coalescence and breakage in gas-liquid systems such as bubble columns and stirred tank reactors, under the heterogeneous flow regime, providing suitable models to predict correctly the bubble size for different operating conditions and different types of flows (air- water or more complex).

The Population Balance Model (PBM) was adopted since it represents an effective method to simulate the bubble size distribution (BSD).The method of moments and, in particular, a simplified version of the Quadrature method of moments (QMOM) was adopted to solve the PBM. The simplified QMOM was based on the idea that it is necessary to solve only the 2^{nd}-order moment transport equation to calculate the Sauter mean diameter d32.

To validate these models, experimental databases are required and thus the experimental observations made byGemello (2018) for bubble columns and Cappello (2019) for stirred tank reactors have been used in the case of air-water systems, whereas, for systems with complex physical properties, the one made by Chaumat et al. (2007) and IFP-NT VonnerRoesler (2018).

Hence, the 0D iterative approach has been used to do a screening of all the breakage and coalescence models; this let us test and validate,in few time, several sets of kernels which provide an accurate bubble size prediction in bubble columns and stirred tank reactors, overcoming the high computational costs related to CFD simulations to carry out results.

Then, the models found with this preliminary approach have been implemented in three-dimensional transient Eulerian-Eulerian CFD simulations in order to have also a better prediction of the hydrodynamics of the system.

The main results of this work can be summarized as follows:

The study done on air-water bubble columns confirmed the ability of the set of models proposed by Gemello (2018) to reproduce the experimental data in the case of air-water system and provided a new set of kernels that represent a valid alternative to the one proposed byGemello (2018). This latter set of kernels consider the breakage model of Laakkonen et al. (2006) model as breakage frequency, the daughter distribution function proposed by Laakkonen et al. (2007), the collision frequency model of Prince and Blanch (1990) (modified by the correction factor) and the film-drainage model for coalescence efficiency proposed by Chesters et al. (1991) considering only inertial collisions. This result is interesting because it lets say that also the coalescence efficiency based on the film drainage model is suitable to describe the bubble size within an air-water bubble column as an alternative to the set of models found by Gemello (2018).

Furthermore, the screening of all the models highlighted that several models predicted bubble size close to the experimental results with a mean error of approximation lower than 20%.

Regarding the screening of the models done for the stirred tank reactor, the results showed that the set of kernels composed by the breakage model of Laakkonen et al. (2006), the modified coalescence efficiency of Coulaloglou and Tavlarides (1977) and the collision frequency of Prince and Blanch (1990) successfully predicted the bubble size distribution in accordance with the experimental observation of Cappello (2019). In a similar way of bubble columns, other models were found to give a prediction of the bubble size close to the experimental observation.

Then, we tried to look for a set of models capable of describing either the systems and we found that the one composed by the breakage model of Laakkonen et al. (2006), the coalescence efficiency of Chesters (1991) and the collision frequency of Prince and Blanch (1990) represented the most universal set of models among the ones tested.

Besides, a study of the use of these model in more complex flow has been done, but unfortunately it did not lead to understand the reasons of the achieved behaviors. Therefore, a more in-depth analysis

of these systems is required and, in particular, some experiments should be done on the breakage and coalescence phenomena separately.
Concerning the CFD simulations done for stirred tank, the Population Balance Model (PBM) has been implemented in the CFD code in order to obtain a better prediction of the hydrodynamics. Apreliminary analysis of the effect of the initial bubble size highlighted that this parameter has only a weak influence on the prediction of the final value and therefore we chose the mean expected bubble size as initialization value.
Then, one-way CFD-PBM coupling simulations (where the BSD has been calculated starting from fully converged simulations of hydrodynamics) were done for different values of superficial gas velocity and stirring rate. Results very close to the experimental data have been collected, confirming again the good prediction capability of the bubble size of the set of models found with the 0D approach. This result is really important since it confirms that also for the case of stirred tanks the simplified QMOM and the 0D approach are successful tools to test and validate models in few time, replacing CFD simulations to screen the models, since they require an extremely high time to carry out simulations.
Due to the lack of time, it was not possible to run simulations with a two-way coupling in order to validate the hydrodynamics inside the tank. Even if the hydrodynamics was well-predicted using a fixed bubble size, as detailed in the thesis of Cappello (2019), the two-way coupling would have been an interesting mean of investigation. Therefore, this approach should be applied in future simulations.

7.Bibliography

Alopaeus, V., Koskinen, J., Keskinen, K. I. &Majander, J. (2002), *'Simulation ofthe population balances for liquid-liquid systems in a nonideal stirred tank. Part2 - parameter fitting and the use of the multiblock model for dense dispersions'*,Chemical Engineering Science 57(10), 1815–1825.

Andersson, B., Andersson, R., Håkansson, L., Mortensen, M., Sudiyo, R., Van Wachem, B. & Hellström, L. (2012), Computational Fluid Dynamics for Engineers, first edn, University Press, Cambridge, UK.

Bakker A. (1992) Hydrodynamics of stirred gas-liquid dispersions. Ph.D. Thesis, Technical University of Delft, The Netherlands.

Bakker A, van den Akker HEA. (1994) *'A computational model for the gas liquid flow in stirred reactors.'* Chem Eng Res Des Trans IchemE. 72 (Part A),594−606.

Bilicki, Z. & Kestin, J. (1987), *'Transition criteria for two-phase flow patterns in vertical upward flow.'*, International Journal of Multiphase Flow 13, 283–298.

Brucato A, Ciofalo M, Grisafi F, Micale G. (1998) *'Numerical prediction of flow fields in baffled stirred vessels: a comparison of alternative modeling approaches.'* Chem Eng Sci. 53,3653−3684.

Brucato A, Ciofalo M, Grisafi F, Rizzuti L. (1989) *'Application of a numerical fluid dynamics software to stirred tanks modelling.'* In: Laforenza D, Perego R, editors. Supercomputing Tools for Science and Engineering. Milan: Franco Angeli, 413−419.

Brucato A, Ciofalo M, Grisafi F, Rizzuti L. (1990) *'Computer simulation of turbulent fluid flow in baffled and unbaffled tanks stirred by radial impellers.'* Proceedings of International Conference on Computer Applications to Batch Processes, Cengio, Italy, 69−86.

Buffo, A., Vanni, M., Marchisio, D.L., 2012. *'Multidimensional population balance model for the simulation of turbulent gas–liquid systems in stirred tank reactors.'* Chem. Eng. Sci. 70,31–44.

Buffo, A., Vanni, M., Marchisio, D. L. & Fox, R. O. (2013), *'MultivariateQuadrature-Based Moments Methods for turbulent polydisperse gas-liquid systems'*, International Journal of Multiphase Flow 50, 41–57.

Buffo A., Vanni M., Renze P., Marchisio D.L. (2016), 'Empirical drag closure for polydisperse gas-liquid systems in bubbly flow regime: Bubble swarm and micro-scale turbulence', Chemical Engineering Res. Des. 113, 284-303.

Cappello, V. (2019), Bubble size and liquid-side mass transfer coefficient measurements in aerated stirred tank reactors with non-Newtonian liquids, PhD thesis, Université Clermont Auvergne, Clermont-Ferrand, France.

Carrica, P. M. &Clausse, A. A. (1993), A Mathematical Description of the CriticalHeat Flux as Nonlinear Dynamic Instability, G. Gouesbet and A. Berlemont.Instabilities in Multiphase Flow, Plenum Press, New York.

Chaumat, H., Billet, A. &Delmas, H. (2007), *'Hydrodynamics and mass transfer inbubble column: Influence of liquid phase surface tension'*, Chemical Engineering Science 62, 7378–7390.

Chesters, A. K. (1991), *'The modeling of coalescence processes in fluid-liquid dispersions:A review of current understanding'*, Chemical Engineering Research and Design: transactions of the Institution of Chemical Engineers: Part A69, 259–270.

Colin, C., Riou, X. & Fabre, J. (2004), Turbulence and shear-induced coalescence in gas-liquid pipe flows, in 'ICMF 2004 - 5th International Conference on Multiphase Flow', Yokohama, Japan.

Coulaloglou, C. A. &Tavlarides, L. L. (1977), *'Description of interaction processesin agitated liquid-liquid dispersions'*, Chemical Engineering Science 32, 1289–1297.

Deen NG, Solberg T, Hjertager BH. (2002) *'Flow generated by an aerated Rushton impeller: two-phase PIV experiments and numerical simulations.'* Can J Chem Eng. 80,638−652.

Friedlander, S. K. (1977), Smoke, Dust and Haze, Wiley, New York.

Gao, Z., Li, D., Buffo, A., Podgórska, W. &Marchisio, D. L. (2016), *'Simulationof droplet breakage in turbulent liquid-liquid dispersions with CFD-PBM:Comparison of breakage kernels'*, Chemical Engineering Science 142, 277–288.

Gemello, L. (2018), Modelling of the hydrodynamics of bubble columns using a two-fluid model coupled with a population balance approach, PhD thesis, Politecnico di Torino, Torino, Italy.

Gimbun J., Rielly C.D., Nagy Z.K. (2009), *'Modelling of mass transfer in gas-liquid stirred tanks agitated by Rushton turbine and CD-6 impeller: A scale-up study'* Chemical Engineering Res. Des., 87, 437-451.

Gordon, R. G. (1981), '*Error bounds in equilibrium statistical mechanics'*, Journal of Mathematical Physics 9, 655–663.

Gosman AD, Lekakou C, Politis S, Issa RI, Looney MK. (1992) *'Multidimensional modeling of turbulent two-phase flows in stirred vessels.'* AIChE J. 38,1946−1956.

Gunawan, R., Fusman, I. & Braatz, R. D. (2004), *'High resolution algorithms for multidimensional population balance equations.'*, American Institute of Chemical Engineering Journal 50, 2738–2749.

Harvey PS, Greaves M. (1982) *'Turbulent flow in an agitated vessel. I. Predictive Model. Trans I.'* Chemical Engineering 60,195−210.

Hibiki, T. & Ishii, M. (2000), *'One-group interfacial area transport of bubbly flows in vertical round tubes'*, International Journal of Heat and Mass Transfer 43, 2711–2726.

Hulburt HM, Katz S. (1964) *'Some problems in particle technology. A statistical mechanical formulation.'* Chem Eng Sci. 19,555−574.

Ishii, M., Zuber, N. (1979). *'Drag coefficient and relative velocity inbubbly, droplet or particulate flows.'* AIChE J. 25,843–855.

Kennard, E. H. (1938), Kinetic Theory of Gases, McGraw-Hill, New York.

Khopkar A.R., Rammohan A.R., Ranade V.V., Dudukovic M.P. (2005) *'Gas–liquid flow generated by a Rushton turbine in stirred vessel: CARPT/CT measurements and CFD simulations.'* Chemical Engineering Science 60, 2215–2229.

Laakkonen, M., Alopaeus, V. &Aittamaa, J. (2006), *'Validation of bubble breakage,coalescence and mass transfer models for gas-liquid dispersion in agitatedvessel'*, Chemical Engineering Science 61, 218–228.

Laakkonen, M., Moilanen, P., Alopaeus, V. &Aittamaa, J. (2007), *'Modellinglocal bubble size distributions in agitated vessels'*, Chemical Engineering Science62, 721–740.

Lane GL, Schwarz MP, Evans GM. (2002) *'Predicting gas-liquid flow in a mechanically stirred tank.'* Appl Math Model. 2,223−235.

Lane GL, Schwarz MP, Evans GM. (2005) *'Numerical modelling of gas-liquid flow in stirred tanks.'* Chem Eng Sci. 60,2203−2214.

Lasheras, J. C., Eastwood, C., Martínez-Bazán, C. &Montañés, J. L. (2002), *'Areview of statistical models for the break-up of an immiscible fluid immersedinto a fully developed turbulent flow'*, International Journal of Multiphase Flow28, 247–278.

Lehr, F. & Mewes, D. (1999), *'A transport equation for the interfacial area density applied to bubble columns'*, Chemical Engineering Science 56, 1159–1166.

Lehr, F., Millies, M. &Mewes, D. (2002), *'Bubble-size distributions and flowfields in bubble columns'*, American Institute of Chemical Engineering Journal48(11), 2426–2443.

Liao, Y. & Lucas, D. (2009), *'A literature review of theoretical models for dropand bubble breakup in turbulent dispersions.'*, Chemical Engineering Science 64, 3389–3406.

Liao, Y. & Lucas, D. (2010), *'A literature review on mechanisms and models for thecoalescence process of fluid particles.'*, Chemical Engineering Science 65, 2851–2864.

Luo, H. &Svendsen, H. F. (1996), *'Modeling and simulation of binary approach byenergy conservation analysis'*, Chemical Engineering Communications 145, 145–153.

Marchisio DL, Barresi AA, Garbero M. (2002) *'Nucleation, growth, and agglomeration in barium sulfate turbulent precipitation.'* AIChE J. 48,2039−2050.

Marchisio DL, Vigil RD, Fox OD. (2003) *'Quadrature method of moments for aggregation-breakage processes.'* J Colloid Interface Sci. 258,322−334.

Marchisio, D. L., Vigil, R. D. & Fox, R. O. (2003a), *'Implementation of the quadrature method of moments in CFD codes for aggregation-breakage problems.'* Chemical Engineering Science 58, 3337–3351.

Marchisio, D. L. & Fox, R. O. (2013), Computational Models for Polydisperse Particulate and Multiphase Systems., Cambridge University Press, Cambridge,UK.

McGraw, R. (1997), *'Description of aerosol dynamics by the quadrature method ofmoments.'*, Aerosol Science and Technology 27, 255–265.

Moilanen P, Laakkonen M, Visuri O, Alopaeus V, Aittamaa J. (2008) *'Modeling mass transfer in an aerated 0.2 m3 vessel agitated by Rushton, Phasejet, and Combijet impellers.'* Chem Eng J. 142,95−108.

Montante, G., Paglianti, A., Magelli, F. (2007). *'Experimental analysis and computational modelling of gas - liquid stirred vessels.'* Chemical Engineering Res. Des. 85, 647–653.

Morud, K.E. and Hjertager, B.H., 1996, '*LDA measurements and CFD modelling of gas–liquid flow in a stirred vessel.'* Chemical Engineering Science, 51: 233–249.

Narasimhan, G., Ramakrishna, D. & Gupta, J. P. (1979), *'A model for transitional breakage probability of droplets in agitated lean liquid-liquid dispersions'*, Chemical Engineering Science 34, 257–265.

Petitti, M., Nasuti, A., Marchisio, D. L., Vanni, M., Baldi, G., Mancini, N. &Podenzani, F. (2010), *'Bubble size distribution modeling in stirred gas-liquidreactors with QMOM augmented by a new correction algorithm.'*, American Institute of Chemical Engineering Journal 56, 36–53.

Prince, M. J. & Blanch, H. W. (1990), *'Bubble coalescence and break-up in air sparged bubble columns'*, American Institute of Chemical Engineering Journal36, 1485–1499.

Placek J, Tavlarides LL, Smith GW, Fort I. (1986) *'Turbulent flow in stirred tanks. II. A two-scale model of turbulence.*' AIChE J. 31,1113−1120.

Raimundo, P. M. (2015), Analysis and modelization of local hydrodynamics inbubble columns, PhD thesis, Université Grenoble Alpes.

Raimundo, P. M., Cartellier, A., Beneventi, D., Forret, A. & Augier, F. (2016),*'A new technique for in-situ measurements of bubble characteristics in bubblecolumns operated in the heterogeneous regime'*, Chemical Engineering Science155, 504 – 523.

Ranade VV, Joshi JB, Marathe AG. (1989) 'Flow generated by pitched blade turbines. II. Simulation using k-e model.' Chem Eng Commun. 81,225−248.

Ranade VV, Joshi JB. (1990) 'Flow generated by a disc turbine. II. Mathematical modelling and comparison with experimental data.' Trans IchemE. 68 (Part A),34−50.

Ranade, V. V. (2002), Computational Flow Modeling for Chemical Reactor Engineering.,Academic Press, San Diego, California, USA.

Roghair, I., Lau, Y., Deen, N., Slagter, H., Baltussen, M., Van Sint Annaland, M., Kuipers, J. (2011). *'On the drag force of bubbles in bubble swarms at intermediate and high Reynolds numbers.'* Chemical Engineering Science 66, 3204–3211.

Roghair, I., Van Sint Annaland, M., Kuipers, H.J.A.M. (2013b). '*Drag force and clustering in bubble swarms.'* AIChE J. 59, 1791–1800.

Scargiali F, D' Orazio F, Grisafi F, Brucato A. (2007) *'Modelling and simulation of gas-liquid hydrodynamics in mechanically stirred tanks.'* Chem Eng Res Des. 85,637−646.

Schiller, L. &Naumann, N. (1935), 'A drag coefficient correlation.', VdiZeitung77, 318.

Simon, M. (2004), Koaleszenz von Tropfen und Tropfenschwärmen, PhD thesis, Teschinschen Universtität Kaiserslautern, Kaiserslautern, Germany.

Simonnet, M., Gentric, C., Olmos, E., Midoux, N. (2007). *'Experimental determination of the drag coefficient in a swarm of bubbles.'* Chemical Engineering Science 62 (3), 858–866.

Simonnet, M., Centric, C., Olmos, E. &Midoux, N. (2008), *'CFD simulation of theflow field in a bubble column reactor: Importance of the drag force formulationto describe regime transitions.'*, Chemical Engineering and Processing 47, 1726–1737.

Sommerfeld M., Decker S., (2004) *'State of the art and future trends in CFD simulation of stirred vessel hydrodynamics.'* Chem. Eng. Technol. 27, 215–224.

Sovova, H. (1981), *'Breakage and coalescence of drops in a batch stirred vessel – ii comparison of model and experiments'*, Chemical Engineering Science 36, 1567–1573.

Sun H, Mao ZS, Yu G. (2006) *'Experimental and numerical study of gas hold-up in surface aerated stirred tanks.'* Chem Eng Sci. 61,4098−4110.

Tabib, M. V., Roy, S. A. & Joshi, J. B. (2008), *'CFD simulation of bubble column- An analysis of interphase forces and turbulence models'*, Chemical Engineering Journal 139(3), 589–614.

Tabor G, Gosman AD, Issa RI. (1996) *'Numerical simulation of the flow in a mixing vessel stirred by a rushton turbine.'* IChemE Symp Ser. 140,25−34.

Tomiyama, A. (1998), *'Struggle with computational bubble dynamics.'*, Multiphase Science and Technology 10(4), 369.

Tomiyama, A., Celata, G.P., Hosokawa, S., Yoshida, S. (2002). *'Terminal velocity of single bubbles in surface tension force dominant regime.'* Int. J. Multiphase Flow 28, 1497–1519.

Venneker BCH, Derksen JJ, Van den Akker HEA. (2002) *'Population balance modeling of aerated stirred vessels based on CFD.'* AIChE J. 48,673−685.

Wang, T. F., Wang, J. F. &Jin, Y. (2005a), *'Population balance model for gas liquid flows: Influence of bubble coalescence and breakup models'*, Industrial &Engineering Chemistry Research 44(11), 7540–7549.

Wang, T. F., Wang, J. F. &Jin, Y. (2005b), *'Theoretical prediction of flow regime transition in bubble columns by the population balance model'*, Chemical Engineering Science 60, 6199–6209.

Wang, T., Wang, J. &Jin, Y. (2006), *'A CFD-PBM coupled model for gas-liquid flows'*, American Institute of Chemical Engineering Journal 52, 125–140.

Wang W, Mao ZS, Yang C. (2006) *'Experimental and numerical investigation on gas holdup and flooding in an aerated stirred tank with Rushton impeller.'* Ind Eng Chem Res. 45,1141−1151.

Wen, C.Y., Yu, Y.H., (1966). *'Mechanics of fluidization.'* Chemical Engineering Progress Symp. Ser. 62, 100–111.

Wheeler, J. C. (1974), *'Modified moments and gaussian quadratures.'*, Rocky Mountain Journal of Mathematics 4, 287–296.

Wright, D. L. (2007), *'Numerical advection of moments of the particle size distribution in eulerian models.'*, Journal of Aerosol Science 38, 352–369.

Wu, Q., Kim, S. & Ishii, M. (1998), '*One-group interfacial area transport in vertical bubbly flow'*, International Journal of Heat and Mass Transfer 41, 1103–1112.

Yuan, C. & Fox, R. O. (2011), *'Conditional quadrature method of moments for kinetic equations.'*, Journal of Computational Physics 230, 8216–8246.

Zhao, H., Maisels, A., Matsoukas, T. & Zheng, C. (2007), *'Analysis of four Monte-Carlo methods for the solution of population balances in dispersed systems'*, Powder Technology 173, 38–50.

8.List of figures

9.List of tables